UNIVERSIDADE TÉCNICA DE LISBOA

INSTITUTO SUPERIOR TÉCNICO

A Wideband Directional Channel Model for Micro-Cells in UMTS

Maria Gabriela Pinto Marques

(*Licenciada*)

Dissertation submitted for obtaining the degree of Master in Electrical and Computer Engineering

Supervisor: Doctor Luís Manuel de Jesus Sousa Correia

Jury: Doctor Carlos António Cardoso Fernandes (President)
Doctor Armando Carlos Domingues da Rocha
Doctor Luís Manuel de Jesus Sousa Correia

May 2001

To my parents

Acknowledgements

First of all, I would like to thank Prof. Luís Correia for having supervised this work. His motivation, discipline and unbeatable patience were the wheel that drove this machine, many times stiff and rusty, through the right path.

I would also like to emphasize the important contribution of *Fundação para a Ciência e a Tecnologia* by means of a Master scholarship.

The working space where the development of this work took place belongs to *Instituto de Telecomunicações*, to which I add my recognition.

This work was produced within the scope of the European IST framework, namely within the ASILUM project, and has been partially funded by it.

The contact with colleagues Lúcio Ferreira, João Gil and Fernando Velez was most of all an inspiration; the teamwork, multiple suggestions and endless fruitful discussions were essential to lighten the way out of loopholes.

From the colleagues with whom I shared the working place, I most owe the pleasant company and working environment. Day-to-day work would have been impossible without it.

From Jorge I got the encouragement and support to go ahead against all the winds.

I also want to thank to my parents for accompanying me in this journey.

Abstract

This work regards the development of a wideband directional channel model to be applicable for simulation of UMTS micro-cells using adaptive antennas. The particular environment of a line of sight street was reproduced.

The proposed model considers single specular reflection from scatterers grouped into clusters. Clusters are uniformly distributed within an (2D) ellipse limited by the street width, while scatterers are Gaussian distributed within each cluster. The theoretical model was implemented and assessed.

When analysing parameter sensitivity, it was concluded that street width is the most influencing input parameter; hence, an effective street width can be used to tune the model. Comparing the model with a set of measurements via Monte-Carlo simulations, a resulting effective street width of 6.5 was obtained within a confidence interval of 68%. Frequency correlation analysis for a pair of up- and down-link UMTS channels lead to the conclusion that correlation does exist, but it depends on the receiving associated delay and angle resolutions.

The model was used to analyse the operational environment in terms of global output parameters and of directional channel impulse response, deriving conclusions about the use of adaptive antennas within UMTS. Typical examples within the city of Lisbon were used for this study.

Keywords

Propagation, Wideband, Directional Models, UMTS, Micro-Cells, Simulation

Resumo

Este trabalho versa o desenvolvimento de um modelo direccional de canal de banda larga aplicável à simulação de micro-células UMTS com antenas adaptativas. Reproduziu-se o ambiente particular de uma rua em linha de vista.

O modelo proposto considera reflexões especulares simples de rerradiadores reunidos em grupos uniformemente distribuídos numa elipse (2D) limitada pela largura da rua. Os rerradiadores seguem uma distribuição Gaussiana dentro de cada grupo. O modelo teórico foi implementado e aferido.

Da análise da sensibilidade aos parâmetros, concluiu-se que o mais influente é a largura da rua, pelo que na afinação do modelo se pode utilizar uma largura efectiva. Comparando o modelo com um conjunto de medições através de simulações de Monte-Carlo, obteve-se um factor de largura efectiva de 6,5 para um intervalo de confiança de 68%. A análise da correlação na frequência para um par de canais UMTS correspondentes a ligação ascendente e descendente leva à conclusão que a correlação existe, mas depende das resoluções de atraso e de ângulo associadas à recepção.

O modelo proposto foi usado para estudar o ambiente operacional a ele associado, em termos de parâmetros globais de saída e resposta impulsiva direccional de canal, inferindo sobre o uso de antenas adaptativas em UMTS. Para tal usaram-se exemplos típicos referentes à cidade de Lisboa.

Palavras-chave

Propagação, Banda Larga, Modelos Direccionais, UMTS, Micro-Células, Simulação

Table of Contents

List of Figures

Chapter 2

Chapter 3

Chapter 4

Annex 1

Annex 2

Annex 3

List of Tables

Chapter 3

List of Abbreviations

AMPS	Advanced Mobile Phone System
AoA	Angle of Arrival
BS	Base Station
CDF	Cumulative Distribution Function
CDMA	Code Division Multiple Access
CIR	Channel Impulse Response
DCIR	Directional CIR
DCM	Directional Channel Model
DL	Down-Link
DoA	Direction of Arrival
EM	Electromagnetic
FDD	Frequency Division Duplex
GAoA	Gaussian Angle of Arrival
GBSB	Geometrically Based Single Bounce
GBSBCM	GBSB Circular Model
GBSBEM	GBSB Elliptical Model
GSM	Global System for Mobile communications
GWSSUS	Gaussian WSSUS
i.i.d.	independent and identically distributed
IMT-2000	International Mobile Telecommunications systems
ISI	InterSymbol Interference

LoS	Line of Sight
MT	Mobile Terminal
NLoS	Non Line of Sight
PDF	Probability Density Function
PDP	Power-Delay Profile
QWSSUS	Quasi-WSSUS
RF	Radio Frequency
SDMA	Space Division Multiple Access
SFIR	Spatial Filtering for Interference Rejection
TD-CDMA	Time Division - Code Division Multiple Access
TDD	Time Division Duplex
ToA	Time of Arrival
UL	Up-Link
ULA	Uniform Linear antenna Array
UMTS	Universal Mobile Telecommunications System
US	Uncorrelated Scattering
VCIR	Vector Channel Impulse Response
WAP	Wireless Application Protocol
WCDMA	Wideband Code Division Multiple Access
WSS	Wide-Sense Stationarity
WSSUS	Wide-Sense Stationary Uncorrelated Scattering

List of Symbols

$a_{k,i}$	scattering complex magnitude of i^{th} reflected scatterer from cluster k
a_w	complex magnitude associated with tap w
b_m	fast fading depth associated with path m
$d(\bullet)$	Dirac delta function
Dj	azimuth angle resolution
Dt	delay resolution
DR	scattering radial range
F_k	mean angle of cluster k
$f_{k,i}$	scattering phase of i^{th} reflected scatterer from cluster k
G	cluster time decay constant
g	ray time decay constant
j	azimuth angle
$\bar{j}$	average azimuth angle
j_0	LoS azimuth angle
j_{0k}	mean AoA of cluster k
j_{BW}	scatterer beamwidth seen from BS
j_i	AoA from scatterer i
$j_{k,i}$	AoA associated with the i^{th} reflected scatterer from cluster k
j_m	AoA from dominant path m
j_w	AoA associated with tap w

L	adimensional azimuth angle spread
λ	wavelength
n_i	Doppler shift of multipath component *i*
q	polar angle
$r(\bullet)$	correlation function
s	standard deviation
s_j	standard azimuth angle spread
s_t	delay spread
t	excess time delay
$\bar{t}$	mean excess time delay
t_{max}	ellipse maximum excess time delay
t_k	excess time delay associated with cluster *k*
t_{ki}	arrival time of the i^{th} ray measured from the beginning of cluster *k*
t_w	excess time delay associated with tap *w*
t_x	*x*% power delay window
v_{ij}	ray angle within a cluster
W	spatial angle
W_i	direction of multipath component *i* relative to the LoS component
W_v	direction of motion relative to the LoS component
A_m	long term fading associated with path m
$\mathbf{a}(j)$	array response vector for the DoA j
B_C	coherence bandwidth
c	speed of light
d	distance
$E\{\bullet\}$	expected value of $\bullet$

f	frequency
f_m	maximum Doppler shift
$f(t)$	transmission system components joint transfer characteristic
$g(t, j)$	BS antenna characteristic
$\mathbf{h}(t)$	vector channel impulse response
$h(t,t)$	time-variant channel impulse response
$h(t,t,j)$	2D direction-dependent time-variant channel impulse response
$h(t,t,W)$	3D direction-dependent time-variant channel impulse response
J	number of scatterers
K	number of clusters
L	distance between ULA elements
M	number of dominant reflectors
N	number of scatterers
n	path loss exponent
N_k	number of scatterers within cluster k
$pdf(j)$	signal power distribution according to j
$P_h(t)$	power density versus excess time delay
P_R	received power
P_T	transmitted power
Q_j	number of additional reflecting points of scatterer j
R	scatterer ring radius
$\boldsymbol{R}_k$	Covariance matrix associated to cluster k
R_{max}	scattering circle maximum radius
R_n	normalised radius to the centre of gravity
$s(t)$	convolution of modulation pulse shape with receiver filter impulse response

t	time
T_C	coherence time
T_k	arrival time of cluster k
U	number of elliptical crowns
v	MT velocity
$\mathbf{v}_{k,b}$	steering vectors superposition during data bust b within cluster k
$x_b(t)$	received signal vector for data burst b
$\lvert\bullet\rvert$	absolute value of $\bullet$
$(\bullet)^H$	complex conjugate transpose (Hermitean) of matrix $\bullet$

Chapter 1

Introduction

This chapter gives a brief overview on the work. Before establishing work targets and original contributions, the scope and motivations are brought up. The work structure is presented as well.

From the birth of cellular mobile communication systems up to the present time being, two decades have passed. Along this period, systems evolved from analog to digital and from bulky portables to others as big as a cigarette lighter. Users in each country increased, in some cases up to more than seventy percent of the population. Also the concept of mobile communications itself was subject to changes: step by step, voice is giving its place to data and to the applications it can bring.

The first systems used analog transmission techniques, namely frequency modulation of voice. Power consumption was large and equipment autonomy was limited to a few hours. Initially, the concept of a mobile phone was something barely portable; larger scale integration made possible the reduction of size, weight and price in later times. Mobility was basically restricted to the country of origin, since several different systems were operating in different countries.

When digital systems came to the scenery, a noticeable increase of capacity was gained. The reduction of the portable size was also possible, due to lower power consumption and larger circuit integration. One particular system should be mentioned here: GSM (Global System for Mobile communications[1]) [MoPa92] was developed as a pan-European standard, making also possible the use of the same mobile phone in different countries. Although this standard was designed essentially for voice, data transmission was foreseen since the beginning, but only up to a data rate of 9.6 kbps. More recently, with the advent of Internet, data gained a wider place in this system, and the standard has been suffering further enhancements in order to provide higher data rates and packet switched data [BuCN99]. A protocol for Internet browsing was also developed, WAP (Wireless Application Protocol).

A third generation of mobile communication systems is about to arrive. It is being developed to provide both voice and data services from the start. From the family of systems created, IMT-2000 (International Mobile Telecommunications systems), attention will be directed onto one in this work: UMTS (Universal Mobile Telecommunications System) [UMTS99]. This system will operate in two different groups of frequency bands, one paired and one unpaired [Tosk99], directed to different types of services. The frequency bands identified here regard to

[1] Initially, these initials stood for “Groupe Spécial Mobile”, the standardisation body where the system was specified.

the European case [Fern99], [Kott99].

The paired band is located in [1920, 1980] MHz and [2110, 2170] MHz, and will use WCDMA (Wideband Code Division Multiple Access) in slices of 5 MHz. Being a paired band, it works in FDD mode (Frequency Division Duplex): the lower portion of the band is used for the up-link, while the upper one is used for the down-link. Due to its characteristics, it is best suited to serve symmetrical applications (the same data rate is used in up- and down-links).

The unpaired band is located in [1900, 1920] MHz and [2010, 2025] MHz and will use TD-CDMA (Time Division - Code Division Multiple Access) in slices of 5 MHz. It works in TDD mode (Time Division Duplex): each band slice is divided into 15 time-slots, which can be used either for up- or down-links. Therefore it can serve equally well symmetrical and asymmetrical applications. However, the nature of TDD imposes a maximum time delay, which restricts its use to pico- or micro-cells.

It is possible to transmit both voice and data on both bands. The supported data rates depend on mobility, and therefore on the scenario/environment. For very low mobility, most likely indoors, it is possible to go up to 2 Mbps, while for medium mobility (micro-cells) and high mobility (macro-cells) it will support up to 384 kbps and 144 kbps, respectively [UMTS98]. Both circuit-switched and packed-switched modes are available. The chip rate to be used in all cases is 3.84 Mcps [Fern99].

From the experience in earlier systems, it is predicted that in certain specific environments capacity will be insufficient in a short term. It is also known that in CDMA (Code Division Multiple Access) based systems like UMTS, capacity is limited by interference from multiple users. These two arguments are strong enough to motivate the use of techniques that try to reduce interference, by ignoring information coming from a certain direction where this interference is originated. These are dynamic situations, for the interference will vary depending on the positions of the mobile terminals. Therefore, to apply these techniques it is necessary that an adaptive antenna be used. This means an antenna array and controlling equipment to take care of the signal processing aspects of these techniques. Several methods are being studied in order to put these concepts into practise.

UMTS being a new system, many questions regarding to its performance under operation are still kept to be answered, concerning services, user capacity, or also at the physical level. This

is the reason why modelling and simulation become so important in any newborn system, so for to obtain a prediction of the system's potentials. By these same means, also new techniques can be compared and chosen.

Steering the attention into the propagation channel, it is needed to know its behaviour within the various environments in which the system will operate. For what concerns the use of adaptive antennas, it is of great importance to evaluate the channel in terms of direction, in order to better exploit this new feature. One way to provide insight into the channel behaviour is by means of creating a model that emulates it. The more realistic and complete this model is, the more reliable are the conclusions about the overall performance of the system. However, the model will not be useful if it is too complicated to implement or to use (it will take too long either to "tune" or to derive simulation results). Therefore, simplifications will have to be done according to certain assumptions, whose validity must be checked. This is the direction followed in this work.

This work aims at the development of a propagation channel model applicable for UMTS micro-cells while regarding the utilisation of adaptive antennas, hence, a wideband directional channel model. The model is to be used for simulations, and, thus, to be implemented in a programming language, assessed, and later used for the analysis of typical scenarios. From the micro-cell environments, a particular operational scenario is chosen, corresponding to the situations where base station and mobile terminal are in one same street.

The original contribution of this work comes from generating a new simulation model, which was implemented, assessed and used for the analysis of typical scenarios. This model was obtained after merging generic specifications from three baseline models (Geometrically Based Single Bounce Elliptical Model, Combined Geometrically Based Single Bounce and Gaussian Wide-Sense Stationary Uncorrelated Scattering Model and Elliptical Sub-Regions Model) adapting these specifications to the particular scenario (operational environment) envisaged. The reached model considers single specular reflections from scatterers grouped into clusters.

Besides this chapter, four others compose this document.

The following chapter is dedicated to the theoretical approach to the problem, by introducing the concepts to be taken into consideration and the status of work done in this area. From this study, the options regarding a further model proposal are taken.

Chapter 3 is dedicated to the model implementation. A description of the model proposed for implementation is produced, the simulation model program is overviewed, and the assessment methods and results are also presented.

The subsequent chapter regards the analysis of some practical application scenarios, based on real street cases from the city of Lisbon. Each case is thoroughly analysed and comparisons are made between these practical scenarios.

Conclusions and further suggestions of work to be done are drawn in the final chapter.

Chapter 2

Channel Modelling

This chapter is intended to familiarise the reader with the theoretical issues and the solutions proposed by different authors for directional channel modelling. The main concepts involved are introduced in a first part, following a general description of the most known models that were developed up till the present moment. The choice of a modelling approach to be used for further implementation concludes the chapter.

2.1 Aspects of Propagation in Mobile Communications

2.1.1 Basic Aspects

Let us consider two isotropic antennas (one transmitting and one receiving) located in free space. If the distance, *d*, between them is such that far-field assumptions can be made, the power measured in the receiving antenna is, according to the well-known Friis' transmission equation [Bala97], inversely proportional to the second power of both the distance *d* and the frequency *f*, *i.e.*,

$$P_R = \left(\frac{l}{4pd} \right)^2 P_T \tag{2.1}$$

where l is the wavelength of the signal and P_T and P_R, respectively, the transmitted and received powers.

The fact that both antennas (from base station - BS - and mobile terminal - MT), and the signal flowing between them, are submerged into a "physical", non-ideal, environment brings a summation of factors to be considered. The signal will necessarily interact with the environment, namely with atmosphere, ground and objects acting as obstacles (*e.g.*, trees, soil irregularities and man-maid objects), both in the down-link (BS to MT transmission) and in the up-link (MT to BS transmission).

In what follows, a closer look into the various possible interactions with the environment is done. The consequences of this interaction, as well as motion, are subject to study in channel modelling and will be addressed in the following subsections.

The presence of the atmosphere can be seen twofold: refractivity variation with altitude forces the ElectroMagnetic (EM) field to curve its course, and atmospheric elements absorb part of the energy. For the range of frequencies and distances involved in the communication system to be studied both these effects can be neglected, therefore, one shall not go into details on them. Extended work on these topics can be found in [Boit83].

Like refractivity variations, the interaction with Nature and artificial objects generates a certain deviation of EM field from its original course. In this case, four different phenomena can be observed: reflection, refraction, diffraction and scattering [HaBH96].

Reflection and refraction are the result of interfacing a plain surface over a certain incidence angle. Part of the energy is returned back (reflected) in a symmetrical angle and part is transmitted trough the surface (refracted), propagating over a different angle. The resulting magnitude and phase of the reflected and refracted signals can be calculated from the Fresnel coefficients, which depend on the material characteristics, and on the signal incidence angle and polarisation.

Diffraction can be seen as a non-abrupt transition between illuminated and shadow areas. Typical examples are illuminated areas behind a sharp edge, a wedge or a round obstacle.

Scattering can be described as a disorganised reflection from a rough surface. A scatterer at a certain distance from the energy source is assumed to isotropically scatter the incident energy that falls on its area.

As one can understand, the effects mentioned above perform changes in the signal arriving to the receiving antenna, both in its direction (DoA - Direction of Arrival) and in its phase and magnitude. Therefore, the main consequences of ground and surrounding "objects" are attenuation increase and multipath. The latter is the cause of fading, *i.e.*, fluctuations on signal magnitude over a period of time or distance. As it is impossible to determine exactly all contributions, the signal can not be seen as purely deterministic, but rather as the sum of a deterministic component (the Line of Sight - LoS - one) with a statistical one, derived from additional attenuation and multipath effect.

Provided the fact that polarisations are treated differently in the interactions with the environment, also polarisation rotation (depolarisation) will occur. In fact, depolarisation will be random. This fact is usually not studied directly in mobile propagation modelling, and it is therefore assumed total polarisation matching between transmitter and receiver. Yet, there are already measurement campaigns reported in literature that have included polarisation.

2.1.2 Path Loss and Fading

The description of median power attenuation along with distance, often named path loss, was the first step taken into the characterisation of a mobile communications channel. Several authors have proposed models that adjust to different environment types and follow different philosophies. The first characterisation attempts accounted for reflections in an ideal flat ground plane. Later, theoretical considerations or measurements conducted to enhanced theoretical and empirical models. Typical examples are COST 231-Walfish-Ikegami and COST 231-Hata models.

COST 231-Walfish-Ikegami Model [COST99] was based on a theoretical model that received an empirical adjustment based on measurements. It is best suited for regular building environments (*e.g.*, downtown Manhattan), when the BS antenna is above the rooftop level, and for distances up to roughly 5 km.

COST 231-Hata Model [COST99] is an empirical model based on measurements performed in different areas within the city of Tokyo. It is suited for irregular areas, typically larger than 3 km, where the purpose is to obtain an average estimation, and so the averaging of urban characteristics is possible. Better results can be achieved for a specific area adjusting the model coefficients with the help of local measurements.

For a better understanding of signal power behaviour along with distance, a sketch of a typical power measurement result for a distancing receiver is depicted in Figure 2.1 [Yaco93]. While the mean value of the signal power tends to decrease with distance, it is possible to observe the occurrence of signal fluctuations over the mean value.

In a more detailed analysis of the picture, three main effects can be noticed. The first one is the decay of power with distance (path loss), which was explored above. The signal fluctuation around the average decay consists of two components: one shows a larger number of variations along with distance; the other shows more prolonged variations along with distance. These two effects are named short-term and long-term fading, respectively.

Long-term fading, or shadow fading (also frequently called "slow fading" [2]) is a power variation due to successive presence or absence of the shadowing effect originated by large obstacles. It is usually described by a lognormal statistical distribution [Pars92].

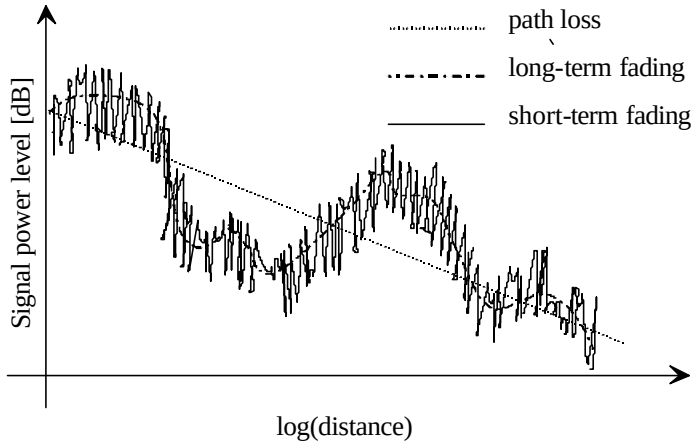

Figure 2.1 – Signal power vs. distance between transmitter and receiver.

Short-term fading, or multipath fading (also frequently called "fast fading" [3]), is naturally the effect due to multipath. The resulting propagated signal is the summation of several components with different orientations; the phases from these components will vary differently within a small distance, therefore, short displacements of the MT can lead to reinforcement or cancellation of the signal. When no *a priori* knowledge of the channel exists, Rice or Rayleigh distributions are assumed for describing this phenomenon [Pars92].

The choice between Rice and Rayleigh distributions depends on the assumption of a LoS or of a Non Line of Sight (NLoS) situation, corresponding to the presence or absence of the deterministic component, respectively. In both cases, the statistical component is assumed to be composed of infinite i.i.d. (independent and identically distributed) rays arriving to the receiver from any direction. As it is well known, the ratio between deterministic and statistical components in Rice distribution is given by the Rice factor; this factor corresponds to the ratio between the LoS power component and the NLoS one, where the NLoS one results from the coherent summation of all the NLoS signal components.

[2] "Slow fading" is also used for one of the sub-effects of short-term fading, and it may lead to misunderstandings.

[3] As in "slow fading", the name "fast fading" is also used for one of the sub-effects of short-term fading.

2.1.3 Wideband Analysis

The multipath phenomenon can be analysed at a more refined scale. As mentioned earlier, the interaction between one single signal sample transmitted and the environment will result in a summation of signal components, each one arriving to the receiving device at a different time instant (Time of Arrival – ToA) and according to a different DoA.

In order to study the temporal behaviour of the resulting signal, as proposed initially by Bello [Stee92], the mobile channel should be seen as a linear time-variant system, where a time-variant impulse response $h(t,\tau)$ can be written [Stee92] (t and τ stand for time and excess time delay, respectively). Likewise, the rest of the well-known "Bello functions" can also be used to describe the channel. Note that all of the 4 functions are related to each other either by direct or inverse Fourier transforms.

When the channel shows Wide-Sense Stationarity (WSS) both in time and frequency domains (*i.e.*, Uncorrelated Scattering –US), it is then called a Wide-Sense Stationary Uncorrelated Scattering (WSSUS) channel; in that case, only power density functions (either in excess time delay or in Doppler shift domains) need to be analysed. This is because WSS channels' fading statistics do not change over an interval of time, therefore, channel correlation functions are invariant with time, while in US channels the contributions from elemental scatterers with different path delays are uncorrelated, thus, autocorrelation of the channel function is singular in the delay variable. Hence, from these two conditions, it results that a delta function relates power density functions and correlation functions.

In practical cases, it is usually not possible to ensure WSSUS during the whole time. However, in many cases, it is possible to ensure stationarity conditions within a restricted period of time (for example, the duration of one frame transmission). Channels with such characteristics are named Quasi-WSSUS (QWSSUS).

Figure 2.2 shows a typical Power Delay Profile (PDP), which is a plot of $P_h(\tau)$, power density versus excess time delay[Pars92].

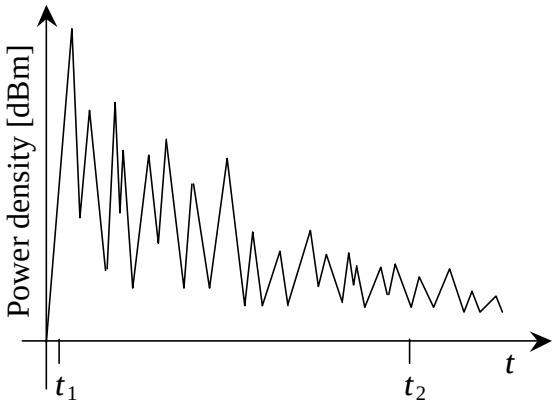

Figure 2.2 – Power-delay profile.

From a PDP it is possible to calculate both mean delay $\bar{t}$ and delay spread s_t (corresponding to the two first statistical moments).

$$\bar{t} = \frac{\int_0^\infty t\, P_h(t)\,dt}{\int_0^\infty P_h(t)\,dt} \tag{2.2}$$

$$s_t = \sqrt{\frac{\int_0^\infty (t-\bar{t})^2 P_h(t)\,dt}{\int_0^\infty P_h(t)\,dt}} \tag{2.3}$$

The PDP allows also for determining the delay window t_x, for a certain percentage of power *x*, which means the minimum interval where this amount of power can be obtained. The delay window can be either fixed or sliding, depending on the lower delay limit, t_1, being zero or another value. Usually, a fixed delay window is used for signals where the LoS component is included, and a sliding one otherwise. A typical delay window considered is the 90% power one.

$$t_x = t_2 - t_1 \tag{2.4}$$

$$\frac{\int_{t_1}^{t_2} P_h(t)\,dt}{\int_0^\infty P_h(t)\,dt} = x\% \tag{2.5}$$

Another useful parameter is the channel coherence bandwidth B_C, which can be estimated from[4] [Yaco93]

$$B_C = \frac{1}{2\pi s_t} \tag{2.6}$$

Delay spread and coherence bandwidth are parameters that describe the time dispersive nature of the channel in a local area.

If the mobile system bandwidth is larger than B_C, it is said that one has a wideband system. In this case InterSymbol Interference (ISI) can occur and equalisation techniques should be employed.

In the opposite case, when the system can be considered narrowband, different path delays are not distinguished (resolved). Hence, only multipath fading needs to be analysed. In this case the channel is called time-flat [Stee92].

Note that a system is considered narrow- or wideband depending on the surrounding environment; hence, it can be considered narrowband in one environment and wideband in another.

2.1.4 Motion and Directionality

When the mobile terminal is in fact moving, Doppler spread will be added to the receiving signal. One should note that this motion can occur in any direction, and that multipath components will suffer different Doppler shifts depending on their DoA. Therefore, each multipath component will be affected by a Doppler shift of

$$\nu_i = f_m \cos(\varphi_i - \varphi_v) = \frac{v}{\lambda} \cos(\varphi_i - \varphi_v) \tag{2.7}$$

[4] A correlation of 0.5 was assumed for an exponential ToA distribution. Note that this is not a rigid rule, giving only a rough estimate of B_C.

where v is the MT velocity, f_m is the maximum Doppler shift, and W_i and W_v are the directions of motion and multipath component relative to the LoS component, respectively.

As an attempt to describe the effect of Doppler shifts, Gans calculated the Radio Frequency (RF) power spectrum based on Clarke's assumptions of uniformly distributed horizontal omnidirectional arriving components [Pars92]. As expected, the resulting power spectrum is symmetrical with respect to the centre frequency, but increasing towards infinity in the edges. Other authors, like Aulin [Pars92] have obtained similar U-shaped curves, but smoothed on the edges, by not considering only horizontal arrivals.

As a complement to delay spread and coherence bandwidth, which describe the time dispersive nature of the channel in a local area, Doppler spread and coherence time are parameters that describe the time varying nature of the channel in a small region, caused by either the relative motion between the MT and the BS, or by objects moving within the propagation scenario.

Coherence time T_C can be seen as a statistical measure of the time duration over which the channel impulse response is essentially invariant (strongly correlated), quantifying the similarity of the channel response at different times. An estimate of T_C can be [Rapp96]

$$T_C = \frac{9}{16\pi f_m} \tag{2.8}$$

If the reciprocal of the baseband signal bandwidth is larger than the coherence time of the channel, this means that the channel will change while the transmission of the baseband message occurs, hence causing distortion at the receiver. Otherwise, the channel can be considered frequency-flat. When the channel is both time- and frequency-flat, it is also called flat-flat. When it is neither time- nor frequency-flat, it is called non-flat [Stee92].

Although Doppler is direction dependent, it should be noted that the study of Doppler is not enough to obtain directional information, because the correspondence between direction and Doppler spread is not unique[5]. Therefore, in order to account for the directional behaviour of

[5] As an example of this fact, two signal components that are symmetrical with respect to the motion direction will present the same Doppler shift.

multipath arrival, an extension to the "Bello functions" is performed: the channel is evaluated through either a direction-dependent time-variant impulse response or a vector time-variant impulse response.

The direction-dependent (or angle-resolved) time-variant impulse response $h(t,\tau,\Omega)$ is often, for shortening, simply called Channel Impulse Response (CIR)[6] or Directional CIR (DCIR). It provides the channel response depending on time, excess time delay and DoA.

The vector time-variant channel impulse response, also called Vector Channel Impulse Response (VCIR), provides the channel response depending on time and excess time delay for each antenna of an array. Naturally, it depends on the receiving antenna array geometry, and it is related to the DCIR through the antenna array factor.

In most cases,- angle discrimination is only 2D, that is, it is performed only in the azimuth coordinate. Therefore, most of the models refer only to the azimuth angle φ and not to the spatial angle Ω (hence, the polar angle θ is neglected). In those cases the impulse response considered is $h(t,\tau,\varphi)$ and the expression "Angle of Arrival" (AoA) is often used instead of DoA.

Although the mobile propagation channel is reciprocal, the directional behaviour of multipath may be different from the points of view of the MT or of the BS, depending on the environment, therefore, DoA statistics from BS and MT will be different. This means that for the full directional knowledge of the channel, a double-directional impulse response should be considered, which is achieved by including Direction of Departure (DoD)[7] information. It is enough to know the full directional behaviour in one link direction (up- or down-). DoA and DoD from one direction correspond to the DoD and DoA, respectively, in the opposite direction.

The same way time-variant channels can be characterised with respect to their delay spread, also angle spread can be characterised. However, due to the non-infinite nature of the angular

[6] Note that, naturally, this is not "the" channel impulse response often mentioned in basic literature (impulse response from time invariant impulse response systems).

[7] This will correspond to the Angle of Departure (AoD) in the 2D case.

domain, the standard metrics used for time are not directly applicable. From the various metrics studied by Eggers [Egge00], two are described here. Both are used for 2D cases, that is, only azimuth is considered. The first one is the "standard" azimuth angle spread metric, obtained through a circular to Cartesian mapping:

$$s_j = \sqrt{E_j\left[j^2\right] - \bar{j}^2} \tag{2.9}$$

where

$$\bar{j} = E_j\{j\} = \arctan\left(\frac{\bar{x}}{\bar{y}}\right) \tag{2.10}$$

$$E_j\{\bullet\} = \int_{\bar{j}-p}^{\bar{j}+p} \bullet \cdot pdf(j)\,dj \tag{2.11}$$

$$\bar{x}_n + j\,\bar{y}_n = E_j\left\{e^{jj}\right\} \tag{2.12}$$

where $pdf(j)$ corresponds to the signal power distribution in j. The second metric is another form of azimuth angle spread. It provides an adimensional result between 0 and 1, and is derived from the normalised radius to the centre of gravity, R_n, which is another dispersion metric. This azimuth angle spread metric is calculated according to:

$$L = \sqrt{1 - R_n^2} \tag{2.13}$$

where

$$R_n = \sqrt{\bar{x}_n^2 + \bar{y}_n^2} \tag{2.14}$$

The inclusion of angular dispersion in channel characterisation allows to classify the rank of the channel. In that sense, it is said that a channel is low-rank if it is narrowband and simultaneously the angle spread is narrower than the 3-dB beamwidth of the system receiver antenna. If one of those conditions is not satisfied, the channel is considered high-rank. Note that depending on both system antennas and the environment, the channel can be considered high-rank in one direction (either up- or down-link) and low-rank in the other.

2.2 Directional Channel Models

2.2.1 General Considerations

To perform a propagation study over a specific communications system, a model must be applied. This model has to be suited to it; that is to say, it has to be sufficiently comprehensive so that the relevant propagation aspects are included. Regarding mobile communication systems, the demands for modelling have changed along with system evolution. Therefore, starting from models considering only narrowband effects like path loss, fading and Doppler spread, then later studying wideband effects (time delay spread), it has come to the point of including direction information, and so the concept of a Directional Channel Model (DCM), or spatial channel model, was created.

The subject of directional channel modelling is not totally brand new. Several authors, following different purposes and approaches, have been contributing to it. This section intends to give an overview on the various models developed under this subject. From the models existing in literature, several approaches can be found: fully deterministic, fully statistical, based on geometric considerations and based on measurements.

Deterministic models make only use of site-specific information to determine the received signal. The tools currently used for the calculations make use of ray-tracing algorithms, based on geometric optics, and can model path loss and delay and angle spreads. These models can provide reproducible information. However, the computational burden and the lack of detailed building and terrain databases do not make them as efficient as desired [MLKS98]. Obviously, also the fact of having site-specific calculations does not allow extrapolation of results. The purpose of this work being to provide a model applicable for a certain environment, but not site specific, makes this sort of models of no special interest, and that is why no deterministic model is approached.

In statistical models, the angle-resolved impulse response is obtained directly by knowing the statistical distribution of each parameter involved. A very precise model demands a quite

large number of parameters, some of which parameters may be correlated, hence, increasing complexity for simulation purposes. Averaging can be used in order to reduce the number of distributions; this causes information loss, and an increase in the error, but in turn a feasible model comes out. In some cases, measurements can be of use to tune such models or to draw the liability of the developed model. Ideally, the less measurements needed the better, for this means additional work and costs in system planning.

Semi-statistical models come halfway between statistical and deterministic ones. The CIR is calculated from geometric considerations regarding the positioning of scatterers. The statistical component comes from the fact that scatterers are not positioned deterministically, but instead according to a certain statistical distribution. This way less statistical distributions need to be known *a priori*, resulting in a simpler model, easier for simulation purposes.

The total of models about to be described embrace most of the approaches mentioned here. For each of the models, a brief description will be given. The development purposes will be mentioned, as well as application conditions and the results that can be drawn from the model.

2.2.2 Extended Tap-Delay Line Model

Recalling the traditional view of a time variant system, *i.e.*, a tap-delay-line composed of W taps with an associated delay t_w and a complex magnitude a_w, [Stee92], the model presented by Klein and Mohr [LiRa99] is an angle dependent extended version of the previous one, whose CIR can be described by

$$h(t,t,j) = \sum_{w=1}^{W} a_w(t)\, d(t - t_w)\, d(j - j_w) \tag{2.15}$$

Each path will then have an associated AoA, j_w.

The above CIR is a generic one, and can be used by most models. The difference between them will reside in the way the different parameters are computed. In this case no particular distribution is assumed *a priori*, and so the statistics of t, j, and $|a|$ must be derived from measurements. This can be achieved by obtaining histograms of these parameters.

Summarising the model's properties:

- it is a wideband 2D directional channel model;
- CIR is computed from the BS point of view, although an equivalent procedure can be used for the MT;
- input parameters are t, j and $|a|$ statistics;
- parameter statistics are to be obtained from measurements;
- no application environment is defined.

2.2.3 Measurement-Based Model

As the previous one, the channel model proposed by Blanz *et al.* [LiRa99] is based on measurements. It basically intends to extract the channel time-variant directional impulse response, $h(t,t,j)$, as it is seen from the BS. This way it will characterise the propagation environment in terms of scattering points.

The time-variant impulse response obtained from measurements at the BS terminals is the result of

$$h(t,t) = \int_0^{2p} h(t,t,j)\, g(t,j)\, f(t)\, dj \tag{2.16}$$

where the impulse responses $f(t)$ and $g(t,j)$ represent the joint transfer characteristic of the transmission system components (modulator, demodulator, filters, etc.) and the characteristic of the BS antenna, respectively.

Note that the $h(t,t,j)$ distribution will vary with the scenery geography and with time, depending on the MT motion characteristics.

Some concluding remarks about this model are:

- it is a wideband 2D directional channel, although easily set for 3D;
- it is drawn from the BS side, but a similar approach can be used for the MT;
- the channel characteristics are totally drawn from measurements;

- the system components' behaviour must be known;
- it is not properly a model, but more of a guideline to extract a channel behaviour from measurements.

2.2.4 Time-Varying Vector Channel Model

Considering the problem of blind adaptive spatial equalisation with a multiple BS antenna, Raleigh and Paulraj [RaPa95] developed a time-variant vector model to estimate inherent time correlation structure existing in fading channels. The model assumes that the MT has a single antenna, while in the BS there is an array of antennas. The propagation environment is composed by M dominant reflectors, and so the array response vector in the DoA of the m^{th} path is given by $\mathbf{a}(\theta_m)$.

It is assumed that, besides short-term fading associated to the Gaussian distributed process parameter $\beta_m(t)$, also lognormal long-term fading exists, accounted by A_m. Therefore, the VCIR is

$$\mathbf{h}(t) = \sum_{m=1}^{M} \mathbf{a}(\theta_m)\ d^{-n/2} \beta_m(t) \sqrt{A_m} \tag{2.17}$$

where n is the path loss exponent.

Final remarks on this model are:

- it is a 2D narrowband[8] directional channel model;
- it provides VCIR;
- VCIR is computed based on short- and long-term fading processes from M dominant paths;
- it also depends on MT-BS distance and path loss exponent;
- no values are suggested for fading and path loss parameters; hence, these must be

[8] No delay profile was included in this model, for it was developed for AMPS (Advanced Mobile Phone System), a first-generation mobile communications system.

derived from measurements;

- presence or absence of LoS is not mentioned, nor the specific type of environment;
- it can be used for simulation (the development purposes were the study of equalisation and tracking).

2.2.5 Gaussian Wide Sense Uncorrelated Scattering Model

While studying the problem of downlink beam steering in GSM, Zetterberg and Espensen [ZeEs96] developed a statistical channel model that makes considerations on the shape of the received signal vector justified by spatial assumptions, the Gaussian WWSUS (GWSSUS) model.

The model assumes that the multipath signal arrives from scatterers that are grouped into *K* clusters, providing different delays; only delay differences within the same cluster are not resolvable within the transmission signal bandwidth (thus, this can still be considered a wideband channel model). There is no correlation between clusters.

The received signal vector is given by

$$\mathbf{x}_b(t) = \sum_{k=1}^{K} \mathbf{v}_{k,b}\, s(t - t_k) \tag{2.18}$$

where *s(t)* is the convolution of the modulation pulse shape with the receiver filter impulse response and $\mathbf{v}_{k,b}$ is the superposition of the steering vectors during the b^{th} data burst within the k^{th} cluster, which may be expressed as

$$\mathbf{v}_{k,b} = \sum_{i=1}^{N_k} a_{k,i}\, e^{j f_{k,i}}\, \mathbf{a}(j_{0k} - j_{k,i}) \tag{2.19}$$

where N_k is the number of scatterers within the k^{th} cluster, $a_{k,i}$ is the scattering complex magnitude, $f_{k,i}$ is the phase and $j_{k,i}$ is the AoA from the i^{th} scatterer belonging to the k^{th} cluster. j_{0k} is the k^{th} cluster mean AoA and $\mathbf{a}(j)$ is the array response vector in the direction of j.

In this model, delays can be assumed stationary over several data bursts, while phases vary significantly. Vectors $\mathbf{v}_{k,b}$ are assumed to be zero mean complex Gaussian distributed wide sense

stationary random processes (stationarity implied during several data bursts in this case). Doppler is accounted indirectly by the change of cluster-BS distance.

When no line of sight is present, the mean will be zero due to the random phase $f_{k,i}$, which is assumed to be uniformly distributed in the range [0, 2π[. When a direct path component is present, the mean becomes a scaled version of the corresponding array response vector, that is,

$$E\{\mathbf{v}_{k,b}\} \propto \mathbf{a}(j_{0k}) \tag{2.20}$$

For the k^{th} cluster, the covariance matrix is given by

$$\mathbf{R}_k = E\{\mathbf{v}_{k,b}\ \mathbf{v}_{k,b}{}^H\} = \sum_{i=1}^{N_k} |a_{k,i}|^2 E\{\mathbf{a}(j_{0k} - j_{k,i})\ \mathbf{a}(j_{0k} - j_{k,i})^H\} \tag{2.21}$$

Concluding remarks on this model are:

- it is a 2D wideband channel model (delay accounted) seen from the viewpoint of the BS;
- although intended for GSM, it can be extrapolated for other systems;
- Doppler effect is implicitly accounted for;
- it provides a received signal vector and a covariance matrix;
- it depends on the number of clusters and on the number of scatterers per cluster;
- it considers both the presence or absence of LoS;
- no specific type of environment is referred to;
- it can be used for simulation;
- scattering input parameters are not specified, which may require measurements.

A particular case of the GWSSUS model is the Gaussian Angle of Arrival (GAoA) channel model [ZeEs96]. In this model, it is assumed that the number of scatterers within each cluster is infinite. Their power distribution regarding the azimuth angle is Gaussian. This leads to a simplified version of the multipath covariance matrix. Given its similarity with the previous model, no comments on the model will be presented. Some confusion may be generated around this model, for other models have been reported with this same name, as is the case of the model presented by Ottersten [Otte95], which is a narrowband model with only one cluster, whose AoA statistics are assumed to be Gaussian distributed around a nominal angle.

2.2.6 Extended Indoor Clustering Model

After analysing indoor measurement data, Saleh and Valenzuela [SaVa87] noticed that a certain type of clustering phenomenon could be observed. It could be seen that multipath components arrived at the antenna in groups, to what was called clusters[9], and that both the clusters and the rays within a cluster decayed in magnitude with time. From that, the following impulse response was derived

$$h(t) = \sum_{k=0}^{\infty} \sum_{i=0}^{\infty} a_{ki}\, d\left(t - T_k - t_{ki}\right) \tag{2.22}$$

where the sum over k corresponds to the clusters and the sum over i represents the rays within a cluster. T_k is the arrival time of cluster k and t_{ki} is the arrival time of the i^{th} ray measured from the beginning of cluster k. The variables a_{ki} are Rayleigh distributed, with a mean square value described by a double-exponential decay given by

$$\overline{a_{ki}^{\,2}} = \overline{a_{00}^{\,2}}\, exp\left(-\frac{T_k}{G}\right) exp\left(\frac{t_{ki}}{g}\right) \tag{2.23}$$

where Γ and g are the cluster and ray time decay constant, respectively, and $\overline{a_{00}^{\,2}}$ is the average power of the first arrival of the first cluster, which is determined by the distance between MT and BS.

An extension of this model accounting for AoA was proposed by Spencer *et al.* [SRJJ97], also based on measurements. Assuming that time and angle are statistically independent, *i.e.*,

$$h(t, \varphi) = h(t)\, h(\varphi) \tag{2.24}$$

the proposed angular impulse response is then given by

$$h(\varphi) = \sum_{k=0}^{\infty} \sum_{i=0}^{\infty} a_{ki}\, d\left(\varphi - \Phi_k - \nu_{ki}\right) \tag{2.25}$$

[9] Note that, for this particular case, delay is resolved within a cluster for the system bandwidth.

where F_k is the mean angle of the k^{th} cluster, assumed uniformly distributed over [0, 2π[, and v_{ki} corresponds to the ray angle within a cluster, modelled as a Laplacian distributed random variable with zero mean and standard deviation s:

Drawing some conclusions on this model:

- it is a 2D wideband directional channel model, potentially extendable for 3D;
- it provides CIR;
- complex magnitudes of the signal components are Rayleigh distributed;
- cluster angle is Laplacian distributed, while ray angle is uniformly distributed;
- LoS is implicit in the first arriving ray;
- Doppler is not mentioned (which is acceptable for an indoor model, where low mobility is implicit);
- it is suited for indoor environments;
- it can be used for simulation;
- parameter values must be drawn from measurements.

This is only one of several indoor models reported on the literature. However, as it is not the intention of this work to focus the study on indoor channels, the remaining models were not analysed in depth, and are therefore not reported here.

2.2.7 Extended GSM Models

The two models hereby presented were developed for simulations, regarding the analysis of downlink beamsteering [ZeEs96]. In order to keep simulations compatible with GSM previous dispositions, the reference channel power delay profiles taken were the ones reported for typical urban and bad urban situations in GSM. The simulation platform was the same used for GWSSUS and GAoA models.

The Typical Urban model uses 120 scatterers randomly placed within a 1 km radius around the mobile. These are held still while the mobile travels a distance of 5 m, at the end of which they are relocated in order to assume their original position with respect to the mobile. Every 5 m gone through, random phases and random lognormal shadowing with a standard deviation of 5-

10 dB are assigned. Exponential path loss law is also applied. The received signal is then computed. Simulations show that this model and the GSM-Typical Urban have nearly identical power delay profiles, Doppler spectrums and delay spreads. Furthermore, the AoA statistics are approximately Gaussian and similar to those of the GAoA model with one cluster.

The only difference between the Bad Urban model and the previous one is the addition of a second scatterer equal to the first one but with 5 dB less average power and a 45º positioning shift. The presence of the second cluster increases both resulting angle spread and delay spread.

Concluding on both models:

- they are 2D wideband directional channel models from the BS viewpoint;
- CIR is computed by "brute force";
- they are based on scatterer positions (moved along the way);
- Doppler effect is implicit;
- shadow fading and path loss are included;
- no reference is made regarding LoS;
- they are designed for sumulation and suited for typical and bad urban macro-cell environments, respectively;
- although the simulation models are designed for GSM, they can be extended to other systems.

2.2.8 Lee's Model

Standing as one of the first to perform spatial considerations, Lee [Lee73] proposed a model to predict the correlation between signals received by two sensors in order to perform considerations about diversity.

As it can be seen in Figure 2.3, according to this model, scatterers are evenly spaced over a circumference surrounding the mobile, blocking LoS. These are *effective scatterers*, *i.e.*, they represent the effect of many scatterers within a region.

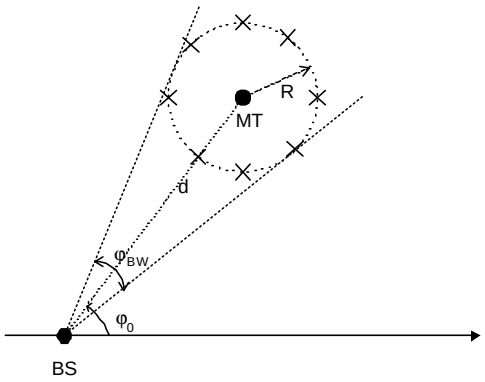

Figure 2.3 – Scatterer placement for Lee's model.

Diversity considerations looked for in the model can be achieved by predicting the level of correlation between the signals received by two sensors as a function of element spacing. This result can be extrapolated for an antenna array of arbitrary size, by considering the correlation between each pair of elements. In general, larger angle spreads and element spacings result in lower correlations, which provide an increased diversity gain. For macro-cell type environments, correlation measurements have provided results with a narrow angle spread at the base station and a large angle spread at the mobile.

Assuming N scatterers equally spaced on the circumference, with R and d as represented in Figure 2.3, the discrete AoA will be

$$j_i = \frac{R}{d} sin\left(\frac{2p}{N} i\right) \quad i = 0, \cdots, N-1 \tag{2.26}$$

Assuming also simultaneous arrival components of complex magnitude with zero mean and unitary variance (for real and imaginary parts), the signal correlation between two array elements spaced a distance equal to L is [Aszt96]

$$r\left(L, j_0, j_{BW}\right) = \frac{1}{N} \sum_{i=0}^{N-1} exp\left[-j \frac{2pL}{l} cos\left(j_0 + j_i\right)\right] \tag{2.27}$$

for d much larger than R.

Although the original model refers the MT velocity, [LiRa99] states that Doppler is not accounted for in this model. Stapleton *et al.* [StCM94], [StCM96] proposed an extension to Lee's model by imposing an angular velocity v to the ring of scatterers, hence, accounting for Doppler

shift. The appropriate maximum Doppler shift is achieved for a scatterer angular velocity equal to v/R.

The joint AoA and ToA channel derives a "U-shaped" power delay [LiRa99], which is not consistent with measurements. A second extension to the model proposed by the same authors [StCM96] considers additional scatterer rings. This way it is possible to obtain the desired PDPs.

The comments on this model are:

- it is a 2D narrowband channel model from BS viewpoint (which can be adjusted for wideband);
- it provides knowledge on the correlation function between two antenna elements;
- it is based on effective scatterer positions (rotated for Doppler effects);
- additional scatterer rings can be used in order to can provide a desired PDP;
- absence of LoS is presumed;
- it is based on the assumption of a macro-cell environment (scatterers are placed only around MT);
- it is not well suited for simulations.

2.2.9 Discrete Uniform Distribution Model

The purpose and analysis capacity of the Discrete Uniform Distribution model [Aszt96] is similar to Lee's "non-extended" model. Basically only the scatterers' placement changes.

The N scatterers are equally spaced within a narrow beamwidth j_{BW} centred at the line of sight to the mobile, as shown in Figure 2.4.

Therefore, the discrete AoA, assuming N is odd, will be

$$j_i = \frac{i}{N-1} j_{BW} \quad i = -\frac{N-1}{2}, \cdots, \frac{N-1}{2} \tag{2.28}$$

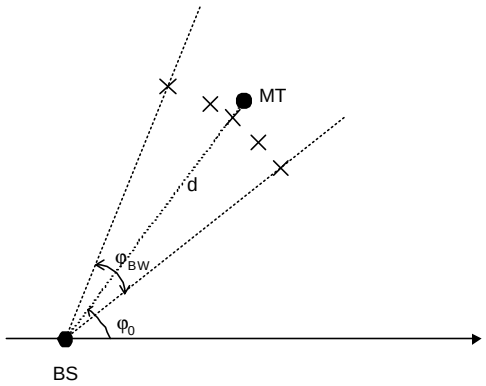

Figure 2.4 – Discrete uniform scatterer distribution.

The signal correlation for the same conditions as the previous model is

$$r(L, j_0, j_{BW}) = \frac{1}{N} \sum_{i=-\frac{N-1}{2}}^{\frac{N-1}{2}} exp\left[- j \frac{2pL}{l} cos(j_0 + j_i) \right] \tag{2.29}$$

The conclusions that can be drawn from this model are the same as for the "non-extended" version of the previous one.

2.2.10 Uniform Sectored Model

Nørklit and Andersen [NøAn94] proposed a model to study the influence of the mobile propagation scenario on the signal received at an antenna. In it, scatterers are randomly placed in a section of a circular crown, as can be seen in Figure 2.5.

It is assumed that scatterers are uniformly distributed within an angle j_{BW} and a radial range of *DR* centred at the mobile. Scattering coefficients have magnitude and phase that are uniformly distributed variables within the intervals [0, 1] and [0, 2π[, respectively.

As the number of scatterers tends to infinity, the signal envelope fading becomes Rayleigh distributed with uniform phase. According to the authors, beam-steering techniques are suited for scatterer distributions with widths slightly larger than the beamwidth.

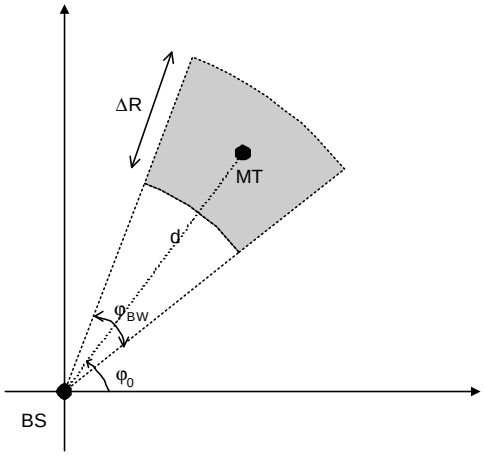

Figure 2.5 – Uniform sectored scatterer distribution.

Concluding:

- this is a narrowband 2D simulation model seen from the BS;
- it computes the channel impulse response;
- it is based on a uniform distribution of scatterers; their associated phases and magnitudes are also uniform; no information is given on scattering area size;
- it accounts only for non-LoS situations;
- it presumes a macro-cell environment.

2.2.11 Geometrically Based Single-Bounce Statistical Channel Models

The concept of GBSB Statistical Channel Models [LiRa99] is based on the definition of a scatterer planar spatial Probability Density Function (PDF). The simplifying assumptions of these models are to consider that, while each multipath signal travels between MT and BS, only a single specular reflection in a scatterer occurs. Therefore, no other effects such as rough surface scattering, diffraction, and multiple bounce by surfaces and volumes are accounted for.

Scatterers are assumed to be omnidirectional re-radiating elements, and are assigned complex scattering coefficients. As mentioned above, a PDF is associated to the scatterers' positioning. This PDF is restricted to a delimited region and the shape of this region will depend on the considered environment.

The mathematical simplicity of the model allows for deriving both joint and marginal statistics for Angle of Arrival (AoA) and Time of Arrival (ToA). These are important to specify and predict adaptive antenna performance. Also, it makes less complex simulations possible. For that, scatterers are placed randomly according to the chosen PDF.

The PDF delimiting region is discussed in what follows, leading to two different models: the GBSB Circular Model (GBSBCM) and the GBSB Elliptical Model (GBSBEM), which are based on a scatterer region of circular and elliptical shapes, respectively. The GBSBCM is applicable to high tier, macro-cellular environments, where the BS is higher than potential scatterers; the MT is surrounded by a circular scatter area centred at the MT. This is why the GBSBCM is also called the GBSB Macro-Cell Model. The GBSBEM is used for low tier, micro-cell systems, where BS and MT are both surrounded by local scatterers (the BS is at about the same height as local scatterers) and where it is assumed that scatterers exist predominantly between the BS-MT axis.

Geometrically Based Single Bounce Circular Model (Macro-Cell Model)

Although it is assumed that the GBSBCM applies to the situation where BS antenna height is relatively large in comparison to that of the MT, which is typical for macro-cell environments [PeRR96], it is a planar model, still, reasonably arguing that the distance *d* is much larger than the difference between BS and MT heights. Therefore, no signal scattering from locations near the BS is involved, which justifies the choice of a circular region surrounding the MT for the scattering region of the GBSBCM, as depicted in Figure 2.6.

The scatterers uniform distribution is delimited by a circle with radius R_{max}, naturally smaller than the BS-MT distance. This is an assumption earlier used for different purposes.

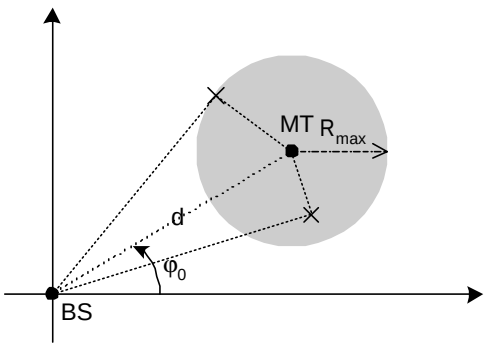

Figure 2.6 – Geometry for the GBSBCM.

Analysing the derived joint ToA*(t)* and AoA*(j)* PDF obtained from the model, some of the model's properties can be drawn. Using Jacobian transformation, it is easy to derive the joint ToA and AoA density function at both BS and MT [LiRa99]. Actually, the resulting PDF is the same for both BS and MT, only differing in the validity region. The joint PDF is then:

$$p_{t,j}(t,j) = \frac{\left(d^2 - t^2c^2\right)\left(d^2c - 2dtc^2\cos(j - j_0) + t^2c^3\right)}{4pR_{max}^2\left(d\cos(j - j_0) - tc\right)^3} \tag{2.30}$$

where c is the speed of light, and d and j_0 are as defined in Figure 2.6. The validity region for the BS and the MT cases are, respectively:

$$\frac{d^2 - 2dtc\cos(j - j_0) + t^2c^2}{tc - d\cos(j - j_0)} \le 2R_{max} \wedge t > \frac{d}{c} \tag{2.31}$$

$$\frac{d^2 - t^2c^2}{d\cos(j - j_0) - tc} \le 2R_{max} \wedge t > \frac{d}{c} \tag{2.32}$$

Out of these validity regions, the PDF's value is zero.

Note that the above PDF only defines the probability of signal paths arriving to the BS or MT; path attenuation differentiation is not accounted for.

Results from this model indicate a high probability of multipath components with small excess delay along the line of sight. Seen from the BS perspective, components are restricted to a small angle range around the LoS direction.

To adjust the performance of the model, R_{max} can be set to match angle spread results given by the model and others derived from measurements.

Geometrically Base Single Bounce Elliptical Model (Micro-cell Model)

The GBSBEM [LiRa96] is based on the fact that, being the BS antenna heights relatively low, it can be assumed that multipath scattering near the BS is just as likely as multipath scattering near the MT; it is also assumed that scattering will be present in the surroundings of an existing LoS path. Therefore scattterers are considered uniformly distributed within an ellipse whose foci are the BS and the MT, as depicted in Figure 2.7.

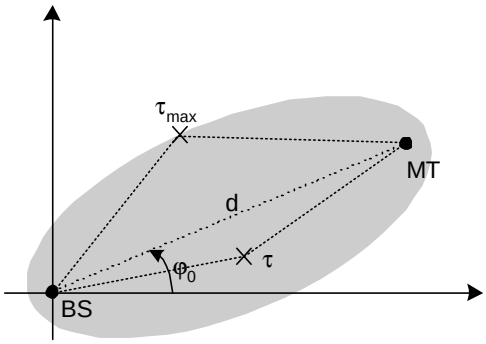

Figure 2.7 – Geometry for the GBSBEM.

As previously mentioned, due to the chosen shape of the scattering region, only multipath signals that arrive with an absolute delay not greater than t_{max} are accounted for in the model. As the model considers equal scattering coefficients, signals with longer delays will experience grater path loss, not being considered below a certain power level. This is equivalent to imposing a receiver power threshold below which signals are not detectable. Choosing a sufficiently large t_{max}, all the power above equipment sensitivity level and AoA of the multipath signals will be accounted for. It must be said that the choice of t_{max} determines both the delay spread and the angle spread.

For this model, the joint ToA*(t)* and AoA*(j)* PDF observed at either the BS or the MT is given by [LiRa99]

$$p_{t,j}(t,j) = \begin{cases} \dfrac{\left(d^2 - t^2c^2\right)\left(d^2c + t^2c^3 - 2tc^2 d\cos\left(j - j_0\right)\right)}{p\,t_{max}c\sqrt{t_{max}^2c^2 - d^2}\left(d\cos\left(j - j_0\right) - tc\right)^3} & \dfrac{d}{c} < t \le t_{max} \\ 0 & \text{elsewhere} \end{cases} \tag{2.33}$$

where c is the speed of light, and d and j_0 are as defined in Figure 2.7. Note that, as in the case of GBSBCM, the above PDF only defines the probability of signal paths arriving to the BS or MT; path attenuation differentiation is not accounted for.

As final remarks on these two models, it can be said that:

- models are 2D wideband channel ones for both BS and MT viewpoints;
- Doppler is accounted for;
- it is possible to compute either the CIR through simulations or the joint and

marginal ToA and AoA PDFs through mathematical algebra;

- models are based on scatterers' spatial PDF;
- scatterers are associated with equal magnitudes and uniform distributed phases;
- only specular reflection is considered;
- R_{max} or t_{max} (for circular or elliptical model, respectively) must be based on measurements;
- for simulation purposes, path loss exponent n and scattering associated magnitude must also be given;
- presence of LoS is assumed for the elliptical model, but is not mentioned in the circular model;
- macro- and micro-cell environments are presumed for the circular and the elliptical models, respectively.

Although Doppler power spectrum can be found, it is not clear how motion affects the spatial PDF, that is, how will scatterers be affected by it.

Other authors can be found suggesting different scattering spatial distributions, as it is the case in [BJLF98] and [MLKS98]; also, a partially 3D model is proposed by [NøAn98], while considering the uniform scattering region to be the intersection between the ground plane and an ellipsoid focused on BS and MT.

2.2.12 Elliptical Sub-regions Model

The model proposed by Lu, Lo and Litva [LuLL97] is dedicated to perform spatial channel simulations. Motivated from the fact that there is a lack of measurement-based information on the joint distributions of ToA and AoA, the model was developed based on a physically defined propagation process.

While concluding that local scatterers around the transmitter, and around the path from the transmitter to the receiver, have more significant effects on the signal components arriving to the receiver, it is proposed, as in the previous model, that scatterers be distributed within a 2D ellipse. Recall that elliptic curves are associated with constant delays. Although this particular

aspect is identical to the previous model, most of the further simulation aspects differ.

The ellipse is divided into U equal width (thus equal delay interval) elliptical crowns. U must be large enough to guarantee the required delay distribution. Given the total number of scatterers, the number of scatterers per crown is given by a Poisson distribution whose mean is chosen in agreement with measurement data. Taking into consideration the fact, observed in measurements, that multipath components tend to arrive in clusters due to the multiple reflective points of the scatterers, it was assumed that there are J scatterers with $1+Q_j$ reflecting points. The additional number Q_j of reflecting points in each scatterer follows a Poisson distribution with the same mean value. The complex path magnitudes are constantly equal, and depend on the number of reflecting points of the scatterer. The phases are uniformly distributed in $[0, 2\pi[$. The AoAs from each reflecting point of the scatterer are assumed to be Gaussian distributed with a variance depending on the scatterer size.

For the cases where the BS antenna is mounted higher than surrounding obstacles, and so scattering effects near by are negligible, a circular area around it can be set scatterer free. Doppler frequency shift of each individual path is also accounted for.

Some final comments on the model:

- it is a 2D wideband channel model from the BS viewpoint (also from MT one) accounting for Doppler;
- it computes CIR through simulations;
- it depends on the distributions for scatterers' spatial positioning, on their number of reflecting points, their angle of arrival and associated phase;
- scaterers are assumed as specular reflectors;
- scatterers are distributed into elliptical crowns, whose number can be adjusted according to measurements;
- the presence or absence of LoS is not mentioned;
- although being more suited for a micro-cell environment type, it can, however, be adapted for macro-cell environments;
- although statistically very complete, variation with time is not explored, and should be quite heavy to implement.

The same way as the previous model, it is not clear how motion affects the spatial PDF,

that is, how will scatterers be affected by it.

2.2.13 Unified Model

Having the notion that earlier models had been developed for particular environments, the model developed by Fuhl, Molisch and Bonek [FuMB98], intends to suit itself to a generalised environment, embracing the situations of macro-, micro- or pico-cells, with or without LoS, and with or without MT motion. In order to account for both macro- and micro-cell characteristics, scattering regions are placed around both the MT and the BS. Also distant reflectors are considered.

The model assumes that the CIR can be computed as the summation of four components: LoS, scattering around the BS, distant reflectors and scattering around de MS. For simplicity, the effect of scattering around the BS is considered in parallel with the remaining effects. While the effect of distant objects is always accounted for as specular reflection, local scatterers can produce either reflection or scattering. The LoS component magnitude is assigned a Rice factor and lognormal shadowing.

A spatial distribution is assumed to the discrete scatterers around the BS and the MT, in order to compute the impulse response at the BS. For this purpose, two distributions are suggested: a uniform distribution within a circle or a single-sided Gaussian. It is said that the second case is a more realistic one, for it does not contain discontinuities. For these components also the envelope and frequency correlation functions are derived.

Considerations about azimuth power spectrum, spatial correlation between antenna elements and frequency correlation are performed, while taking into consideration the local scattering around the MT. Besides Doppler consideration, the temporal variations of the channel are considered for a moving MT through the introduction and removal of scatterers. It is not explicit, though, how this is consistent with a non-uniform scatterer distribution.

In order to perform simulations in the various types of environments, the authors suggest ranges of values for the different parameters involved, also distinguishing high-rank and low-rank environments.

Finalising:

- the presented model is a wideband 2D one from the BS viewpoint , also accounting for Doppler;
- it computes CIR through simulations;
- it is based on distributions of scatterers' spatial positioning, distant reflectors, LoS and shadowing effects; scatterers can produce either specular reflection or scattering;
- path loss attenuation exponent depends on scattering behaviour;
- a broad number of environments is covered with this model; typical values are suggested for the different environments, including (non) LoS variants and high/low rank channels.

It is indicated how scatterers are included in or discarded from an influence region moving along with an MT. It is not explicit, though, how this is consistent with a non-uniform scatterer distribution.

2.2.14 Combined GBSB and GWSSUS Model

The model approach proposed by Piechocki and Tsoulos [PiTs99] for the simulation of a directional channel makes use of combined characteristics between GBSB and GWSSUS models. The GBSB model does not provide information about the temporal evolution of the CIR, hence, consecutive snapshots of the channel are assumed uncorrelated, which is unrealistic. As for the GWSSUS, it is totally dependent on measured data. The combination of these two models takes place by considering a GBSB model consisting of clusters instead of discrete scatterers; these clusters will satisfy GWSSUS assumptions. Within the assumption of a moving MT, Doppler spectrum is analysed.

The cluster spatial distribution assumptions are such that clusters are fixed in space according to a uniform distribution. During MT motion, the scattering influence region will move along with it and so new multipath components will be added and others will be discarded, therefore, the number of multipath components will vary with time. The authors prove that this number is Poisson distributed. Also the statistics for the multipath components lifetime is

derived. The AoA statistics are presented in order to derive the channel angle spread.

This model can simulate different type of environments, and so the authors present some suggestions for the respective simulation (Macro-cell Urban, Bad Urban, Suburban and Micro-cell Urban). The presence of LoS will depend on the particular environment. Since the model is driven by GBSB assumptions, the channel characteristics of delay spread, angle spread and correlation functions remain the same as the original model.

To conclude:

- the model is wideband 2D from the BS viewpoint (extendable for the MT), also accounting for Doppler;
- it computes CIR through simulations;
- it depends on the distributions for cluster spatial positioning (uniform) and for cluster angle of arrival (Gaussian);
- dependence on path loss is mentioned;
- LoS considerations are made;
- it can cover several types of environments; simulation suggestions are made for those.

2.3 Modelling options

In this work it is intended to develop and implement a directional model, which is to be conditioned by a certain number of specifications. Naturally, models already developed by other authors, which were presented herein, will serve as background to build this model. From the intended specifications, the final start-up models will be derived.

The purpose of the model to be built is simulation, more precisely the evaluation of typical micro-cell environments. The target-system for the model is UMTS, therefore, wideband analysis must be possible. Summarising, the model shall be a micro-cell wideband directional simulation model. For the simulations, a non-deterministic modelling approach is preferable, for it can be considered for system evaluation in general terms and for performing its assessment in general scenarios, instead of a particularly well-defined situation.

The GBSBEM is a model that fulfils these first requirements, and will therefore be used. Although the model only accounts for specular reflections, and more precisely single reflections, other phenomena can be implicitly accounted for by modifying the scattering coefficients. However, the concept of isolated scatterers will also be changed. The additional proposal is to substitute single scatterers by clusters comprising a group of scatterers. This is motivated by two facts. On one hand, measurement campaigns have detected signals arriving in clusters from a certain direction [KLTH00]. On the other hand, as scatterers within each cluster will fall below system resolution, this allows for the simulation of short-term fading while keeping the correlation between consecutive time samples. The use of clusters is also supported by the Elliptical Sub-regions Model and by the Combined GWSSUS and GBSB Model.

Once more, it should be stated that for an efficient use of simulations, a good compromise between precision and complexity must be achieved. This is also one of the targets of the model to be built.

Chapter 3

Model Implementation

This chapter regards implementation issues. The proposed model is described, the simulation model programme functioning is explained and model results are assessed.

3.1 Model Description

As mentioned in the previous chapter, the model proposed in this work is based on the GBSBEM Model, with additional support from two other models: the Elliptical Sub-regions Model and the Combined GBSB and GWSSUS Model.

The model is proposed for a micro-cell environment. In this case it is assumed that the BS is below rooftop level. From the micro-cell environment, a particular operational environment will be chosen, leading to a simplification of the problem: the LoS street operational environment considers both BS and MT positioned along the same street.

From the geometrical bases of the model, it is considered that scatterers are placed according to a chosen PDF within a certain region. The resulting signal is calculated assuming that each scatterer, being an omnidirectional re-radiating element, produces single specular reflection between BS and MT. In agreement with the operational environment to be studied, and also the GBSBEM Model, the scattering region will be an ellipse, whose foci are BS and MT, assuming that a similar environment is seen from BS and MT viewpoints. The elliptical scattering region size will be dimensioned according to the street width. This means that the maximum delay t_{max} will decrease in opposition to the distance between BS and MT. For this environment, also the LoS path will be accounted for.

This being a 2D model, one of the inherent limitations comes from the fact that all scatterers and incoming waves are assumed to be at the horizontal level; therefore, although scatterers do not block each other's signal, as if they were positioned at different heights, no additional delay is included from this difference. Another considered assumption is that BS and MT are aligned at the centre of the street, which obviously simplifies the positioning of the ellipse within it.

Instead of considering isolated scatterers, these will be grouped into clusters, as considered in both the Elliptical Sub-regions Model and in the Combined GBSB and GWSSUS Model, which shows more consistency with reported measurement campaigns [KLTH00]. Signals resulting from scatterers within the same cluster will fall below angular and temporal resolution;

therefore, with this option, the correlation between consecutive time/space samples in short-term fading, which is expected to exist in real environments, will naturally be kept. The resolution limitation will also lead to the same ToA and AoA resulting statistics as for the original GBSBEM case. Note that these statistics are independent of the clustering density, for they assume a continuous scattering PDF. However, when performing simulations, cluster density will be a parameter to take into account.

Clusters will be uniformly distributed within the scattering region, as suggested for isolated scatterers in GBSB models. This is a reasonable approach for a simulation model where displacement of the MT is to be considered. When the MT is displaced, the region shape will change, and therefore some scatterers will be added to the new region, while others are discarded. If the environment is supposed stationary, with a uniform distribution of scatterers, their positioning may be reused in consecutive displacements of the MT, only changing the region boundaries, which would not be possible in any other distribution. The possible disadvantage of uniform distribution is that it yields to an abrupt signal power variation at the maximum delay.

For the distribution of scatterers within a cluster, a Gaussian distribution was chosen. The same standard deviation will be used in both axes, which means cluster orientation will not be differentiated. The number of scatterers in each cluster is Poisson distributed, as in the Elliptical Sub-regions Model.

GBSBEM considers scatterers with a reflection coefficient whose magnitude is fixed and equal for all scatterers, and only the phase is random. In the proposed model, reflection coefficients are random variables both in magnitude and phase, assumed uniformly distributed within the intervals [0, 1] and [0, 2π[, respectively. In this way, the ambiguity regarding the reflecting materials and angles of incidence is added. This is also a way of, implicitly, considering other scattering phenomena besides specular reflection. These reflection coefficients are kept fixed for any position of the MT. This is a simplification, for it is known that in real physical environments these coefficients change according to the incidence angle (magnitude close to unity in grazing incidences, smaller magnitude in perpendicular incidences), thus, depending on MT position. However, as no particular orientation is considered for the clusters, it is not meaningful to vary the reflection coefficients, and so the values obtained from the random distribution can be considered as mean ones.

Figure 3.1 represents an example of the operational environment and the resulting

scatterers positioning. The elliptical scattering region for a particular MT position is also represented. As proposed, the groups of scatterers (*i.e.*, clusters) present a uniform distribution, that is, the expected cluster density is constant along the whole street both in length and width. Each cluster has a larger density of scatterers in the centre, as it is the case in Gaussian distributions. Some exemplifying signal paths are also represented in the picture.

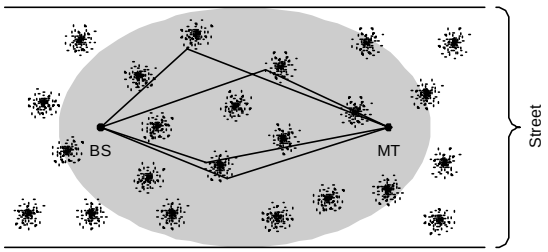

Figure 3.1 – Spatial distribution of scatterers within a street.

It is known that in micro-cell environments the street guiding effect is important, namely through multiple-reflections along the street. However, the chosen model assumptions only account for single reflections. One way to overcome this limitation in a simple way is to consider an effective street width, emulating multiple specular reflections through longer distanced single reflections, as in geometric optics methods. In this way, longer delays are considered in the simulations for the same physical environment, compensating for the longer spread delays and angles that characterise such effect.

The model will also encompass signal Doppler shifts in each path, for the cases where the MT has an associated velocity. Due to the operational environment chosen, it is assumed that the MT moves along the street length, parallel to it.

In order to account for temporal and angular finite resolution, after the calculation of every signal component, components within the same delay and angle slot are coherently summed. The sizes of these delay and angle slots correspond to the intended delay resolution Dt and azimuth angle resolution Dj. In this process, signal components below a desired noise margin are discarded. This "filtering" process is exemplified in Figure 3.2.

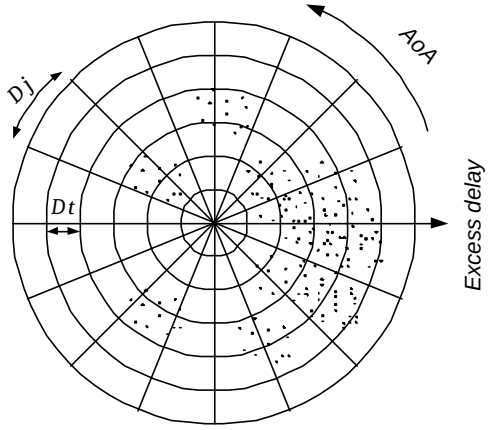

Figure 3.2 – Signal resolution limitation.

The model is generic for any frequency; thus, statistics of AoA and ToA are assumed to be equal, for example, for both up- and down-links from an FDD connection in UMTS. However, some difference is expected to occur in terms of scattering in different frequencies, thus, in different UMTS channels. Scattering coefficients will most likely not vary significantly in terms of magnitude, but relevantly will in terms of phase. To account for this, scatterers will be given different random phases for the two links of an FDD connection.

For a better overview of the proposed model, Table 3.1 summarises all its aspects and parameters. These parameters concern scatterer and cluster specific properties, and also generic properties like path loss exponent and Doppler shift. Some parameters are fixed for any implementation of the model, while others can be chosen at each simulation process, and in that case are identified as "simulation dependent". This is the case for every numerical value (*e.g.*, cluster density).

As this is a model with statistical assumptions for scattering, its analysis should be performed by means of the Monte-Carlo method, that is, deriving global results from multiple consecutive simulations.

scattering region	shape		ellipse (2D)
	foci		BS and MT
	delay limit		(effective) street width
clusters	distribution		2D-Uniform
	range		scattering region
	density		simulation dependent
scatterers within cluster	distribution		Gaussian
	standard deviation (cluster half-size)		simulation dependent
	no. of scatterers per cluster	distribution	Poisson
		average	simulation dependent
scattering coefficients	magnitude	distribution	Uniform
		range	[0, 1]
	phase	distribution	Uniform
		range	[0, 2π[
path loss exponent			simulation dependent
LoS path			present
Doppler shift			accounted for
MT velocity			simulation dependent
delay resolution			simulation dependent
angle resolution			simulation dependent
noise margin			simulation dependent

Table 3.1 – Characterisation of the proposed model.

3.2 Programming

The proposed model has been implemented in C programming language and prepared for performing simulations and deriving parameters resulting from a group of simulations. Each simulation process is performed as represented in the flowchart in Figure 3.3.

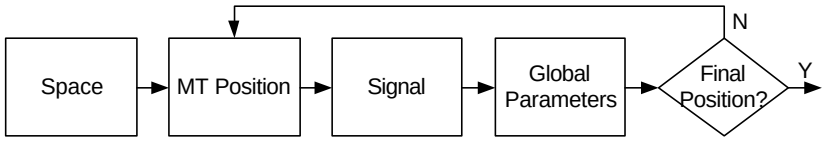

Figure 3.3 – Simulation flowchart.

In the beginning of every simulation, a new space of scatterers is generated according to the parameters set in Table 3.1, as represented in the flowchart in Figure 3.4. This space is then used to calculate the resulting signal arriving to the BS at every MT position along the street[10]. From the resulting signal, global parameters are derived.

The space generation is performed twofold. In an outer cycle, a subspace of clusters centres is generated (2D uniformly). To guaranty equal proportion in both dimensions (street length and width), XY positions are generated within a square containing the whole street. For this, X and Y positions are generated independently (and thus uncorrelated) according to a uniform distribution. The inner cycle generates the final scatterer positions around the original cluster centre, after which the centre point is discarded. The standard deviation of the Gaussian clusters is equal in both dimensions, as previously mentioned. While scatterer positions are generated, also their complex scattering coefficients are randomly generated.

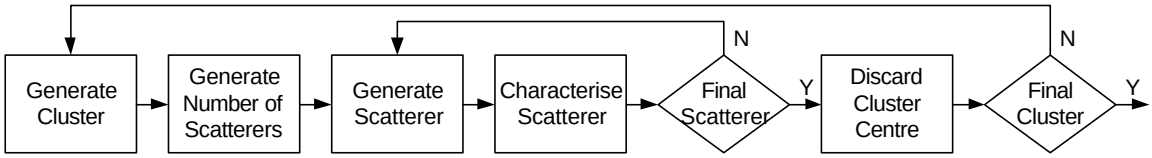

Figure 3.4 – Space generation flowchart.

All the random generators used were extracted from [PTVF92]. All of the non-uniform generators (Gaussian and Poisson) are based on a uniform one, which can be chosen from several ones with different computational complexity and robustness. "ran1" was chosen because, according to the authors, no statistical test is known to fail with it. It allows for the use of the same *seed* for every of the used random variables and for a group of consecutive simulations, because consecutive sequences of samples generated with this function are still

[10] As it was earlier stated, in the chosen operational environment, the signal arriving to the BS is in statistical terms equal to the one arriving at the MT, and so only one direction needs to be analysed in terms of global parameters.

uncorrelated. This uncorrelation is guaranteed for a number of samples up to 10^8, which is an acceptable threshold for this problem. This threshold is of the same order of magnitude of an area with 1 km length, a cluster density of 10^{-2} m^{-2} and 20 scatterers per cluster, which is a reasonable limit for a simulation environment. A limitation from the used uniform random generator is the fact that the boundary values are never reached. This means that the scattering coefficients proposed will in fact have uniform magnitudes and phases within]0, 1[and]0, 2π[, which presents no problem.

Signal calculation is sketched in Figure 3.5. After calculating the LoS path signal, to calculate the scattered signals each scatterer position is analysed to check if it is contained within the current scattering region. If so, the signal resulting from that scatterer is calculated. Calculating each signal involves the computation of magnitude, phase shift (resulting from the path length, the scattering coefficient and the Doppler shift), excess delay and AoA. The path loss exponent is set to 2. After obtaining every signal component, the resulting signal is then filtered to cope with system resolution limitation. The noise level is set at –120 dBm, assuming a transmitted power of 1 W (30 dBm).

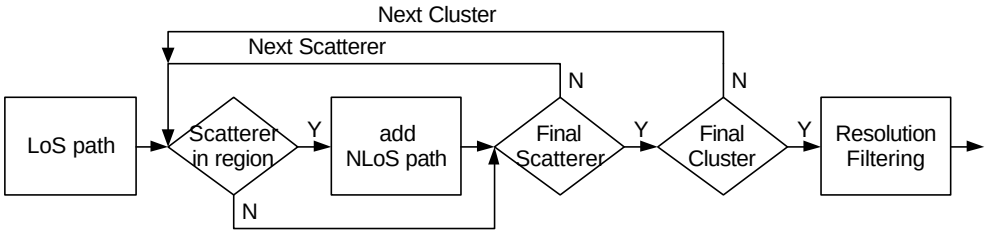

Figure 3.5 – Signal calculation flowchart.

The Monte-Carlo analysis is to be made for sets of 100 simulations, which provides a reasonable compromise between result averaging and simulation time. To conclude the analysis, the global parameters calculated in each simulation are used to derive average values and its standard deviation, which will be used for the model assessment and later for the model analysis. The calculated global parameters are the Rice factor, average delay, 90% power delay window, delay spread and azimuth angle spread.

3.3 Assessment

3.3.1 Parameters Influence

As can be seen in Table 3.1, there is a group of parameters which can vary in each simulation in order to satisfy more specific environment characteristics. From those, two have already been set as fixed in the previous subsection: path loss exponent will be set to 2 and the noise margin will be –120 dBm for a transmitted power of 1 W. This subsection intends to study the influence of the remaining input parameters in terms of the resulting global parameters. For this study, frequency will be set to the centre frequency of the lower up-link FDD channel, which is 1922.5 MHz [Fern99]. Delay and angle resolution are also set fixed to 65.1 ns (one fourth of the chip time) and 1º, respectively. The influence of frequency will be studied in a subsequent subsection. The influence of delay resolution is also evaluated in the subsequent chapter.

The input parameters to study here are cluster density, cluster standard deviation, average number of scatterers per cluster, MT velocity and street width. These parameters will be evaluated in terms of resulting delay and angle spread along BS-MT distance, for averaged results over 100 simulations. The ranges of values chosen for the parameters are represented in Table 3.2. The values tested for BS-MT distance are also contained in this table.

Parameter	Minimum	Maximum	Step Size
cluster density [m^{-2}]	0.005	0.020	0.005
cluster standard deviation [m]	0.5	2	0.5
average number of scatterers per cluster	10	40	10
MT velocity [ms^{-1}]	0	30	10
street width [m]	10	40	10
BS-MT distance [m]	20	160	20

Table 3.2 – Input parameters variation ranges.

The chosen values try to be consistent with the physical reality observed. The ones for MT velocity correspond to values up to 108 km/h, which largely overcomes speed limit allowed

within a city. The cluster standard deviation range is in agreement with possible signal scatterers like persons, cars and trees. The cluster densities encompass low to high traffic flow or tree density. The average numbers of scatterers are sufficiently large to apply the central limit theorem and to assume cluster fading. The values for cluster size and density and number of scatterers are also consistent with the ones reported in [PiTs99]. The simulation results are depicted in the following figures (Figure 3.6 to Figure 3.10). The simulations were performed varying only one parameter at a time, while all the others were kept at the minimum value.

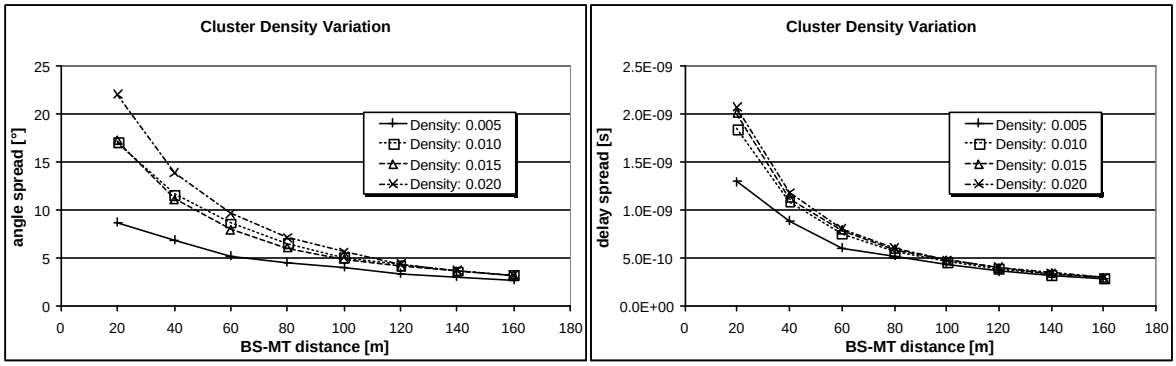

Figure 3.6 – Angle and delay spread behaviour with cluster density variation.

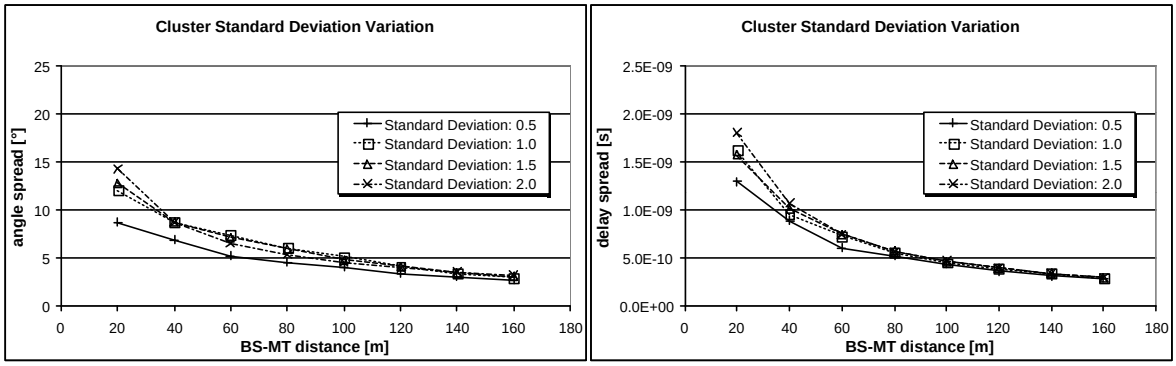

Figure 3.7 – Angle and delay spread behaviour with cluster standard deviation variation.

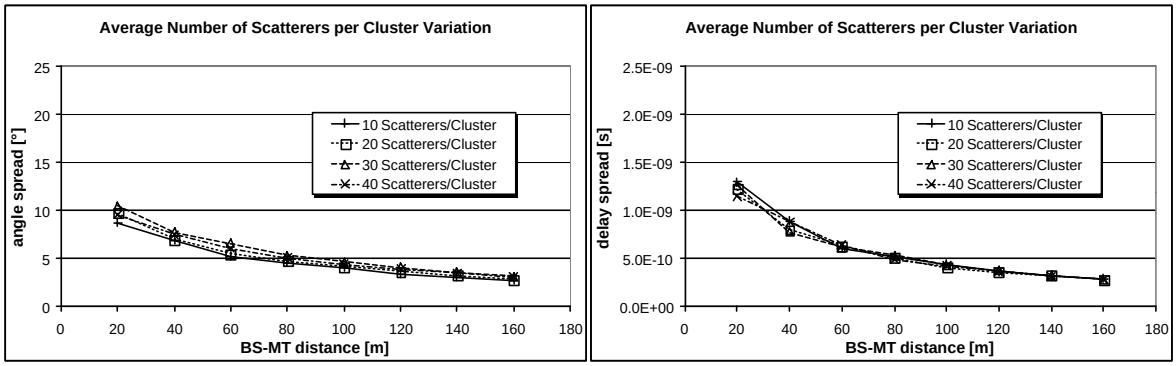

Figure 3.8 – Angle and delay spread behaviour with average number of scatterers per cluster variation.

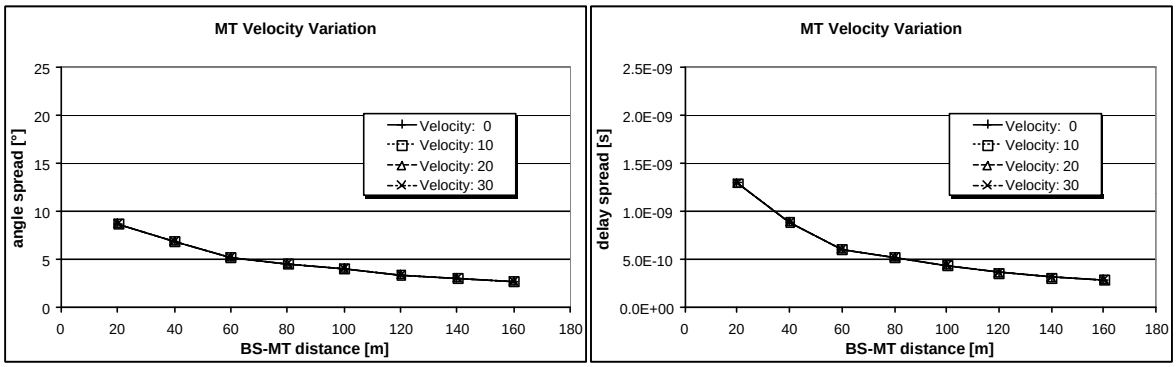

Figure 3.9 – Angle and delay spread behaviour with MT velocity variation.

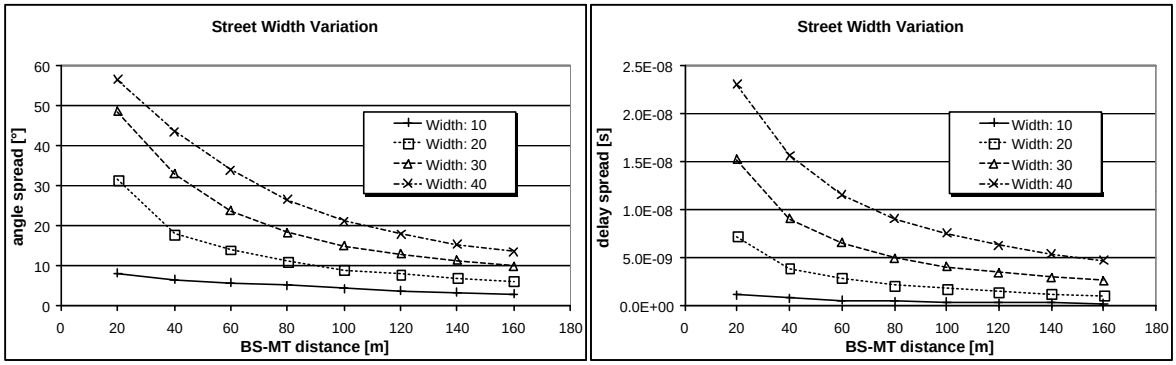

Figure 3.10 – Angle and delay spread behaviour with street width variation.

Analysing the results contained in the graphics above, it can be seen that, for both angle and delay spread, the most affecting input parameter is street width. In fact, comparing its influence with the second most influencing parameter (cluster density), it is an order of magnitude higher in terms of delay spread and roughly 2.5 times in terms of angle spread.

Comparing cluster density influence with cluster standard deviation, it is comparatively more influencing on angle spread than street width is: angles spread variations have a ratio of 2 and delay spread variation ratio is 1.5.

The output parameters show a slight variation with the number of scatterers per cluster, but there is no particular trend in, thus in average terms it can be considered that this parameter does not influence angle and delay spreads. Yet, it is expected to influence the total amount of power received.

MT velocity, as would be expected, does not influence angle and delay spread.

As angle and delay spreads decrease with BS-MT distance, the influence of all the analysed parameters tends to dissipate with it.

Being the street width the most influencing parameter, it can be used for coarse or more rapidly tuning the model, while the parameters regarding clusters and scatterers can be used for a finer tuning and also to tune the total amount of power received. A list of the values chosen for the input parameters is presented in Table 3.3.

Parameter	Value
cluster density [m^{-2}]	0.01
cluster standard deviation [m]	1
average number of scatterers per cluster	20

Table 3.3 – Input parameter chosen values.

3.3.2 Comparison with measurements

The theoretical model proposed is not a purely measurement-based model. Nevertheless, a measurement campaign is essential to assess it, validating the options taken while choosing parameter values. The input parameters used for the model cannot be deduced directly from measurements. Instead, resulting global parameters are extracted from these measurements and compared with the same parameters extracted from simulations of the theoretical model. As the model has a statistical behaviour, it is not expected to have simulation and measurement results matching completely. Alternatively, one should look for the matching of the measurements with the statistical behaviour of the model; that is to say, by comparing the global parameters' average and standard deviation by means of Monte-Carlo simulations.

Although a measurement campaign was foreseen in this work, its results were not obtained in time to include in this thesis. Therefore, the assessment of the model through comparison with measurements was performed resorting to measurement campaigns reported in literature. One particular campaign described in [PLNR99] was chosen for this purpose; it contains a fairly complete description of the measurement process and one of the measured streets matches quite reasonably the operational environment of the proposed model.

The measurements from [PLNR99] were performed through a 200 MHz channel sounder at a centre frequency of 2.1 GHz. The measurement bandwidth was 50 MHz (delay resolution of 20 ns). Measurements were performed at 30 km/h, at a sampling of 5 Hz, which corresponds to

a distance step of 1.67 m. The measurement subset chosen used a receiver (which can be seen here as the BS) at lamp-post level (2.3 m) and a transmitter (MT) at a car roof. According to the map, the route chosen had BS-MT distances from 20 to 280 m, at an approximately 10 m wide street. The receiver (BS) antenna was a ULA with measurable angles of ±60º relative to boresight, which, according to the report's map, is shifted 45º relative to the street axis. Results shown are the 50 percentile of the Cumulative Distribution Function (CDF) for both angle spread (14.5º) and delay spread (16 ns).

In order to compare the proposed model with the measurements, an equivalent scenario was derived into the model simulations. The antenna receiving angle limitation was also included, but without including any additional antenna radiation pattern. An angle resolution of 1º was chosen. The resulting CDF of angle and delay spread was then compared with the 50 percentile values extracted from the measurements.

From a first analysis, it was concluded that for a 10 m street width simulation, delay and angle spread were much lower than the ones measured. The conclusion reached from this analysis was that, as previously suggested, multiple reflections are indeed important and thus the concept of *effective* street width must be considered. Therefore, in order to tune the model, an effective street ratio should be derived from the comparison with measurements.

Several simulation processes were run in order to obtain a best match, which was achieved with a ratio of 6.5 (*i.e.*, an effective street width of 65 m). Figure 3.11 represents the results obtained for this case. The graphics represent the CDF for the average results of angle and delay spread, and for average ± standard deviation. It should be noted that, assuming that Monte-Carlo simulations behave as a Gaussian process, the use of these standard deviation boundaries correspond to a 68% confidence interval.

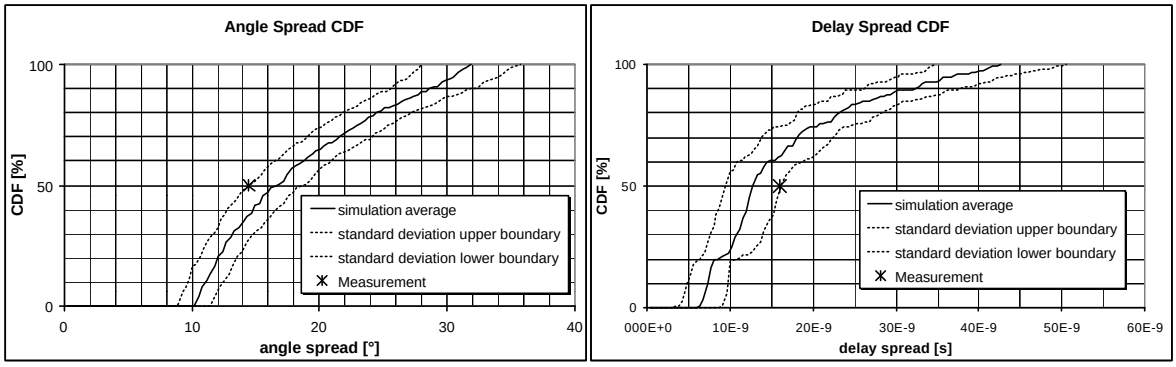

Figure 3.11 – Comparison with measurements: angle and delay spread CDF for an effective street width of 65 m.

From the results obtained, it can be said that, on average, the first 6.5 multiple reflections at a street are important in terms of angle and delay spread accounting, although in terms of cumulative power they may be despised.

3.3.3 UL / DL behaviour

It is intended with this subsection to perform some considerations about the correlation between up-link (UL) and down-link (DL) in FDD. This information will be important while using adaptive antennas, for, in some cases, up-link information can be used to derive down-link beamforming. As it is known, in UMTS TDD the same band is to be used for both up- and down-links, and in that case, if stationarity is maintained in between up- and down-link time-slots, correlation is total, although interferers may vary from one link direction to the other. However, in FDD two different sub-bands are used. Therefore, a correlation analysis should be performed.

The proposed model assumes scattering coefficients with random phase rotation between UL and DL. If resolution were not finite, meaning an infinite bandwidth, correlation would be fully kept. As this is not the case, some decorrelation between the two link directions is expected to exist. To analyse this, single simulations were performed, maintaining the environment from last subsection. The lowest FDD pair was analysed, *i.e.*, UL and DL channels whose centre frequencies are 1922.5 and 2112.5 MHz, respectively. Results for angle and delay spread were obtained for BS-MT distance steps of 20 m. Several values of delay and angle resolutions were used, in order to evaluate their influence (delay resolution: 10 ns, 20 ns, 40 ns; angle resolution: 1º, 2º, 4º). The following figures (Figure 3.12 to Figure 3.16) represent the results obtained. Although a deeper study would have to be performed, in order to derive a consistent expression for correlation dependence as a function of resolution, it can anyhow be stated that correlation indeed depends on the resolution used for both angle and delay.

Looking at the depicted graphics, it can be seen that for the resolution values presented, a coherent trendline can still be seen. However, although correlation is naturally not total (it would mean a 45º trendline slope), it indeed exists.

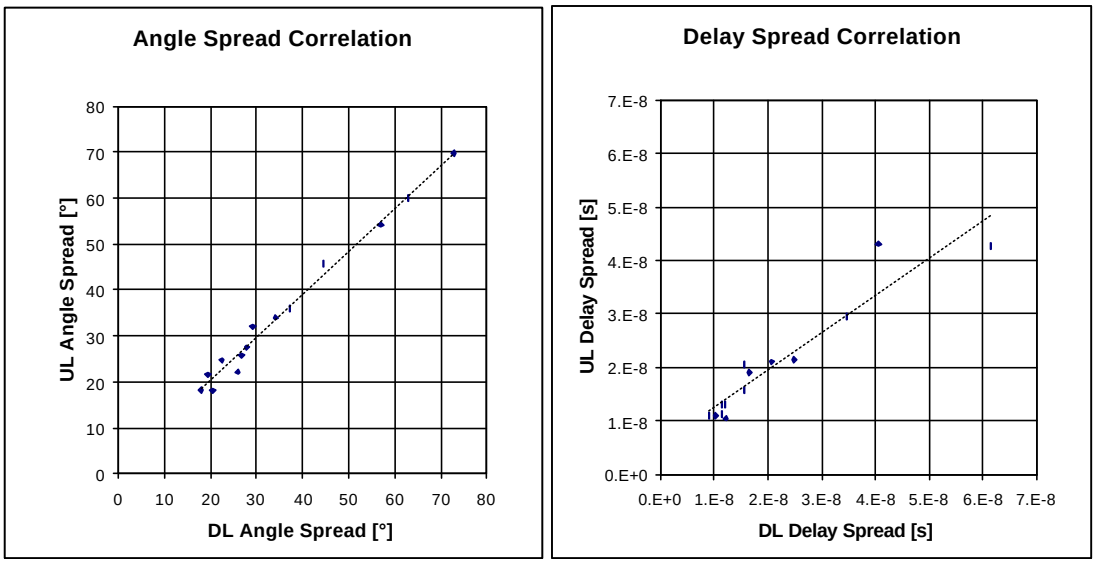

Figure 3.12 – Correlation analysis; angle resolution = 1º; delay resolution = 10 ns.

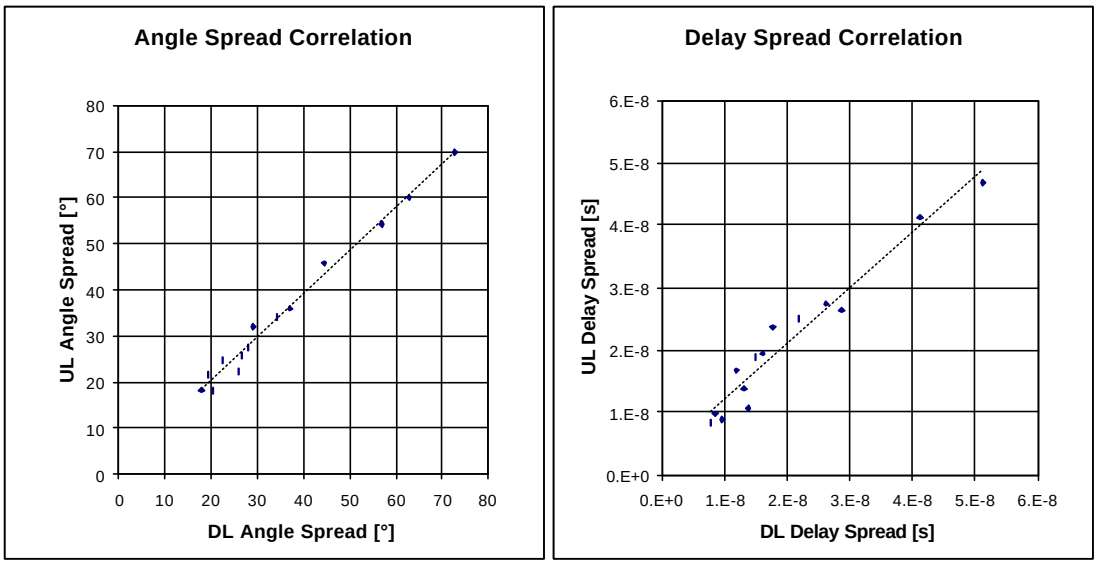

Figure 3.13 – Correlation analysis; angle resolution = 1º; delay resolution = 20 ns.

For the delay spread correlation, when varying the delay quantisation, the variation of the trendline slope is not straightforward (for an increasing quantisation value it decreases and increases); when varying the angle quantisation, the slope variation is smaller; in both cases the trendline does not cross the plot origin. For the angle spread correlation it can be observed that, for the range of values analysed, variations are much smaller in comparison with the ones for the delay spread; moreover, the trendline roughly crosses the plot origin in all cases.

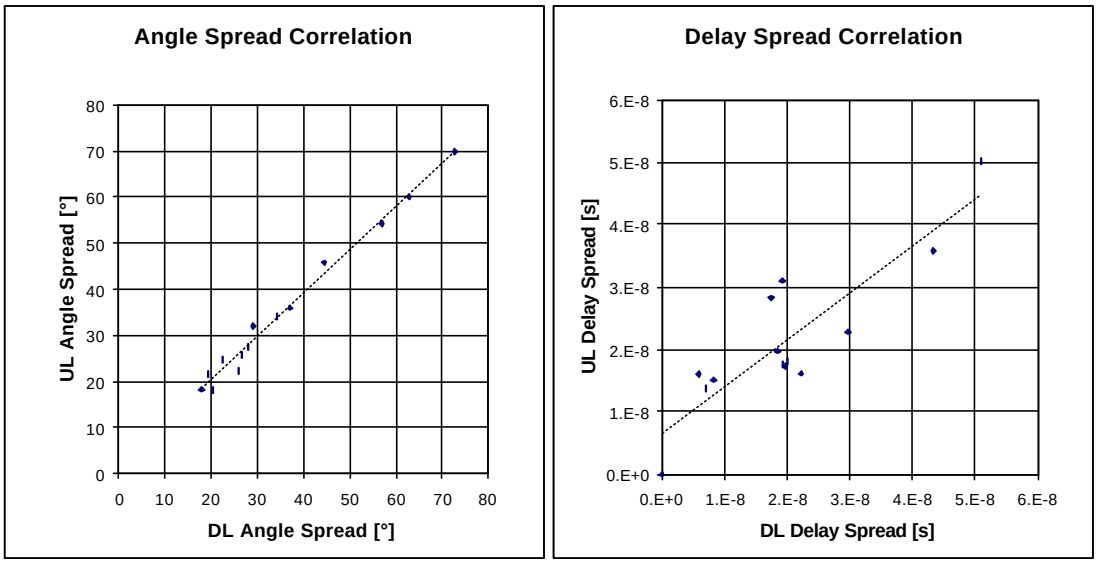

Figure 3.14 – Correlation analysis; angle resolution = 1º; delay resolution = 40 ns.

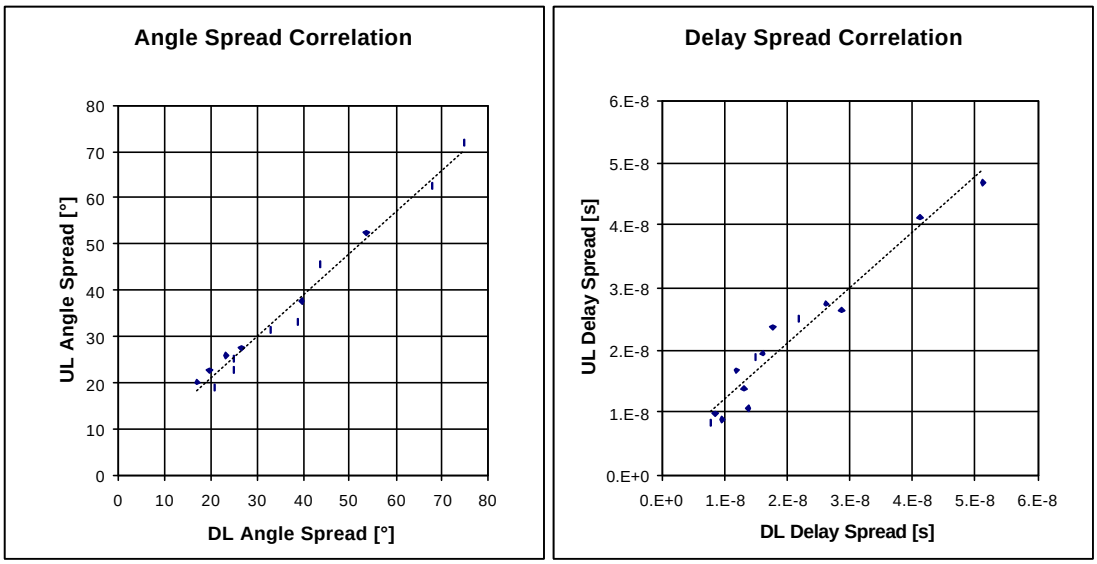

Figure 3.15 – Correlation analysis; angle resolution = 2º; delay resolution = 40 ns.

As some sort of conclusion, it can be said that, in general terms, delay spread correlation is more sensitive than angle spread correlation. Moreover, delay spread is more sensitive to delay resolution variation than to angle resolution variation.

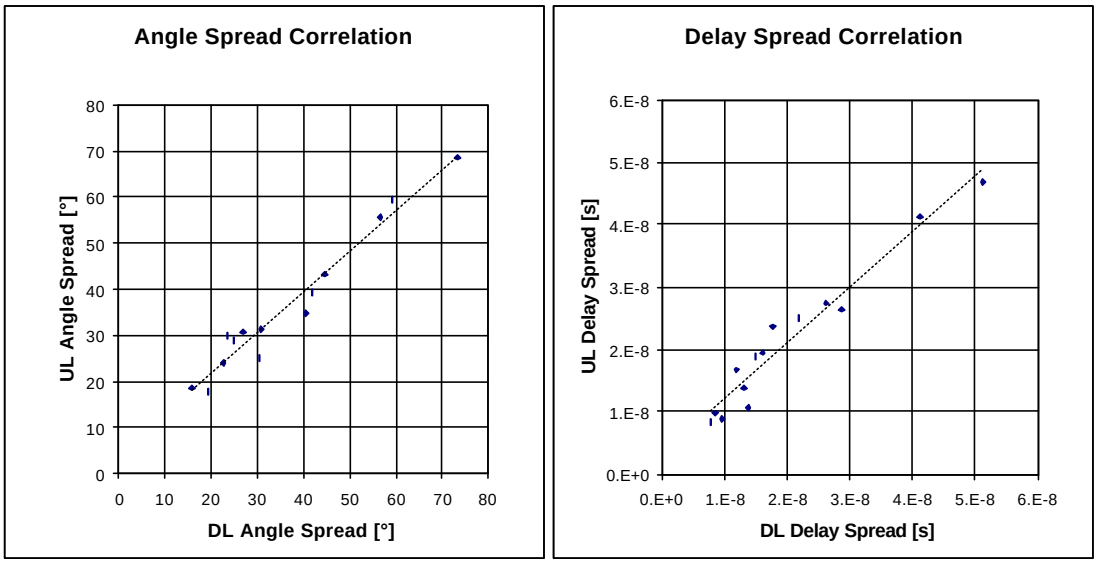

Figure 3.16 – Correlation analysis; angle resolution = 4º; delay resolution = 40 ns.

3.3.4 Model behaviour

In this chapter the proposed model's assumptions were explained in detail and justified. After its implementation, the influence of input parameters on output global parameters was analysed. The model was assessed by comparing it with measurements reported in literature, providing a general coarse tuning of the model, and frequency correlation was studied.

Although without direct results from a measurement campaign, which would allow for a more precise tuning of the model, the general tuning produced guarantees reasonable confidence in future results to be derived from the model in terms of global parameters and also in the global power variation with delay and angle, that is, in terms of directional impulse response. Therefore, the proposed model can and will be used for the analysis of the operational environment for which it was developed.

Chapter 4

Model Analysis

In this chapter, the proposed model is used to analyse the operational environment in terms of global output parameters and of directional channel impulse response, in order to derive conclusions about the use of adaptive antennas within UMTS. Typical examples are used for this study.

4.1 Scenarios and Simulations

The use of adaptive antennas in mobile communications, namely in UMTS, involves the behavioural study of the mobile channel in terms of delay and angle for the general environments (macro- micro. and pico-cells) and for the operational environments within. This can be achieved by performing simulations with a wideband directional channel model.

Simulations at a wideband directional channel model can be done with omnidirectional, directional and adaptive antennas, fulfilling different purposes. Using omnidirectional antennas naturally provides a comprehensive result on the incoming signal. Conclusions can be drawn about which type of antenna to use, and if it is expected to obtain improvements with a directional antenna or with an adaptive one; this type of simulation can serve as a comparison basis. Using directional antennas, and, in particular, realistic radiation patterns, makes it possible that the conclusions drawn from the omnidirectional case can be confirmed for static cases. Finally, the model can be used for link-level simulations, where an adaptive antenna is incorporated. Moreover, the model can then be used to simulate both the desired and interfering signals, therefore, it is important for the assessment of the used adaptive techniques.

Once the proposed model in this work has been assessed, it can be used to perform the simulations described above. The first type of simulations will be addressed here. A group of typical examples was chosen to represent the operational environment to which the model is associated (LoS street). These comprehend residential, non-residential, pedestrian and vehicular areas, with and without green areas. Four streets within the city of Lisbon were chosen:

- "Rua Gomes Leal": this street belongs to a residential neighbourhood of villas with a maximum of three stories high; it is approximately 5 m wide by 160 m long and has got no trees;
- "Rua do Ouro": this street belongs to a business area at downtown Lisbon; it is approximately 10 m wide by 650 m long and has also got no trees; both pedestrian and vehicular traffic exists;
- "Rua Augusta": this is a street parallel to "Rua do Ouro" at the same business area downtown Lisbon; it is approximately 15 m wide by 650 m long and has also got no

trees; it is a pedestrian street, where there are also esplanades along the centre;

- "Avenida da Liberdade": this is a traffic mainstream leading to the geographic centre of the city; it is approximately 80 m wide by 1350 m long, and it is mainly a vehicular street with some pedestrian flow; approximately half of the street width belongs to green areas positioned at each side of the street, also having some cafés with esplanades within those areas.

For the simulations, the same frequency was used as for Section 3.3.1, corresponding to the centre frequency of the first FDD UL channel. Scatterer and cluster parameters were kept the same for all the streets for two reasons. First, it was seen that, in terms of the global output parameters used to assess the model, the influence of those input parameters was not significant. Secondly, considering that those input parameters correspond to size and density of physical reality like trees, people and vehicles, on average terms these can be set as equal.

Simulations were performed along the four streets with three different set-ups:

1. BS-MT distances between 10 and 30 m with a step of 5 m for "Rua Gomes Leal", "Rua do Ouro" and "Rua Augusta";
2. BS-MT distances between 100 and 600 m with a step of 100 m for "Rua do Ouro" and "Rua Augusta";
3. BS-MT distances between 100 and 1000 m with a step of 100 m for "Avenida da Liberdade".

The first set-up intends to evaluate variations along a short distance scale; as the 3 streets have increasing widths from 5 to 15 m, it is possible to perform a comparison between them. The other two set-ups focus on longer distance scales; although "Avenida da Liberdade" is much wider than "Rua do Ouro" and "Rua Augusta", thus results being expected to be reasonably different, graphic comparison of these three streets (within set-ups 2) and 3)) will be performed using one common plot for each parameter.

The chosen angular resolution was 10º, while two different delay resolutions were analysed: 65.1 ns, corresponding to one fourth of the chip time, and 20 ns, corresponding to one thirteenth of the chip time.

4.2 Simulation Results

Results for the typical examples chosen were obtained from a set of 100 simulations. Two types of results were obtained: global output parameters and DCIR. These results were averaged over the 100 simulations. Also the standard deviation for spread parameters and for the DCIR was derived. As explained in the previous chapter, in each simulation the incoming signal is calculated from the previously positioned scatterers. Figure 3.1 depicts the scatterers positioning obtained for one simulation for "Rua Gomes Leal". The BS and MT positions for the simulation set-up used in this street are also marked.

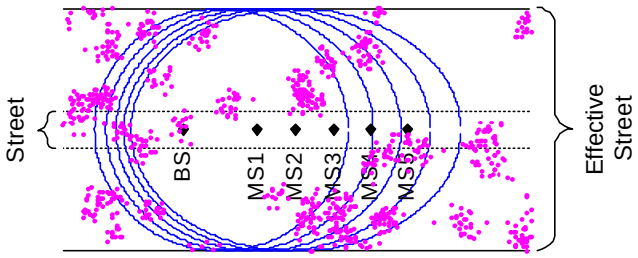

Figure 4.1 – Spatial distribution of scatterers within a street – simulation example.

The derived results can be divided into three groups: delay, angle and power parameters. Delay parameters encompass delay spread, average delay and 90% power delay window. Delay spread standard deviation was also calculated. Angle was studied according to the two angle spread metrics - standard and adimensional - referred to in Chapter 2. The standard deviation for these two metrics was also derived. For power considerations, Rice factor was calculated.

Results for 65.1 ns delay resolution are represented in this sub-section. Annex 1 contains equivalent results for a 20 ns delay resolution. For each parameter, two sets of plots are presented: one first plot depicts simulation set-up 1); a pair of plots depicts set-ups 2) and 3).

Delay Analysis

Figure 4.2 refers to the average result of the delay spread for a 65.1 ns delay resolution.

Figure A1.1 in Annex 1 refers to the same results for a 20 ns delay resolution.

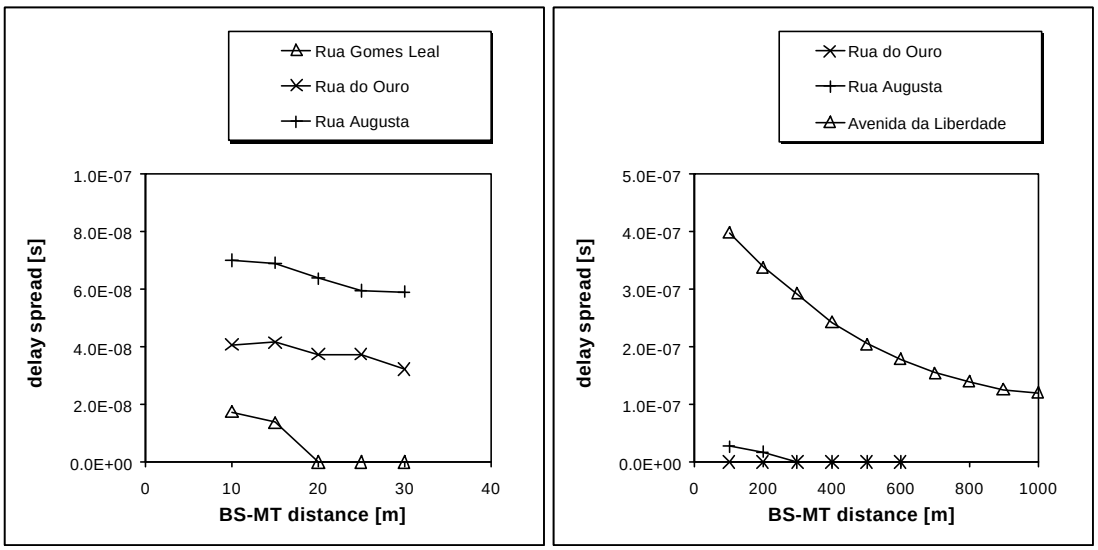

a) set-up 1). b) set-ups 2) and 3).

Figure 4.2 – Delay spread results.

The delay spread is directly related with the relative difference between signal component path lengths. Therefore, this parameter should be lager for wider streets and also for smaller distances between MT and BS. In fact, as can be seen from the graphics plotted for this parameter, it decreases with BS-MT distance increase, as it would be expected. Also the wider streets have larger delay spreads.

For the streets in set-ups 1) and 2), delay spread is in the order of magnitude of tens of ns. For these set-ups it reaches a value of zero for a BS-MT distance between 20 (for the narrowest street) and 300 m (for the widest street of these three); this occurs when all the signal components arrive within the same delay slot, or delay quantisation interval, which occurs earlier for narrower streets.

In the case of set-up 3) the street is much wider than the remaining examples, thus results are in the order of hundreds of ns. For this case the delay resolution limitation is never reached, and so results do not get to zero within the distances considered.

Analysing the results for 20 ns delay resolution, it can be seen that the global behaviour of the parameter is alike. However, the exact values obtained are different, because of the different quantisation error associated (half delay slot = 10 ns). The difference between values from the two cases comes within a range equal to the difference between their respective quantisation

errors. One consequence of this difference is the position where zero delay spread value is reached in each street. Obviously, for 20 ns delay resolution this value is only obtained for larger BS-MT distances.

Delay spread results are again plotted in Figure 4.3 (and in Figure A1.2 from Annex 1); in this case, not only average results, but also standard deviation boundaries are depicted. The solid lines regard average delays, while the dotted lines stand for the standard deviation boundaries. Streets within the plot can be distinguished through the associated colour.

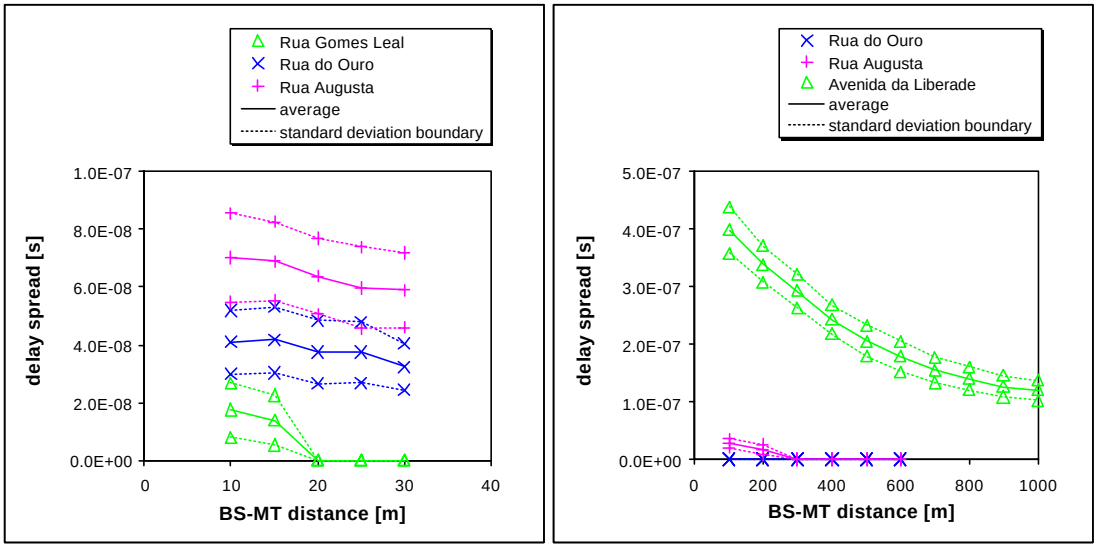

a) set-up 1). b) set-ups 2) and 3).

Figure 4.3 –Delay spread results (average values with standard deviation boundaries).

Analysing results for 65.1 ns delay resolution, delay spread standard deviation for set-ups 1) and 2) is roughly 10 ns; it shows a slight decrease when the average value decreases, becoming zero simultaneously with it (this means values from all 100 simulations are zero, thus, average and delay spread obtained from these results are also zero). For set-up 3), standard deviation is smaller than 40 ns. For 20 ns delay resolution, standard deviation is between 5 and 10 ns for set-ups 1) and 2), and smaller than 25 ns for set-up 3).

Considering that a Gaussian process can be assumed for the number of simulations used in the Monte-Carlo simulation method (100), the standard deviation boundary provides a 68% confidence interval for the results. From the graphics it can be seen that even in set-up 1) results are disjoint in almost every situation, therefore, the degree of certainty for the values obtained is high.

Figure 4.4 (and Figure A1.3 in Annex 1) refers to the average delay.

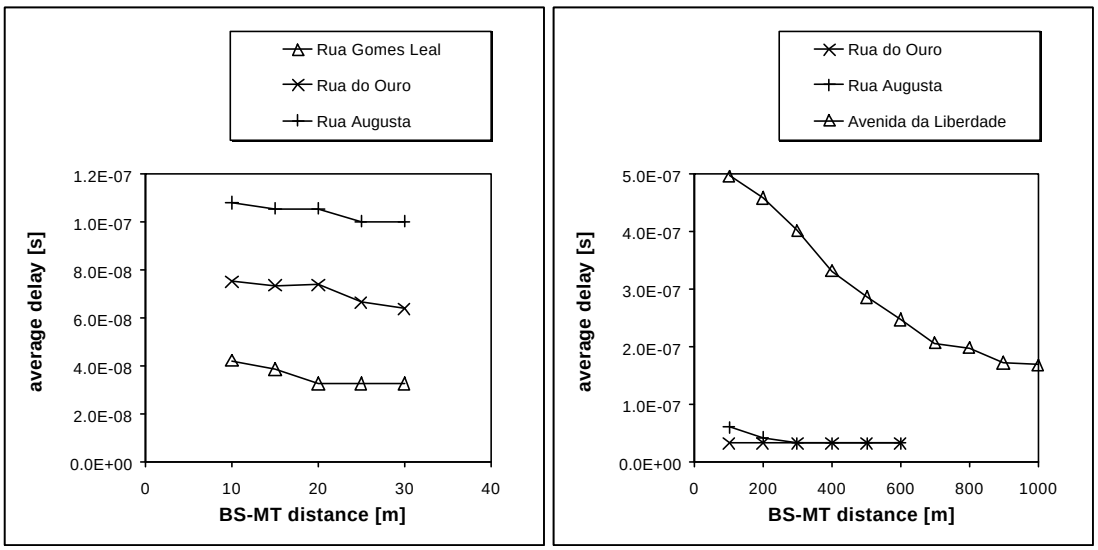

a) set-up 1). b) set-ups 2) and 3).

Figure 4.4 – Average delay results.

As the delay spread, average delay depends on the relative difference between signal component path lengths. Therefore, the same behaviour as delay spread is expected, that is, decreasing with BS-MT distance and being smaller for narrower streets. Its values are also of the same order of magnitude as for the delay spread, but slightly larger. Unlike the delay spread, values do not decrease until zero, and the minimum value is half of the quantisation interval, as can be seen for both resolutions.

This metric is naturally a complement to the delay spread one. For an ideal Gaussian process, these two metrics would be enough to characterise it.

Figure 4.5 (and Figure A1.4 from Annex 1) represents the 90% power delay window results.

The power delay window provides somehow a combination of the results of average delay and delay spread with a different power percentage. Continuing the assumption of a Gaussian process, an interval centred about the average delay with a half size equal to the delay spread corresponds roughly to a 68% floating power delay window; the double of this interval will correspond to a 95.5% one. Therefore it is expected that the values for the 90% power delay window have the same behaviour as the delay spread but having values between two and four times larger than it, which in fact happens for both resolutions. Due to the method used for its

calculation, the metric's minimum value is not zero, but half of the quantisation interval.

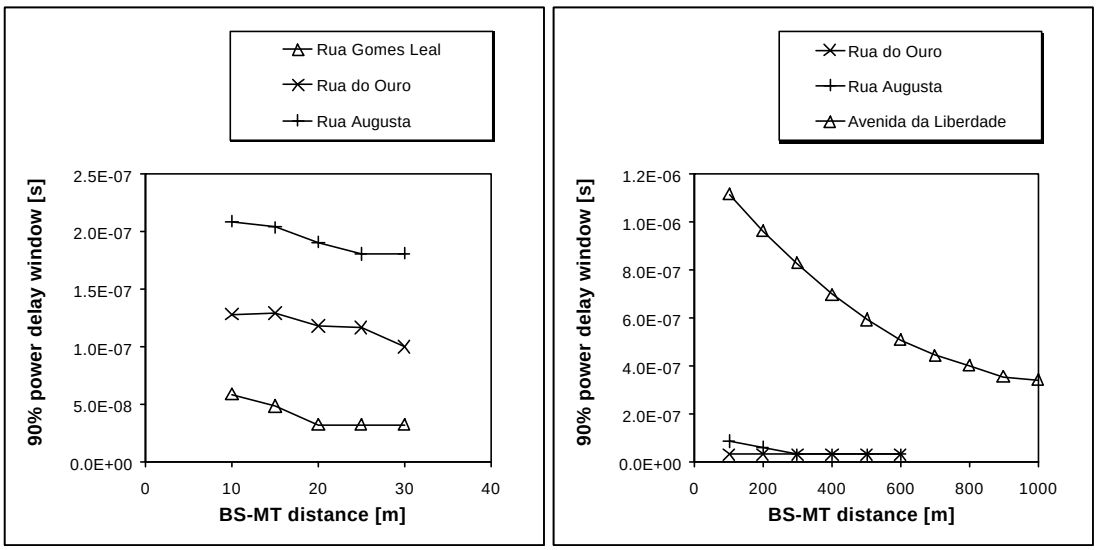

a) set-up 1). b) set-ups 2) and 3).

Figure 4.5 – 90% power delay window results.

Angle Analysis

Figure 4.6 (and Figure A1.5 in Annex 1) represents the average values for the standard angle spread metric. The standard deviation boundary of these results is plotted in Figure 4.7 (and Figure A1.6 in Annex 1).

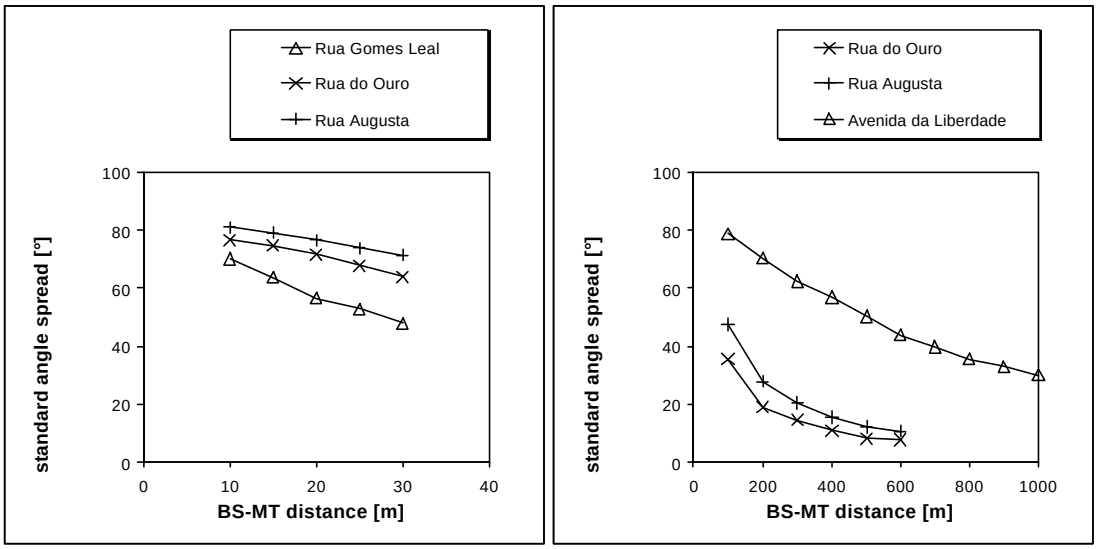

a) set-up 1). b) set-ups 2) and 3).

Figure 4.6 – Standard angle spread results.

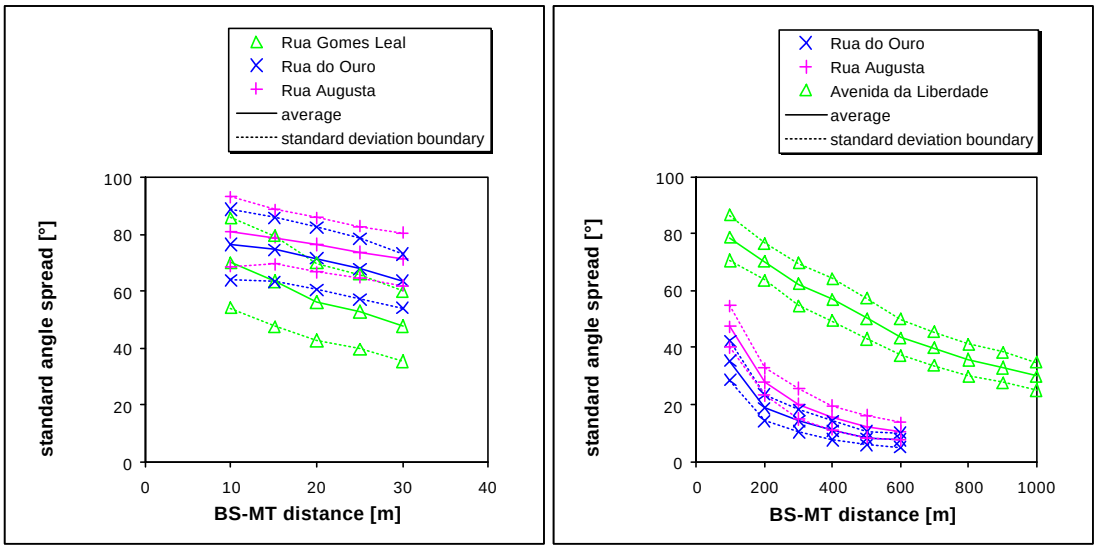

a) set-up 1). b) set-ups 2) and 3).

Figure 4.7 – Standard angle spread results (average values with standard deviation boundaries).

Angle spread, in a qualitative analysis, is expected to perform as the analysed delay parameters, decreasing with BS-MT distance and having smaller values for narrower streets. This is in fact what can be observed in the plots. For set- up 1) values between 80 and 40º are obtained, which are quite high values, denoting a low angular discrimination for the distances under consideration. Set-up 2) starts with values between 50 and 70º, but rapidly decreases for values close to 10º; the variation for higher distances decreases, as some sort of saturation; it should be noted that 10º corresponds to the angle resolution. Values for set-up 3) decrease from 80 to 30º with a nearly constant slope. Unlike for the delay spread case, angle spread never gets to be zero, which means there is always signal arriving from more than one angle slot.

As delay spread standard deviation, angle spread standard deviation also decreases with distance. However, the tolerance drawn from its boundaries is much higher, leading to a higher degree of uncertainty. The standard deviation values for set-up 1) are rather high, but this can be understood when looking at Figure 3.1. It can be seen that for this case the scattering region is almost circular, which necessarily derives a high angle spread. In such cases, the sensitivity to scatterer positioning will be high, thus the standard deviation results can be expected to be as obtained.

As would be expected, delay resolution does not affect angle spread global parameters, thus equal results are obtained for both delay resolutions.

The adimensional metric for the angle spread is represented in Figure 4.8 (and Figure A1.7

in Annex 1). Its standard deviation boundaries are derived in Figure 4.9 (and Figure A1.8 in Annex 1).

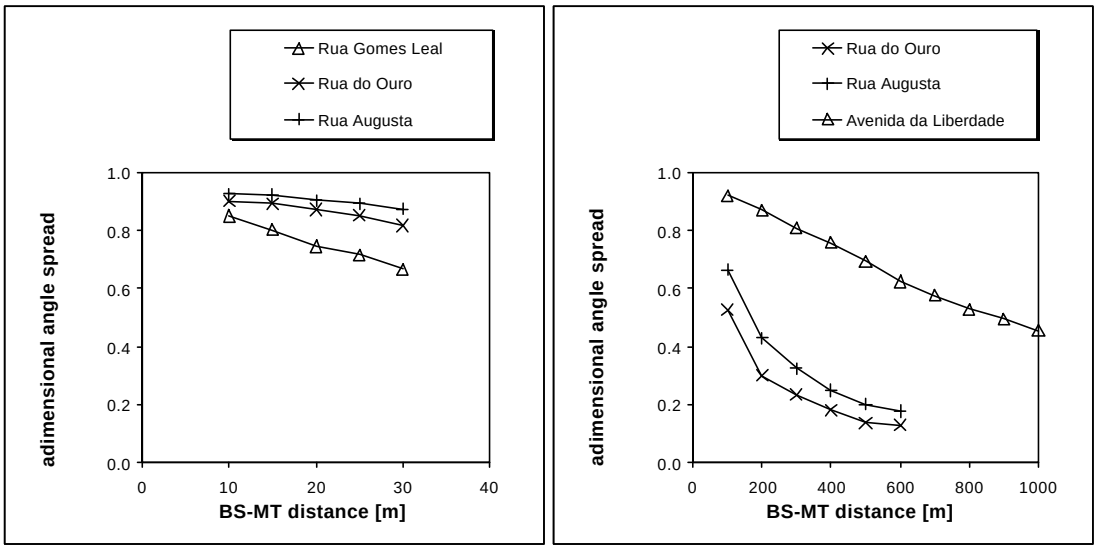

a) set-up 1). b) set-ups 2) and 3).

Figure 4.8 – Adimensional angle spread for results.

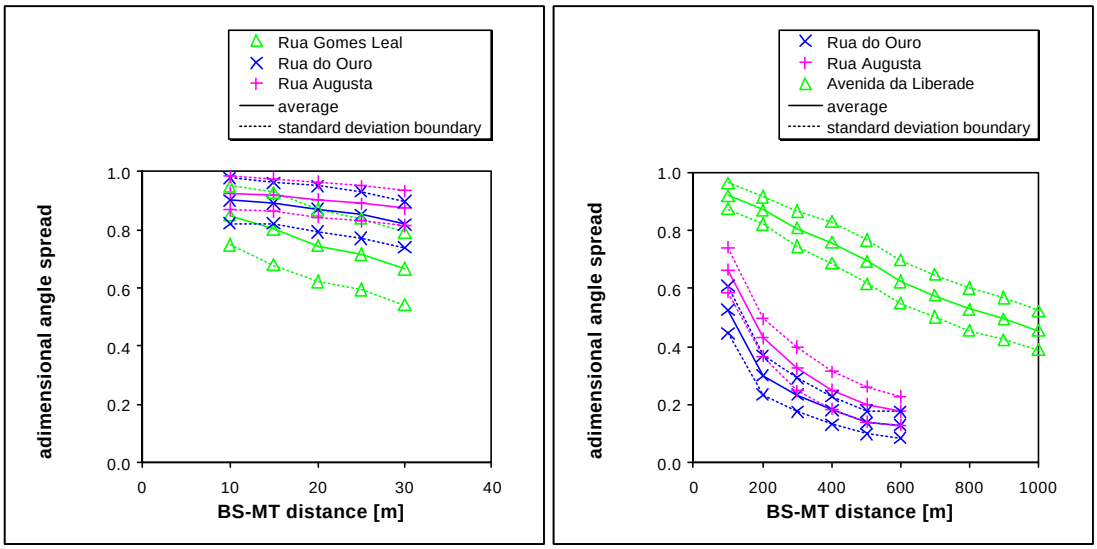

a) set-up 1). b) set-ups 2) and 3).

Figure 4.9 – Adimensional angle spread results (average values with standard deviation boundaries).

The generic analysis stated above for the standard angle spread can also be drawn from the adimensional metric, for the global behaviour is the same in both cases. However, the values obtained seem to be higher with the adimensional metric (values get close to 1, which is the maximum) than with the standard metric (the highest values are close to 90º). Although

according to [Egge00], the standard metric is expected to be less robust when the angle spread is high, which is the case, the contrary seems to happen in this case. An example quoted by [DuRa99] justifies this fact: the expression for the adimensional delay spread is derived for a theoretical situation where two discrete multipath components arrive at a receiver with a separation of j; for equal power components the result is $sin(j/2)$; as in the case of the proposed model multiple discrete signal components arrive at the receiver with random separation, high values are naturally expectable to obtain from the metric.

Power Analysis

The Rice factor obtained from the simulations is depicted in Figure 4.10 (and Figure A1.9 in Annex 1).

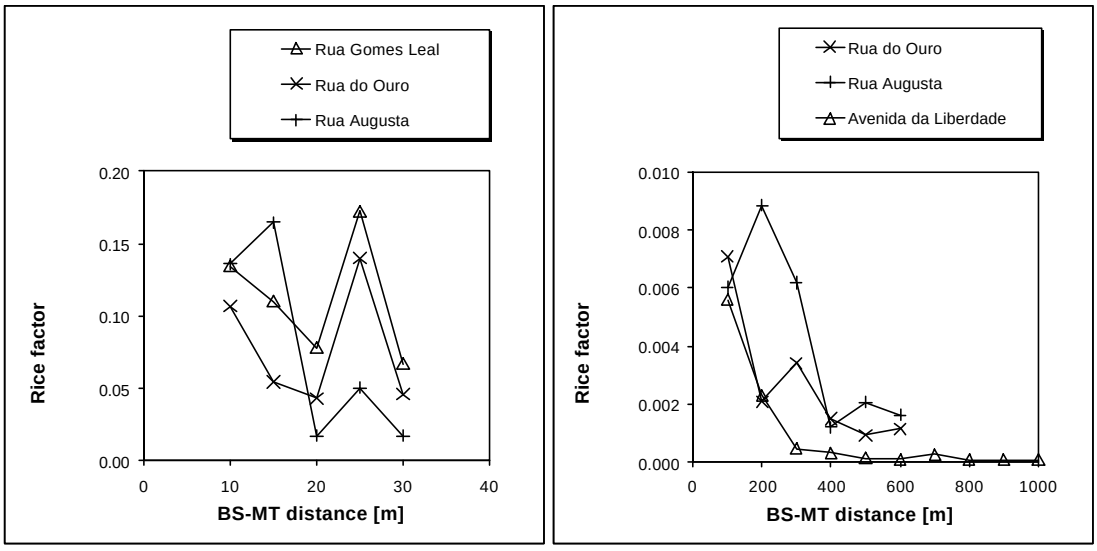

a) set-up 1). b) set-ups 2) and 3).

Figure 4.10 – Rice factor results.

As can be seen, very low values are obtained for this parameter. This is due to the fact that a large number of scatterers are included in the model, and therefore the relative importance of the LoS path becomes low with comparison to the scattered paths. Large oscillations of the parameter are observed for set-ups 1) and 2), while this is not observed at set-up 3). This should be due to certain sensitivity to scatterers relative positioning in the street. The robustness of set-up 3) to this phenomenon should be caused by the larger number of scatterers in this case, which are enough to provide the averaging effect. It should be remembered that the Rice factor is calculated from the ratio between LoS signal power and scattered signal power, where the

scattered signal components are coherently summed up. This parameter does not depend on the delay or on the angle resolution.

DCIR

For the analysis of DCIR, two types of results were extracted from simulations: incoming signal average (in terms of delay and angle) and incoming signal standard deviation. These two results are used to derive the DCIR and its standard deviation.

The DCIR is essentially the resulting normalised incoming signal. Therefore it can be obtained by calculating the incoming signal and dividing it by the maximum signal component. Normally this component will be the one arriving from the LoS direction at the first delay slot. This method was used to obtain the average results for the DCIR in the considered examples.

Results for the DCIR are plotted in polar surface coloured representations; the number of depicted rings corresponds to the number of delay slots where incoming signal exists; angle analysis can be proceeded with respect to LoS, which is assumed to exist for an AoA of 0º; colour provides signal power strength information. For a better visualisation of the signal behaviour, a logarithmic (dB) representation was adopted. An example of this representation is depicted in Figure 3.2.a). Results are grouped per simulations set-up. To minimise space and information redundancy, scale and axis titles, which would be the same in each plot, are omitted, leading to the example depicted in Figure 3.2.b). In some cases the delay and angle slots are small, and therefore the slot contours reduce drastically the visualising capacity of the graphics. For that reason, these same plots are repeated in Annex 2, but omitting the slot angle and delay contour, as depicted in Figure 3.2.c).

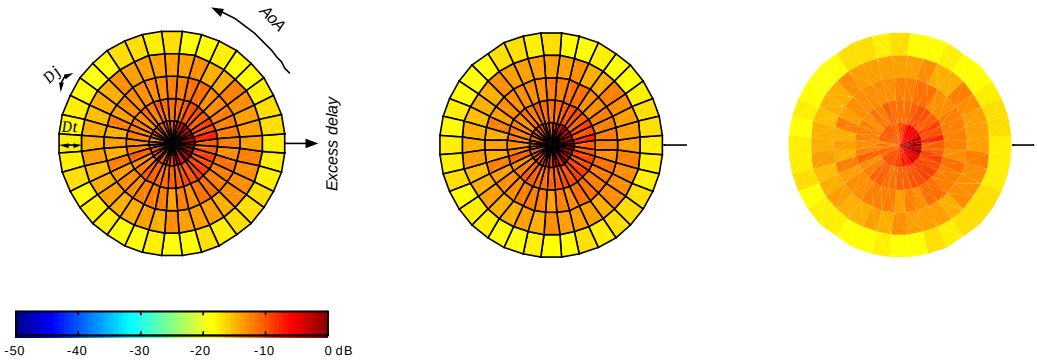

a) baseline b) without scale legend c) without scale legend and resolution contour

Figure 4.11 – DCIR logarithmic scale representation.

Results plotted in this chapter refer to a resolution of 65.1 ns, 20 ns resolution results being depicted in Annex 3.

The average DCIR in logarithmic scale for simulation set-ups 1), 2) and 3) are represented in Figure 4.12, Figure 4.13 and Figure 4.14, respectively. The same results are plotted without resolution contour in Figure A2.1, Figure A2.2 and Figure A2.3 from Annex 2. Equivalent results for 20 ns delay resolution are depicted in Figure A3.1, Figure A3.2 and Figure A3.3 (with resolution contours) and in Figure A3.4, Figure A3.5 and Figure A3.6 (without resolution contours).

Analysing the three set-ups along the increasing BS-MT distance, it can be seen that the number of delay rings decreases. This is analogous to the decrease of the delay parameters with distance, which was observed before in this chapter. Quoting the example of "Rua Gomes Leal" at 65.1 ns delay resolution (Figure 4.12), it can be seen that 20 m is the lowest distance with only one delay ring; this matches the position where the delay spread becomes zero and the average delay reaches its minimum value (Figure 4.2a) and Figure 4.4a)). It should be mentioned that for the situations where only one delay ring exists, narrowband approaches are valid.

Also in agreement with the delay parameters, wider streets show a larger number of delay rings for the same positions. Furthermore, a larger number of rings exist for the same positions when the quantisation interval is smaller, as in the case of 20 ns delay resolution.

For set-up 1) the angular discrimination is not very intense, therefore, signal power colours represented are nearly uniform in any direction, and only a slight difference can be seen for higher distances; this colour difference is better noticed at the narrowest street. Although this discrimination is not very obvious in the graphics depicted above, where a logarithmic scale is employed, other graphics depicted further down in linear scale can show more obviously this discrimination.

In set-up 2) better angle discrimination can be noticed, therefore, a larger colour variation is observed in the graphics, corresponding to concentration of signal around the LoS AoA. For DCIR cases where more than one delay ring exists, a phenomenon similar to a pair of lobes can be observed at peripheral rings: for these rings signal is weaker in LoS direction; signal is stronger in two groups of directions close to the LoS and symmetrical with respect to it. This phenomenon can be better observed in Figure A3.5 from Annex 3.

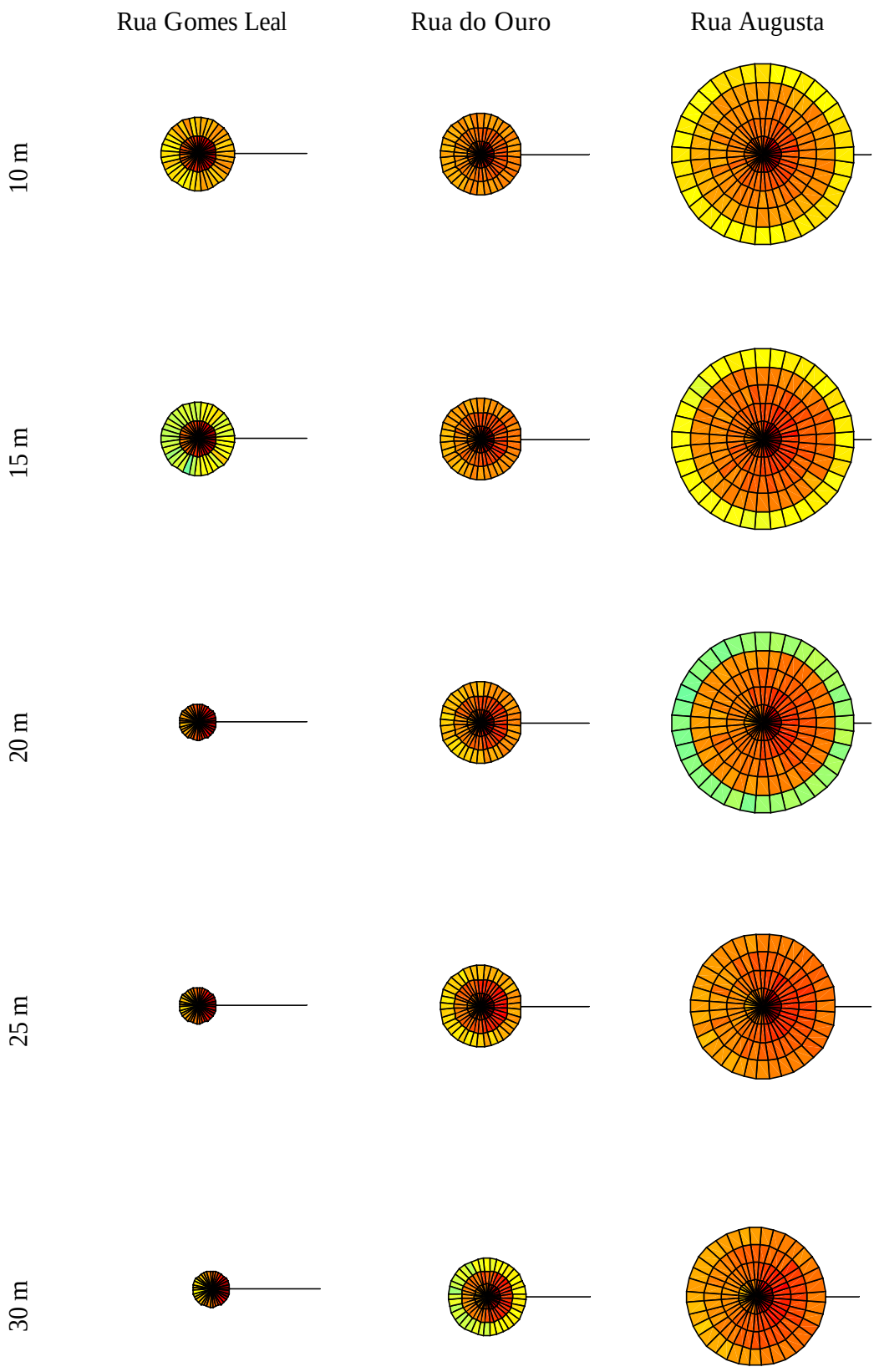

Figure 4.12 – DCIR logarithmic results for simulation set-up 1).

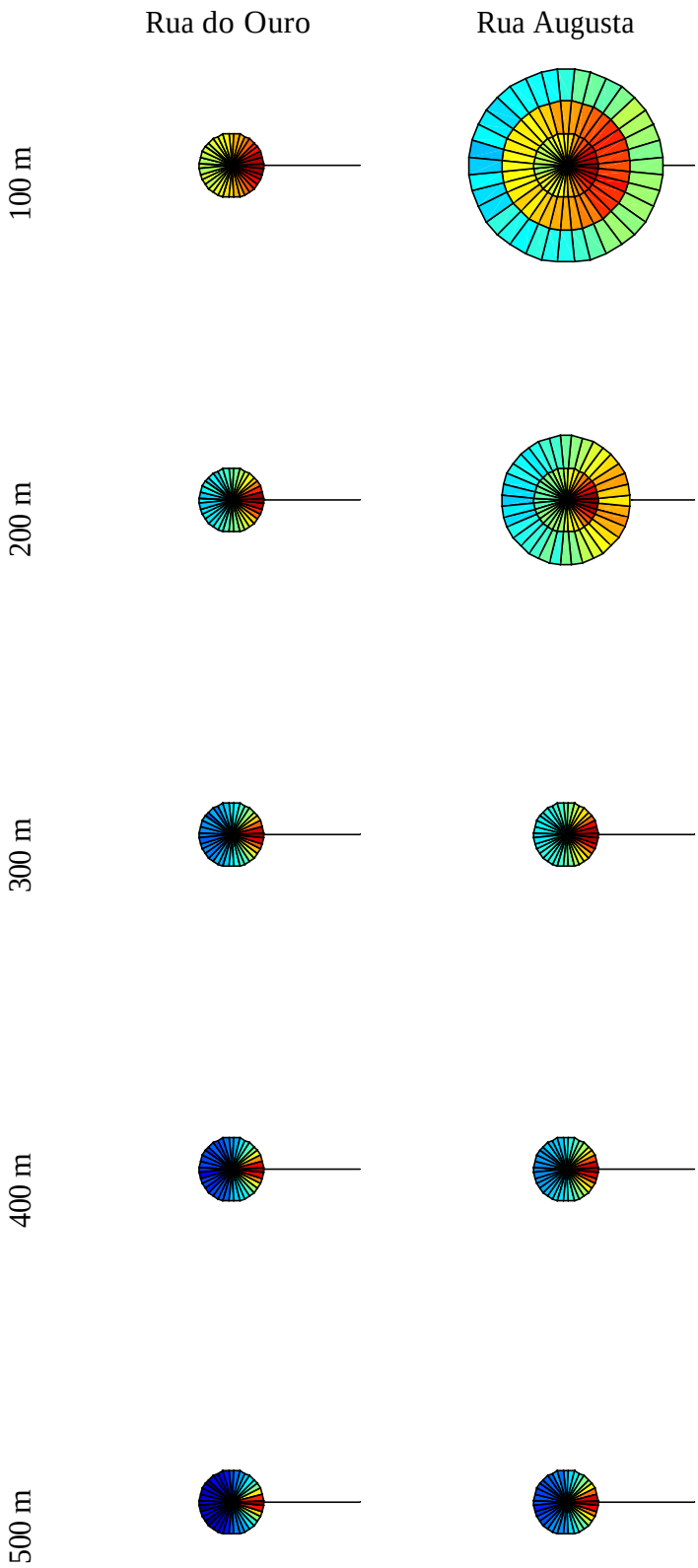

Figure 4.13 – DCIR logarithmic results for simulation set-up 2).

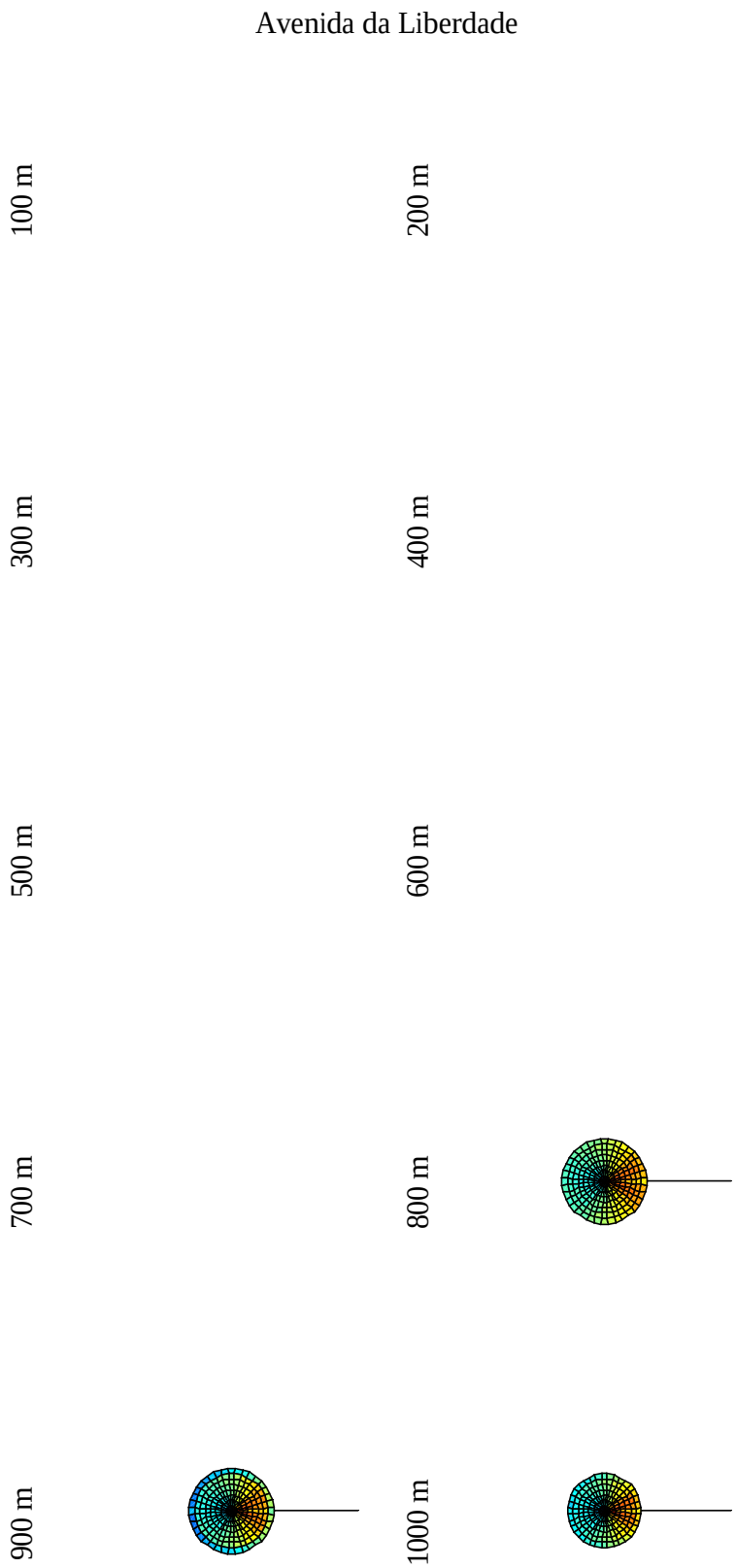

Figure 4.14 – DCIR logarithmic results for simulation set-up 3).

The simultaneous decrease of delay rings and increase of signal discrimination can be observed in more detail in the street example used for set-up 3), namely in Figure A2.3 from Annex 2.

In some of the polar plots an abrupt colour variation in the last delay ring can be observed. This is due to the signal quantisation within delay slots, when the elliptical region boundary does not match an exact number of delay slots, therefore, some signal is accounted in this last ring, but in average terms signal power in this ring is less then in the remaining ones. This fact was expected, and was previously mentioned in Chapter 3.

As earlier mentioned, the standard deviation calculated in the model simulations corresponds to the standard deviation from the resulting signal. To obtain standard deviation results that can be more directly related to the DCIR, two types of calculation methods are used. One, which will simply be named standard deviation, is to divide the signal standard deviation by the maximum signal component (as was done to obtain the DCIR). The other method, whose result will be named normalised standard deviation, is to divide each standard deviation component by its correspondent signal component. This way the standard deviation is normalised for the specific component.

It makes no sense to perform logarithmic representations for standard deviation results, thus linear representation will be adopted. For a better understanding, each plot will represent three different results: the linear average DCIR result, the so-called standard deviation and the normalised standard deviation. An example of such plot is depicted in Figure 4.15. Note that these are adimensional results. As in the average delay previously depicted, visualisation can be difficult, and therefore representations without contour will be adopted; delay and angle slot dimensions can be derived from the observation of the average DCIR results, and so the need for these contours cesses to exist. Also scales will be omitted. The resulting example is depicted in Figure 4.16. Due to the larger amount of results to be presented in comparison to the average DCIR case, results will be only grouped per street and within the same simulation set-up.

As for the case of average DCIR, results plotted in this chapter refer to a resolution of 65.1 ns. The linear scale representations of average DCIR, standard deviation and normalised standard deviation are represented in Figure 4.17, Figure 4.18 and Figure 4.19 for simulation set-up 1), Figure 4.20 and Figure 4.21 for set-up 2) and Figure 4.22 and Figure 4.23 for set-up 3).

Equivalent results for 20 ns delay resolution are depicted in the plots from to Figure A3.7 to Figure A3.13 in Annex 3.

Average Standard deviation Normalised Stnd. Dev.

Figure 4.15 – DCIR baseline linear representation

Average Standard deviation Normalised Stnd. Dev.

Figure 4.16 – DCIR linear representation without scale legend and resolution contour

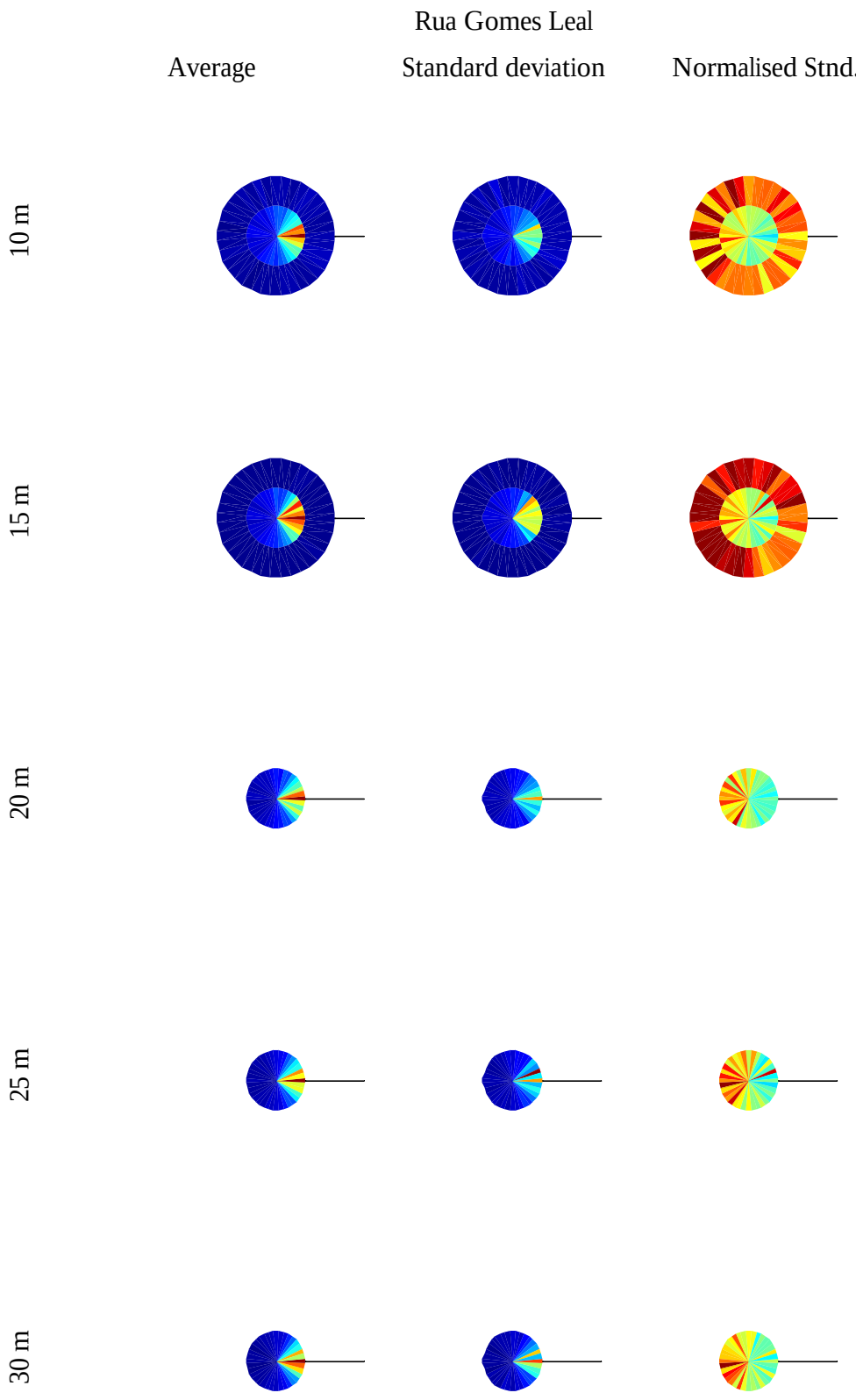

Figure 4.17 – DCIR average and standard deviation results for “Rua Gomes Leal” (simulation set-up 1)).

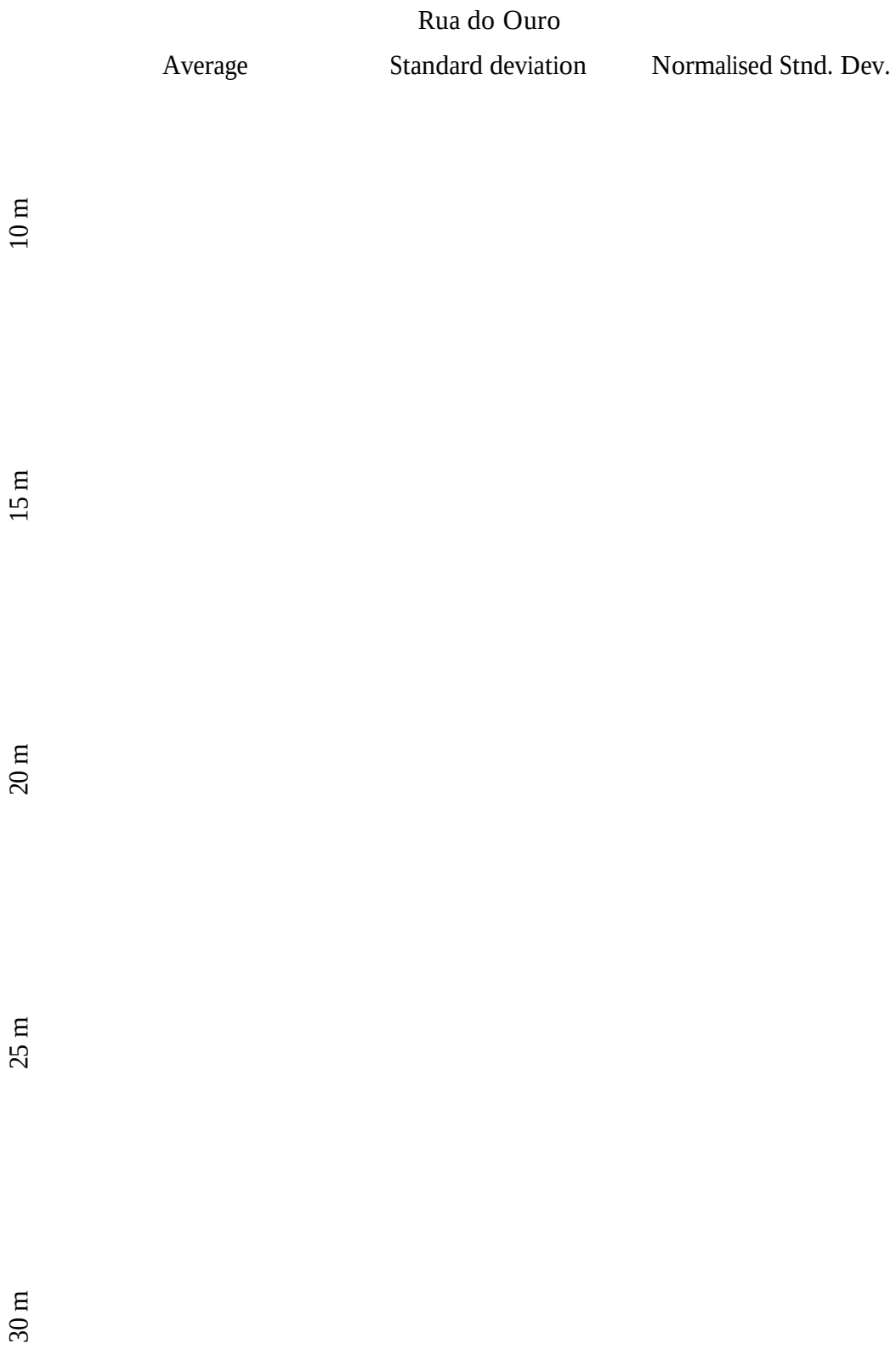

Figure 4.18 – DCIR average and standard deviation results for “Rua do Ouro” at simulation set-up 1).

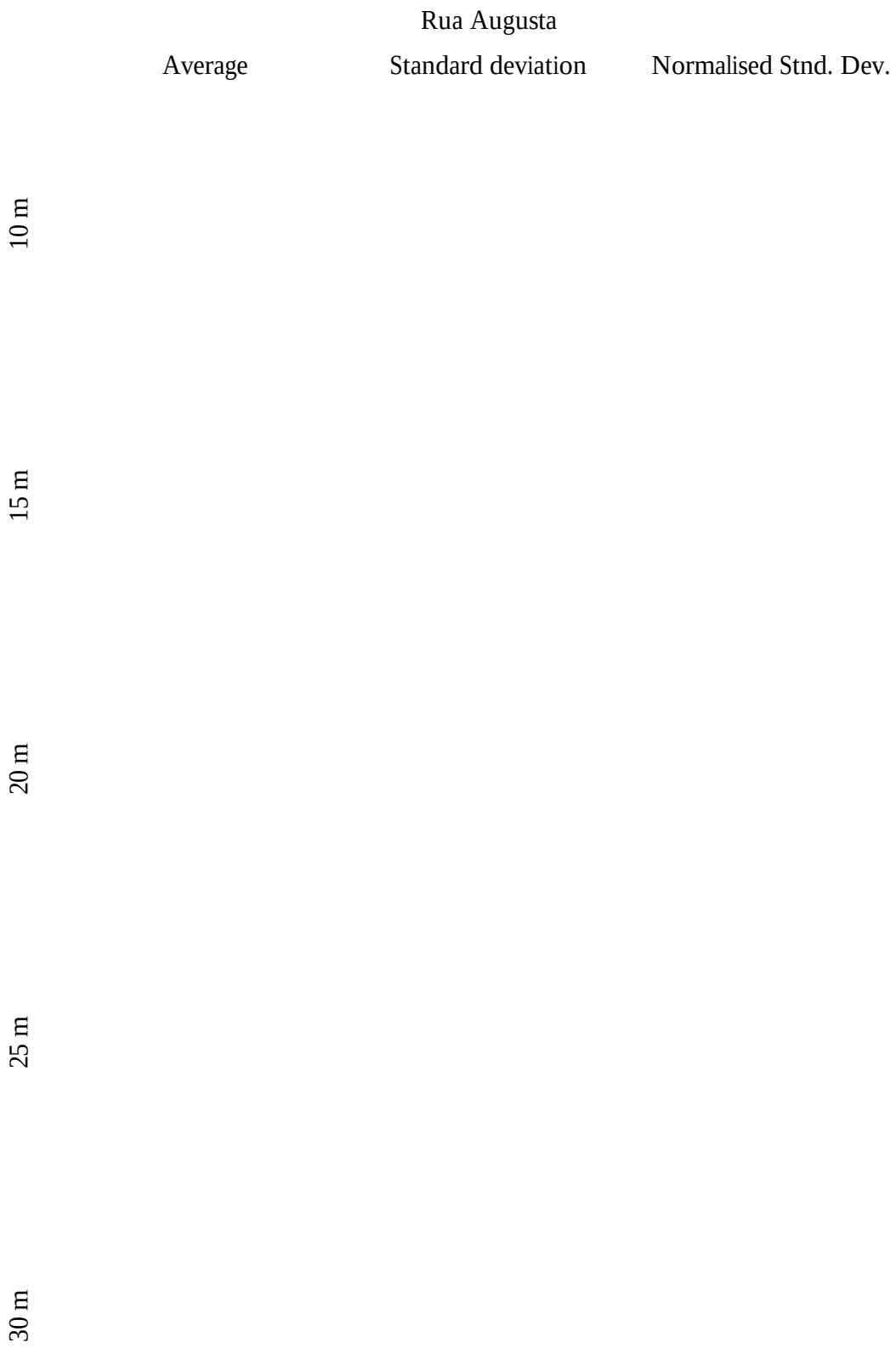

Figure 4.19 – DCIR average and standard deviation results for “Rua Augusta” at simulation set-up 1).

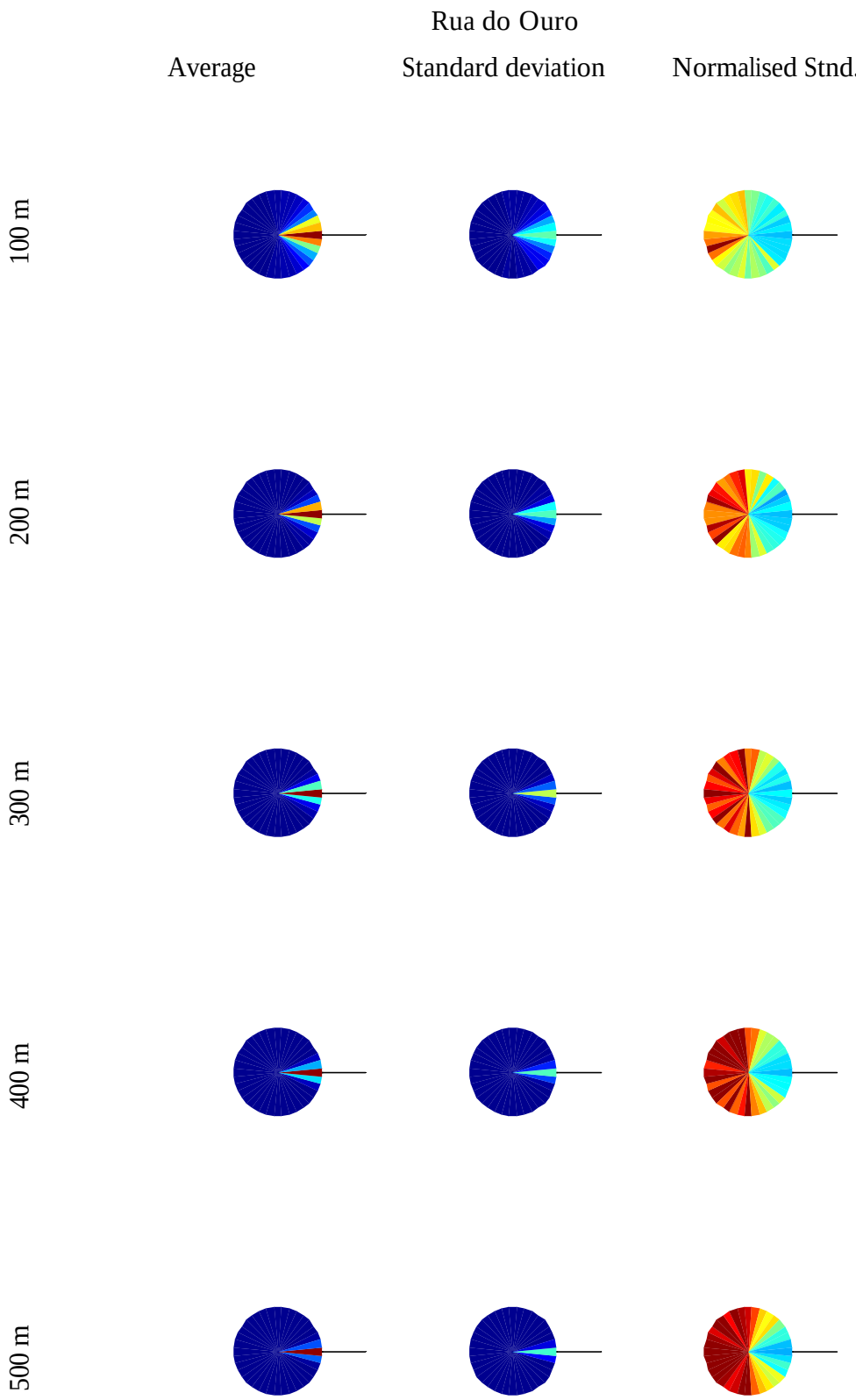

Figure 4.20 – DCIR average and standard deviation results for “Rua do Ouro” at simulation set-up 2).

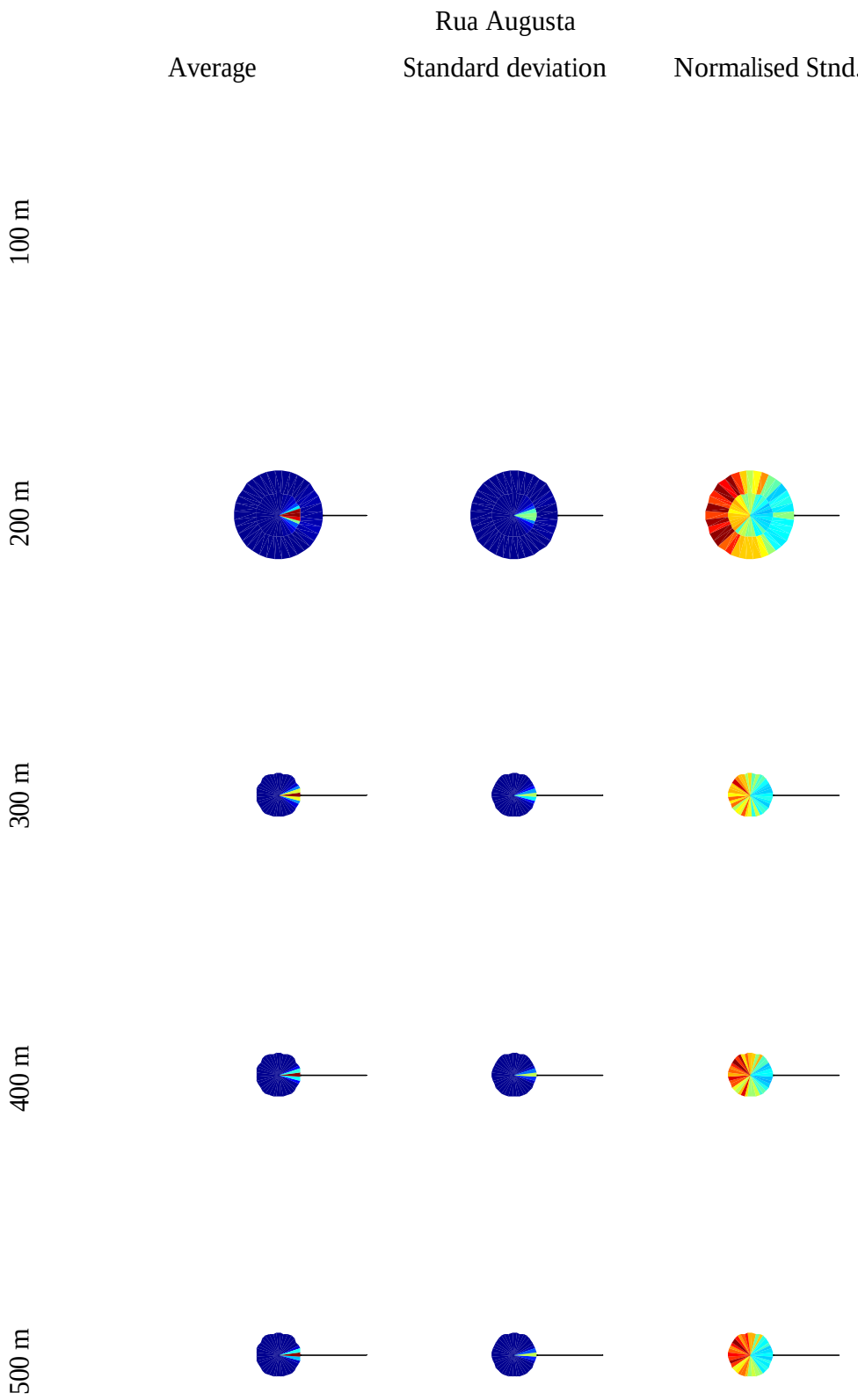

Figure 4.21 – DCIR average and standard deviation results for “Rua Augusta” at simulation set-up 2).

Figure 4.22 – DCIR average and standard deviation results for “Avenida da Liberdade” at the first half of set-up 3).

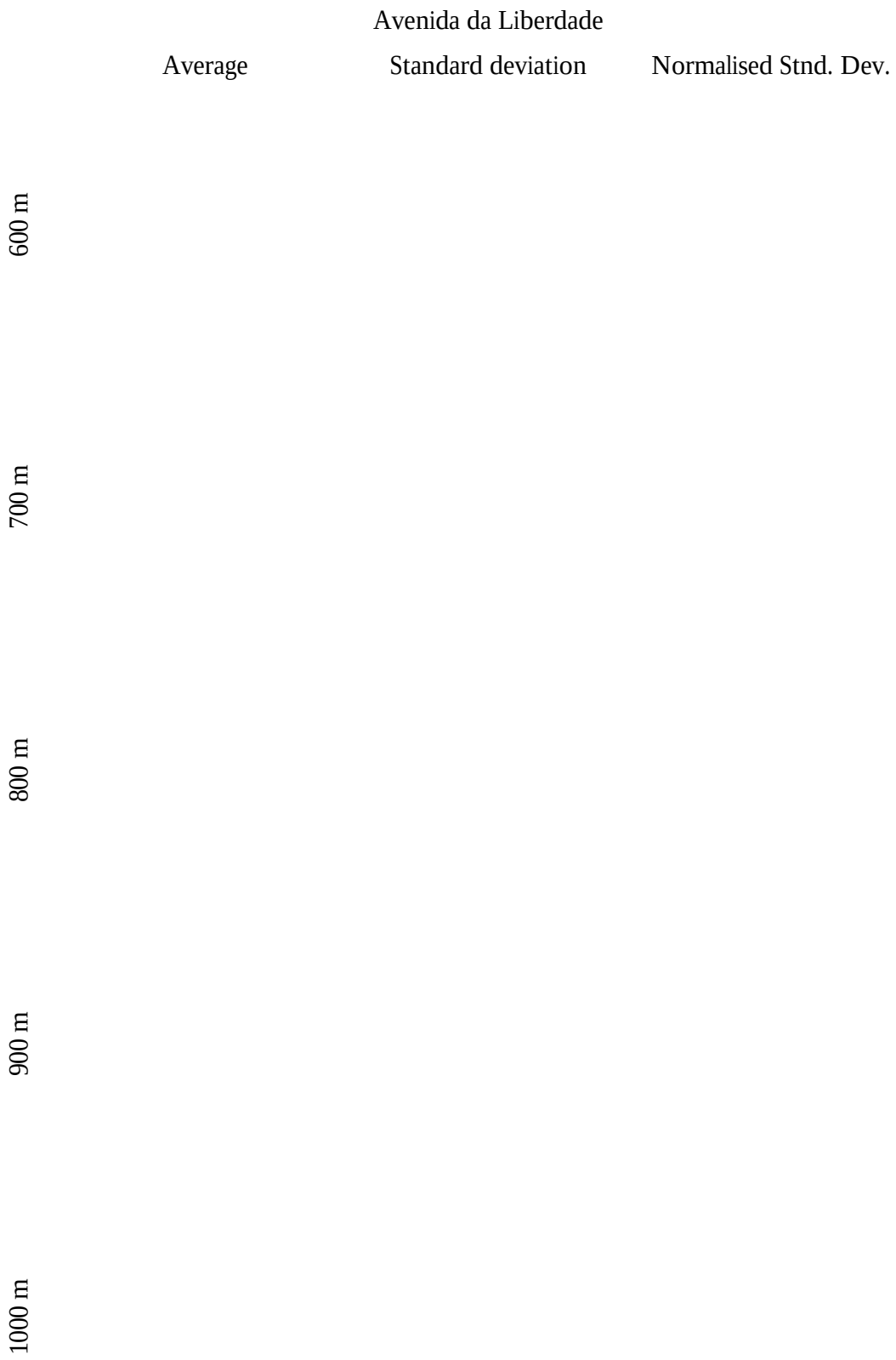

Figure 4.23 – DCIR average and standard deviation results for "Avenida da Liberdade" at the 2nd half of set-up 3).

As can be observed from the graphics, standard deviation is about on the same order of magnitude as the DCIR itself, which can be better noticed with the help of the normalised standard deviation, where values up to 3 can be observed. Thus, there seems to be a large uncertainty associated to the results. This is naturally related to the DCIR sensitivity in respect to scatterer positioning and its relation to the signal delay and angle quantisation, when cluster resulting signals move in between slots within simulations. This uncertainty is naturally larger for smaller quantisation intervals, as is the case for 20 ns delay resolution.

It can also be seen that the associated error is larger for the cases of lower signal power than in higher signal power slots, thus, higher power slots will necessarily be less sensitive to scatterer positioning differences. This is more notorious in two different situations: the last delay ring and in good angle discriminating streets. In the delay rings where an abrupt power variation occurs, the standard deviation, thus, the related error, is larger than the one observed for the other rings, as can be seen for instance in "Rua Augusta" at a 20 m distance (set-up 1) - Figure 4.12 and Figure 4.19). In the cases where good angle discrimination exists, the AoAs with lower received signal power are consequently more sensitive to scattering position variation, thus resulting in a larger normalised delay spread (see for instance "Rua do Ouro" at set-up 2) - Figure 4.13 and Figure 4.20).

Finally, from the results obtained, it is possible to draw conclusions about the expected performance of adaptive antennas for the examples studied. It is expected that no particular improvement be achieved for shorter BS-MT distances (although a narrower radiation pattern could prevent from receiving interference, it will be difficult for the adaptive antenna to derive a meaningful direction discrimination). However, for larger distances, it is possible to discriminate signal directions. This way signal reception is maximised comparatively to interferers. Larger distances correspond to cases where more sensitivity to inter-cell interference occurs, therefore, it is likely that adaptive antennas may reduce both intra- and inter-cell interference.

In many cases spatial and temporal processing should be performed, for multiple delay slots are expected, particularly when a smaller delay quantisation is used; other cases need only spatial processing, for they can be considered narrowband.

Chapter 5

Conclusions

This chapter finalises this work, summarising conclusions and pointing out aspects to be developed in future work.

This work intended to develop a model for UMTS with the capability to serve as support to the study of adaptive antennas. This demanded a wideband simulation model providing angular information. The target environment chosen was a micro-cell, from which the operational environment of LoS (line of sight) street was chosen, meaning that both the base station (BS) and the mobile terminal (MT) are positioned in this same street.

To get in touch with the context and language of the problem, the key topics that rule the study of this area were approached. As background platform for this work, an overview on directional channel modelling state-of-the-art reported in the literature is presented. A wide range of models has already been developed to fulfil different purposes. From these models, the starting-point approaches were chosen in order to obtain the desired purpose. The chosen approaches were based on the GBSBEM (Geometrically Based Single Bounce Elliptical Model) and additionally supported by the Combined GBSB (Geometrically Based Single Bounce) and GWSSUS (Gaussian Wide-Sense Stationary Uncorrelated Scattering) model and by the Elliptical Sub-Regions model.

Based on the afore-mentioned approaches, the model is formulated and thoroughly described, while justifying each parameter option taken. The resulting model considers single-specular reflection from scatterers grouped into clusters. The clusters are uniformly distributed within an ellipse, while scatterers are Gaussian distributed within each cluster. The size of the ellipse is limited by the width of the desired street. Scatterers are associated a complex scattering coefficient with uniformly distributed phases and magnitudes within [0, 1] and [0, 2π[, respectively.

The resulting model, implemented in C programming language, is described and then assessed in three stages: parameter analysis, comparison with measurements and frequency correlation analysis. Monte-Carlo simulations were used for this purpose. After this set of assessment analysis the model was considered fit for result analysis to be proceeded in a further chapter.

The parameter analysis is performed to derive the model sensitivity regarding input parameters. The variation of results of each parameter is analysed and compared, in terms of average values for angle and delay spread resulting from Monte-Carlo simulations. It is concluded that the most influencing parameter is the street width, whose influence, compared to the second

most influencing parameter (cluster density), is one order of magnitude higher for the delay spread and 2.5 times higher for the angle spread. This parameter can be used for a generic tuning of the model, creating the concept of an effective street width.

Model simulation results are compared with measurements reported in literature. The measurement conditions are reproduced in the simulations. Average and standard deviation results for angle and delay spread are derived from the Monte-Carlo simulations, which produce a 68% confidence interval (assuming a Gaussian process). Measurement results fall within this interval when an effective street width ratio of 6.5 is chosen.

The correlation between up- and down-links in an FDD transmission is also analysed for the lowest UMTS FDD channel pair, reaching the conclusion that correlation depends both on the used delay and angle resolutions, although the influence of delay resolution is stronger.

From the assessed model, several representative cases within the operational environment associated to the proposed model are chosen to exemplify expectable results in terms of global output parameters and of directional channel impulse response. Two delay resolutions are used for this purpose: 65.1 ns, corresponding to one fourth of the chip time, and 20 ns, one thirteenth of the chip time. Results are used to evaluate expected performance improvements when using adaptive antennas.

All parameters decrease with distance between BS and MT, and are larger for wider streets. Average delay spread becomes zero when its real values fall below the used delay resolution. Delay spread is in the order of tens of nanoseconds for streets between 5 and 15 m wide, and angle spread comes in the order of tens of degree. The evolution of these parameters can also be evaluated through the directional channel impulse response, namely from the number of circular crowns and signal power strength variation within them: less circular crowns exist for larger distances and for narrower streets.

Regarding the use of adaptive antennas for the considered operational environment, it is seen that for small BS-MT distances the expected improvement is poor, while for increasing distances, an increase of performance is indeed expected, thus justifying their use.

This is not at all a finalised work. A wide range of issues can be improved. Some of them are left as suggestions for work continuation. First of all, a thorough model assessment would be

advisable, this time directly from measurement campaign results. The extension of the model to other operational environments would also provide an added value to this work, as well as scatterer mobility introduction and shadow fading assumptions. Some improvement could additionally be provided to the behaviour in between frequency channels, in order to achieve control on the resulting inter-frequency correlation. These improvements would lead to a more complete model for performing micro-cell simulations with adaptive antennas.

References

[Aszt96] Asztély,D., *On Antenna Arrays in Mobile Communication Systems: Fast Fading and GSM Base Station Receiver Algorithms*, Masters Thesis, Royal Institute of Technology, Stockholm, Sweden, Mar. 1996.

[Bala97] Balanis,C.A., *Antenna Theory: Analysis and Design*, John Wiley & Sons, New York, NY, USA, 1997.

[BJLF98] Bronzel,M., Jelitto,J., Lohse,N., Fettweis,G., Thomä,R., Sommerkorn,G., Hampicke,D., Trautwein,U. and Richter,A., "Experimental Verification of Vector Channel Models for simulation and Design of Adaptive Antenna Array Receivers", in *Proc. of ACTS Mobile Communication Summit*, Rhodes, Greece, June 1998.

[Boit83] Boithias,L., *Radiowave Propagation in Earth Environment* (in French), Dunod, Paris, France, 1983.

[BuCN99] Bull,D., Canagarajah,N. and Nix,A. (eds.), *Insights into Mobile Multimedia Communications*, Academic Press, Bodmin, UK, 1999.

[COST99] COST Action 231, *Digital Mobile Radio Towards Future Generation Systems (Final Report)*, COST Telecom Secretariat, European Commission, Brussels, Belgium, 1999.

[DuRa99] Durgin,G. and Rappaport,T., "Three Parameters for Relating Small-Scale Temporal Fading Statistics to Multipath Angles-of-Arrival", in *Proc. of PIMRC´99 – 10th IEEE International Symposium on Personal, Indoor and Mobile Radio Communications*, Osaka, Japan, Sep. 1999.

[Egge00] Eggers,P., "Comparison of Angular Dispersion Metrics in Synthetic and Measured Radio Channels", in *Proc. of AP2000 – Millennium Conference on Antennas&Propagation*, Davos, Switzerland, Apr. 2000.

[Fern99] Fernandes,E. (ed.), *UE Radio transmission and reception (FDD)*, 3GPP Technical Specification, No. 25.101, Ver. 3.1.0, Oct. 1999, http://www.3gpp.org.

[FuMB98] Fuhl,J., Molisch,A. and Bonek,E., "Unified Channel Model for Mobile Radio Systems with Smart Antennas", *IEE Proceedings - Radar, Sonar Navigation*, Vol. 145, No. 1, Feb. 1998, pp. 32-41.

[HaBH96] Hall,M., Barclay,L. and Hewitt,M., *Propagation of Radiowaves*, IEE Press, London, UK, 1996.

[KLTH00] Kalliola,K., Laurila,J., Toeltsch,M., Hugl,K., Vainikainen,P. and Bonek,E., "3-D Directional Wideband Dual-Polarized Measurement of Urban Mobile Radio Channel With Synthetic Aperture Technique", in *Proc. of AP2000 – Millennium Conference on Antennas & Propagation*, Davos, Switzerland, Apr. 2000.

[Kott99] Kottamp,M. (ed.), *UE Radio transmission and reception (TDD)*, 3GPP Technical Specification, No. 25.102, Ver. 3.1.0, Oct. 1999, http://www.3gpp.org.

[Lee73] Lee,W.C.Y., "Effects on correlation between two mobile base-station antennas", *IEEE Transactions on Communications*, Vol. COM-21, No. 11, Nov. 1973, pp. 1214-1224.

[LiRa96] Liberti,J. and Rappaport,T., "A Geometrically Based Model for Line-of-sight Multipath Radio Channels", in *Proc. of VTC'96 - IEEE 46th Vehicular Technology Conference*, Atlanta, GA, USA, Apr. 1996.

[LiRa99] Liberti,J. and Rappaport,T., *Smart Antennas for Wireless Communication: IS-95 and Third Generation CDMA Applications*, Prentice Hall, Upper Saddle River, NJ, USA, 1999.

[LuLL97] Lu,M., Lo.,T. and Litva,J., "A Physical Spatio-Temporal Model of Multipath Propagation Channels", in *Proc. of VTC'97 - IEEE 47th Vehicular Technology Conference*, Phoenix, AZ, USA, May 1997.

[MLKS98] Molisch,A., Laurila,J., Kuchar,A. and Schmalenberger,R., "Test scenarios for mobile radio systems with adaptive antennas", in *Proc. of the COST252/259 Joint Workshop "Communications for the Millennium"*, Bradford, UK, Apr. 1998.

[MoPa92] Mouly,M. and Pautet,M.-B., *The GSM System for Mobile Communications*, published by the authors (Michel Mouly and Marie-Bernadette Pautet), Palaiseau, France, 1992.

[NøAn94] Nørklit,O. and Andersen,J.B., "Mobile Radio Environments and Adaptive Arrays", in *Proc. of PIMRC'94 - 5th IEEE International Symposium on Personal, Indoor and Mobile Radio Communications*, The Hague, The Netherlands, Sep. 1994.

[NøAn98] Nørklit,O. and Andersen,J.B., "Diffuse Channel Model and Experimental Results for Array Antennas in Mobile Environments", in *IEEE Transactions on Antennas and Propagation*, Vol. 46, No. 6, June 1998, pp. 834-840.

[Otte95] Ottersten,B., "Spatial Division Multiple Access (SDMA) in Wireless communications", in *Proc. of Nordic Radio Symposium*, Saltsjöbaden, Sweden, Apr. 1995.

[Pars92] Parsons,D., *The Mobile Radio Propagation Channel*, Pentech Press, London, UK, 1992.

[PeRR96] Petrus,P., Reed,J. and Rappaport,T., "Geometrically Based Statistical Channel Model for Macro-cellular Environments", in *Proc. of Globecom'96 - IEEE Global Telecommunications Conference*, London, UK, Nov. 1996.

[PiTs99] Piechocki,R. and Tsoulos,G., "Combined GWSSUS and GBSR Channel Model With Temporal Variations", in *Proc. of COST259/260 Joint Workshop "Spatial Channel Models and Adaptive Antennas"*, Vienna, Austria, Apr. 1999.

[PLNR99] Pettersen,M., Lehne,P., Noll,J., Røstbakken,O., Antonsen,E. and Eckhoff,R., "Characterisation of the Directional Wideband Radio Channel in Urban and Suburban Areas", in *Proc. of VTC'99-Fall - IEEE 50th Vehicular Technology Conference*, Amsterdam, The Netherlands, Sep. 1999.

[PTVF92] Press,W., Teukolsky,S., Vetterling,W. and Flannery,B., *Numerical Recipes in C: The Art of Scientific Computing*, 2nd ed., Cambridge University Press, Cambridge, UK, 1992.

[RaPa95] Raleigh,G. and Paulraj,A., "Time Varying Vector Channel Estimation for Adaptive Spatial Equalisation", in *Proc. of Globecom'95 - IEEE Global Telecommunications Conference*, Singapore, Nov. 1995.

[Rapp96] Rappaport,T., *Wireless Communications*, IEEE Press, New York, NY, USA, 1996.

[SaVa87] Saleh,A.M. and Valenzuela,R.A., "A Statistical Model for Indoor Multipath Propagation", *IEEE Journal on Selected Areas in Communications*, Vol. SAC-5, No. 2, Feb. 1987, pp. 128-137.

[SRJJ97] Spencer,Q., Rice,M., Jeffs,B. and Jensen,M., "A Statistical Model for Angle of Arrival in Indoor Multipath Propagation", in *Proc. of VTC'97 - IEEE 47th Vehicular Technology Conference*, Phoenix, AZ, USA, May 1997.

[StCM94] Stapleton,S.P., Carbo,X. and McKeen,T., "Spatial Channel Simulator for Phased Arrays", in *Proc. of VTC'94 - IEEE 44th Vehicular Technology Conference*, Stockholm, Sweden, June 1994.

[StCM96] Stapleton,S.P., Carbo,X. and McKeen,T., "Tracking and Diversity for a Mobile Communications Base Station Array Antenna", in *Proc. of VTC'96 - IEEE 46th Vehicular Technology Conference*, Atlanta, GA, USA, Apr. 1996.

[Stee92] Steele,R. (ed.), *Mobile Radio Communications*, Pentech Press, London, UK, 1992.

[Tosk99] Toskala,A. (ed.), *Physical layer - General Description*, 3GPP Technical Specification, No. 25.201, Ver. 3.1.0, Oct. 1999, http://www.3gpp.org.

[UMTS98] UMTS Forum, *Minimum spectrum demand per public terrestrial UMTS operation in the initial phase*, Report No.5, London, UK, Oct. 1998.

[UMTS99] UMTS Forum, *UMTS/IMT-2000 - Assessing global requirements for the next century*, Report No.6, London, UK, Feb. 1999.

[Yaco93] Yacoub,M.D., *Foundations of Mobile Radio Engineering*, CRC Press, Boca Raton, FL, USA, 1993.

[ZeEs96] Zetterberg,P. and Espensen,P.L., "A Downlink Beam Steering Technique for GSM/DCS1800/PCS1900", in *Proc. of PIMRC'96 - 7th IEEE International Symposium on Personal, Indoor and Mobile Radio Communications*, Taipei, Taiwan, Oct. 1996.

Annex 1

Global output parameters for a 20 ns delay resolution

This annex represents the global output parameters obtained for a 20 ns delay resolution.

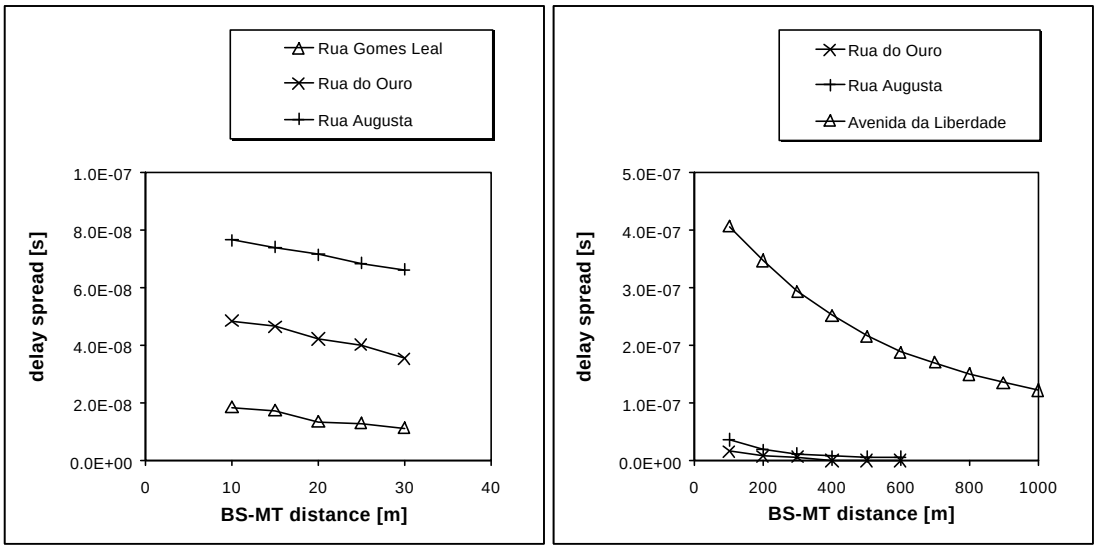

a) set-up 1). b) set-ups 2) and 3).

Figure A1.1 – Delay spread results.

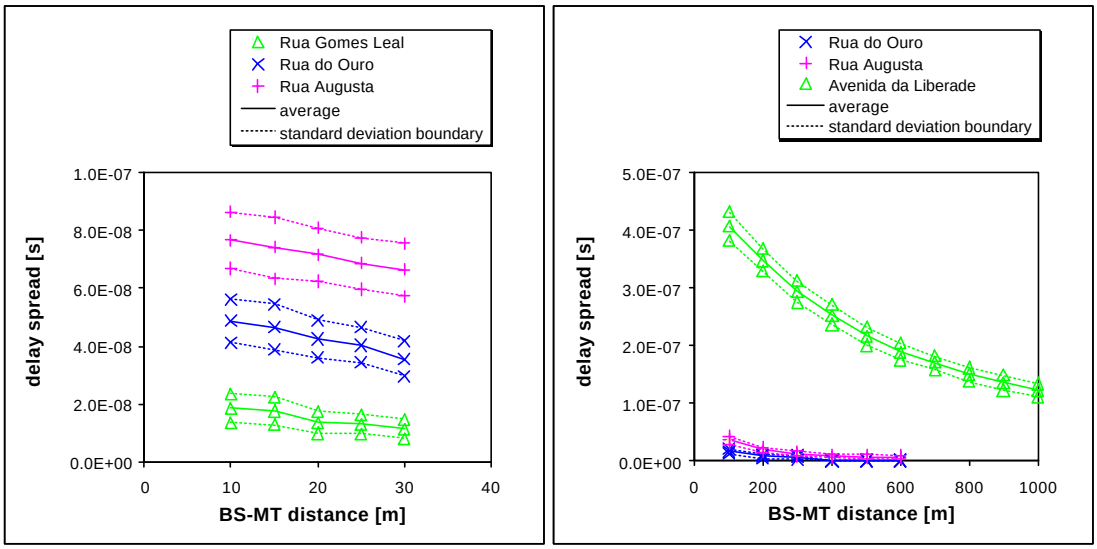

a) set-up 1). b) set-ups 2) and 3).

Figure A1.2 – Delay spread results (average values with standard deviation boundaries).

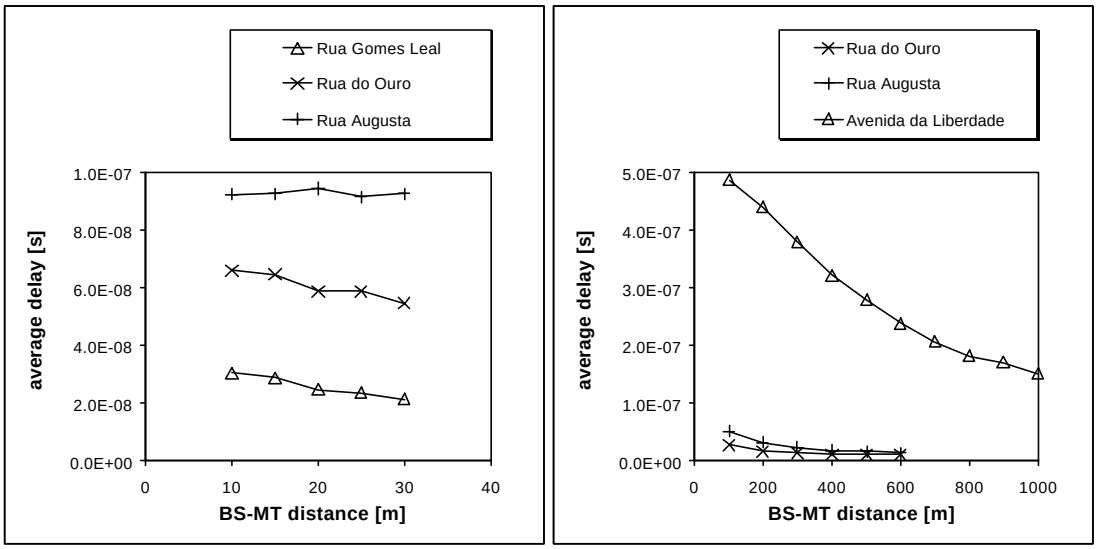

a) set-up 1). b) set-ups 2) and 3).

Figure A1.3 – Average delay results.

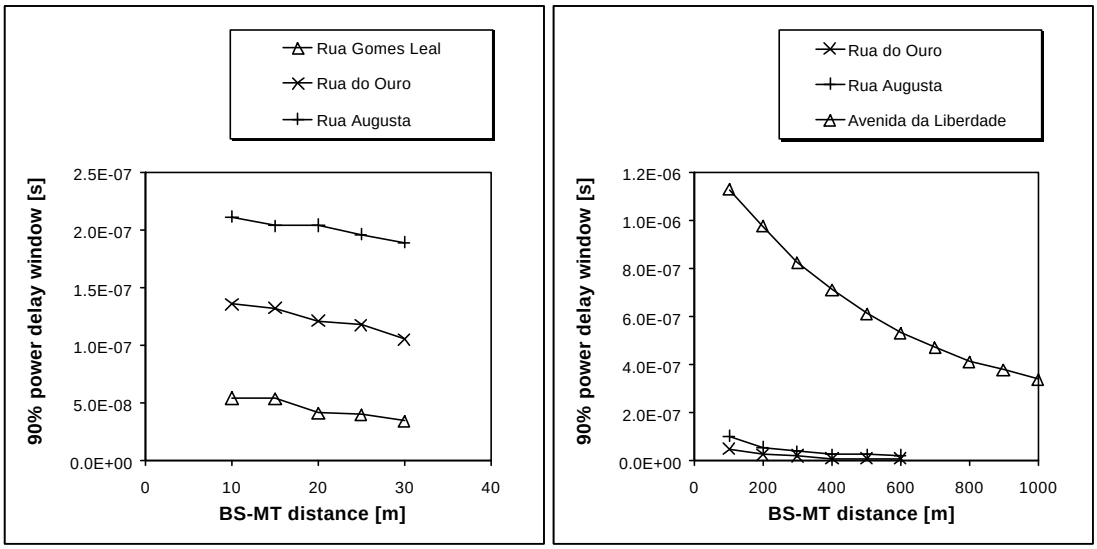

a) set-up 1). b) set-ups 2) and 3).

Figure A1.4 – 90% power delay window results.

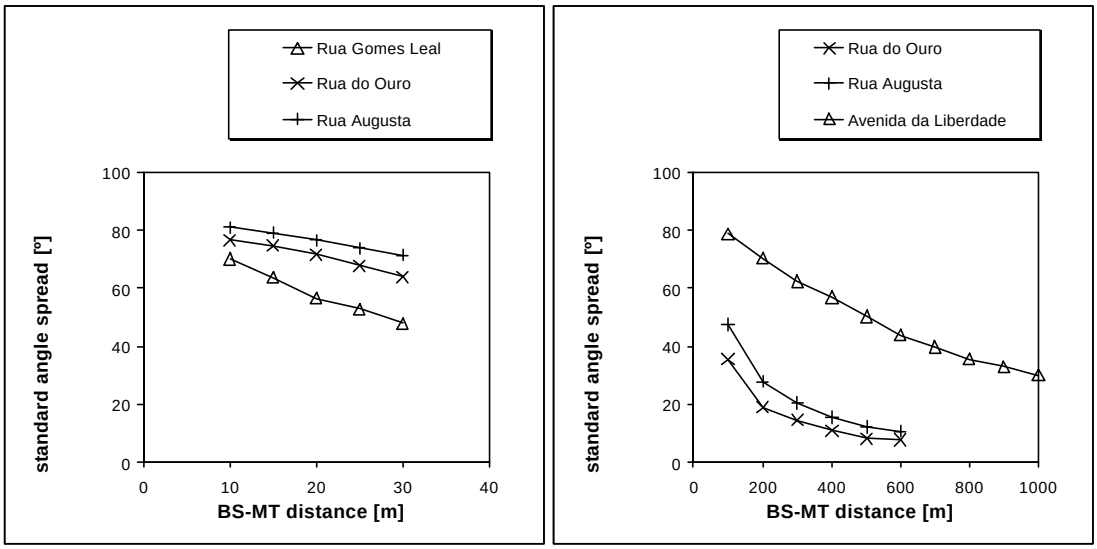

a) set-up 1). b) set-ups 2) and 3).

Figure A1.5 – Standard angle spread results.

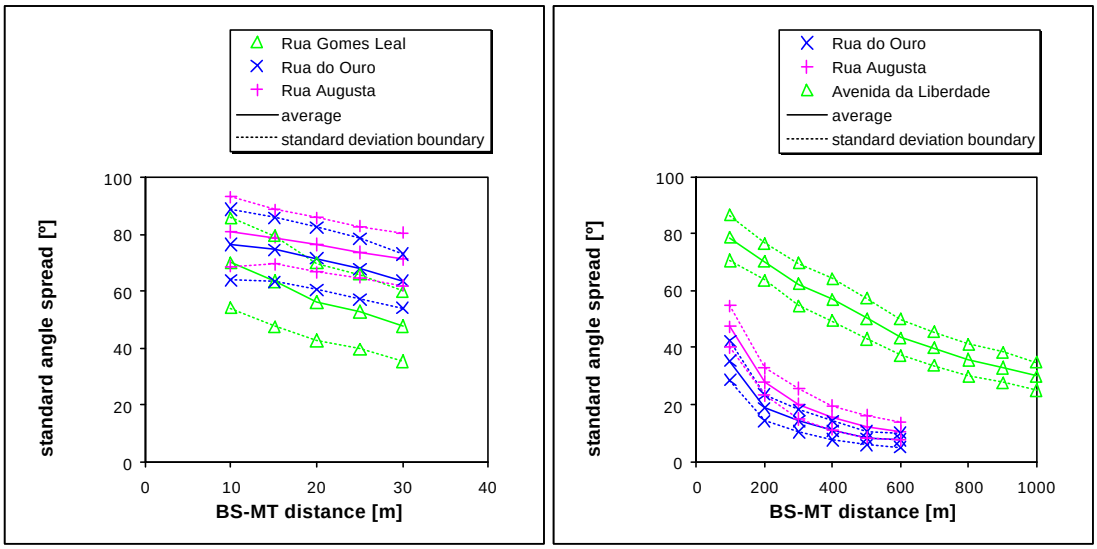

a) set-up 1). b) set-ups 2) and 3).

Figure A1.6 – Standard angle spread results (average values with standard deviation boundaries).

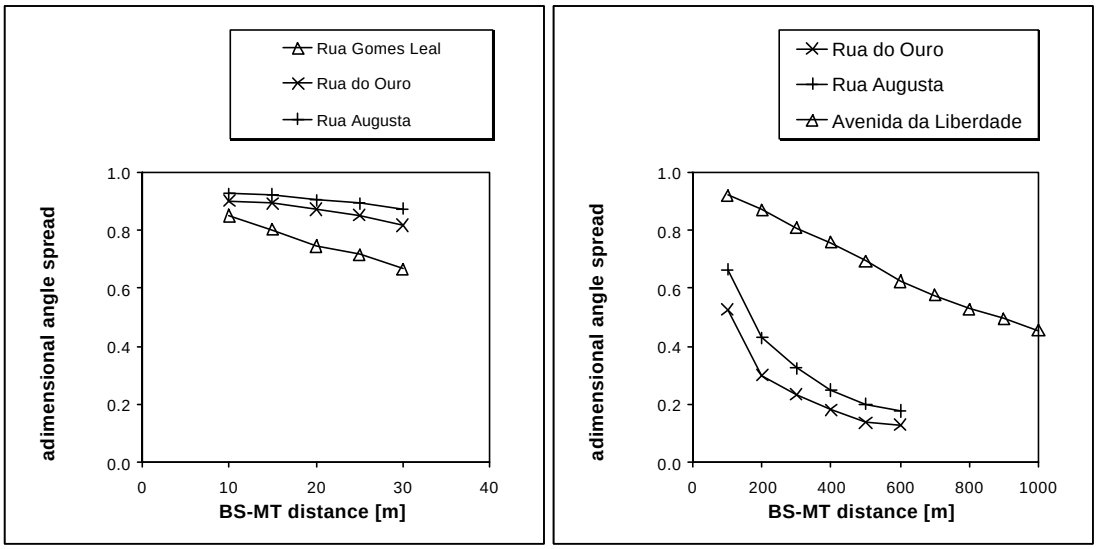

a) set-up 1). b) set-ups 2) and 3).

Figure A1.7 – Adimensional angle spread for results.

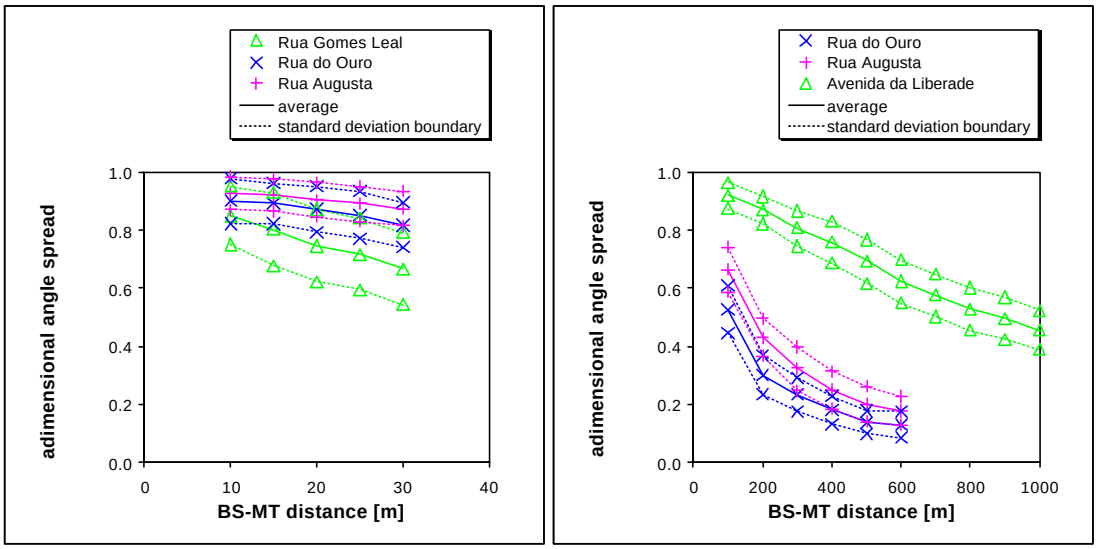

a) set-up 1). b) set-ups 2) and 3).

Figure A1.8 – Adimensional angle spread results (average values with standard deviation boundaries).

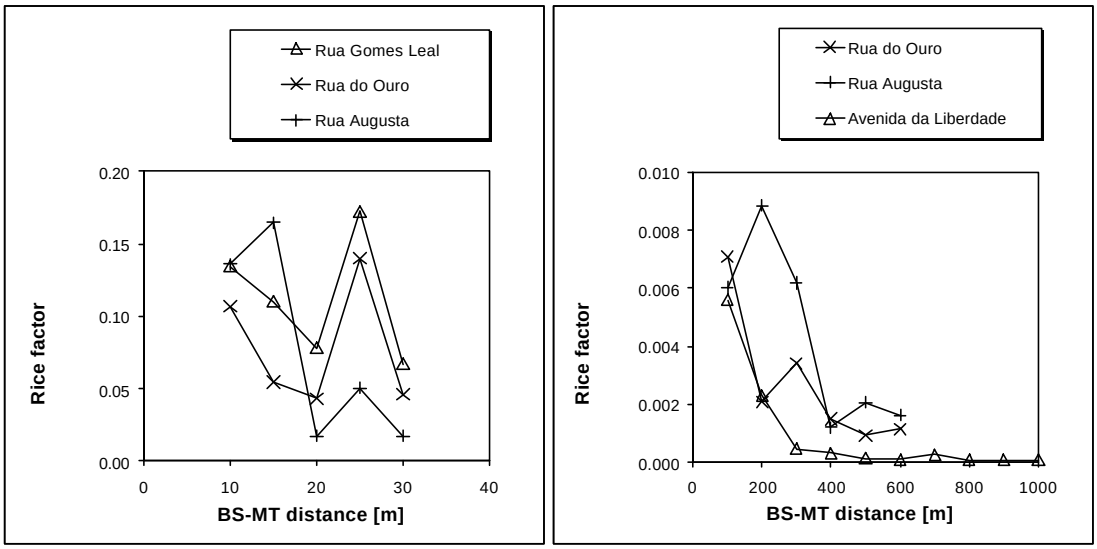

a) set-up 1). b) set-ups 2) and 3).

Figure A1.9 – Rice factor results.

Annex 2

DCIR without contours for a 65.1 ns delay resolution

This annex presents the results for DCIR in logarithmic scale for 65.1 ns delay resolution after extracting the resolution contour.

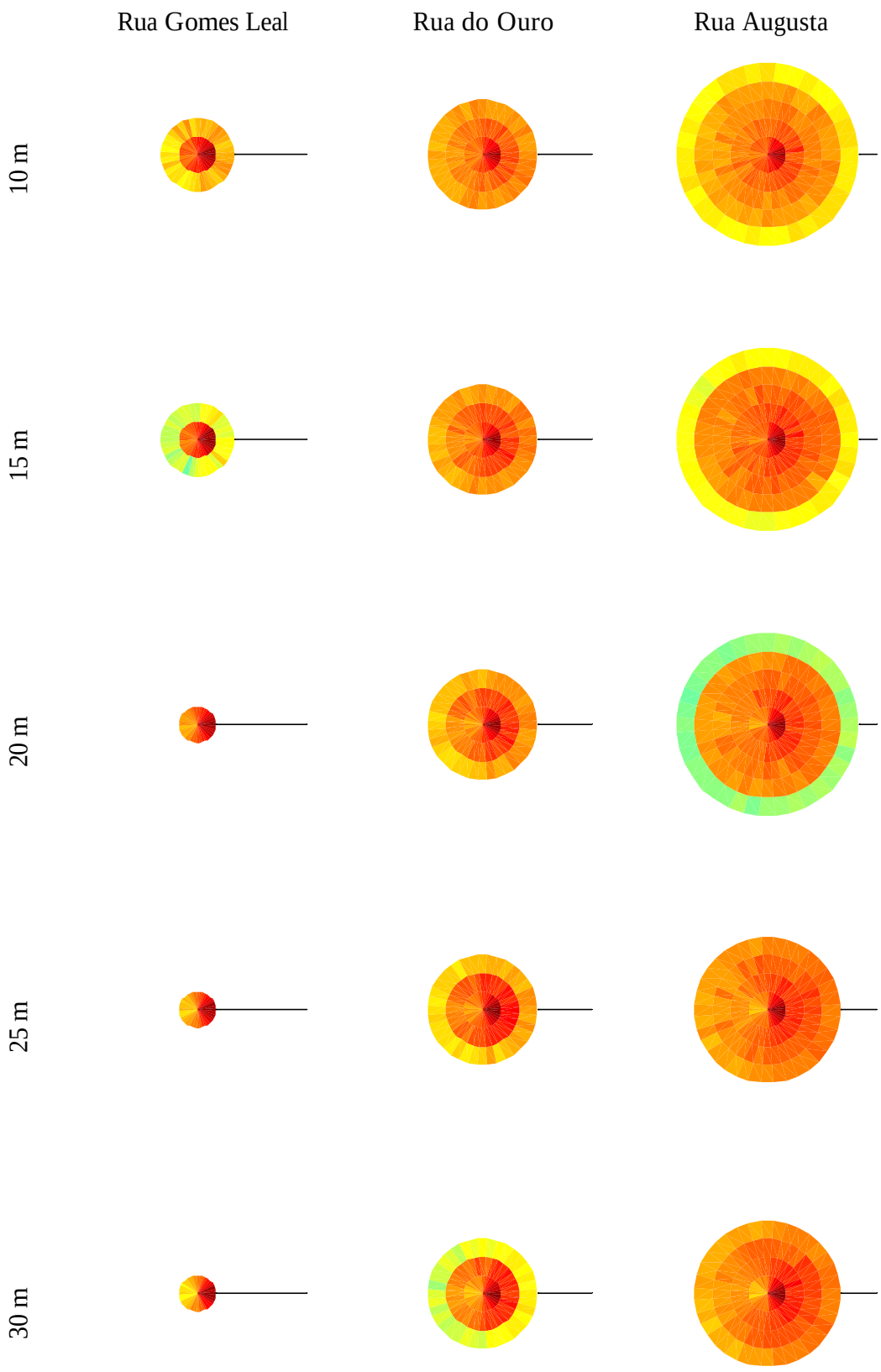

Figure A2.1 – DCIR logarithmic results for simulation set-up 1).

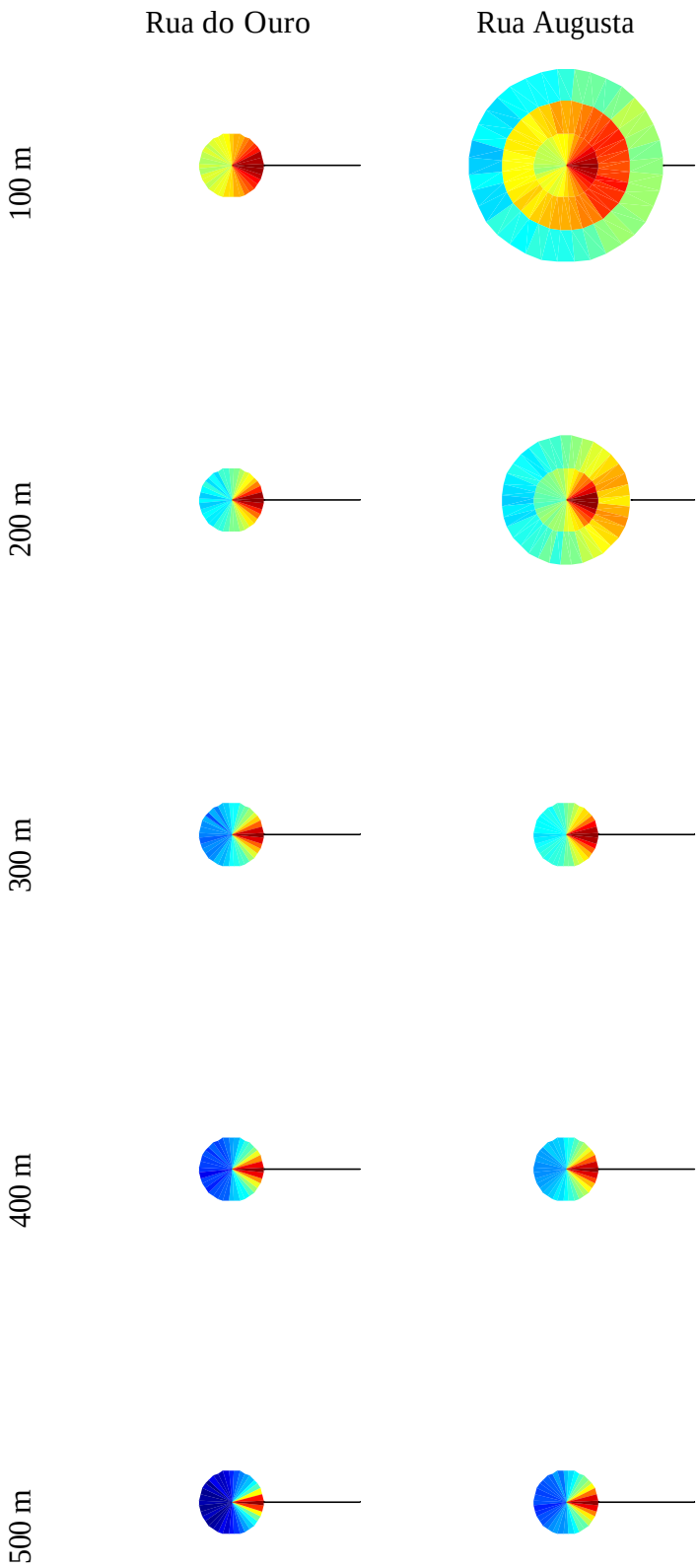

Figure A2.2 – DCIR logarithmic results for simulation set-up 2).

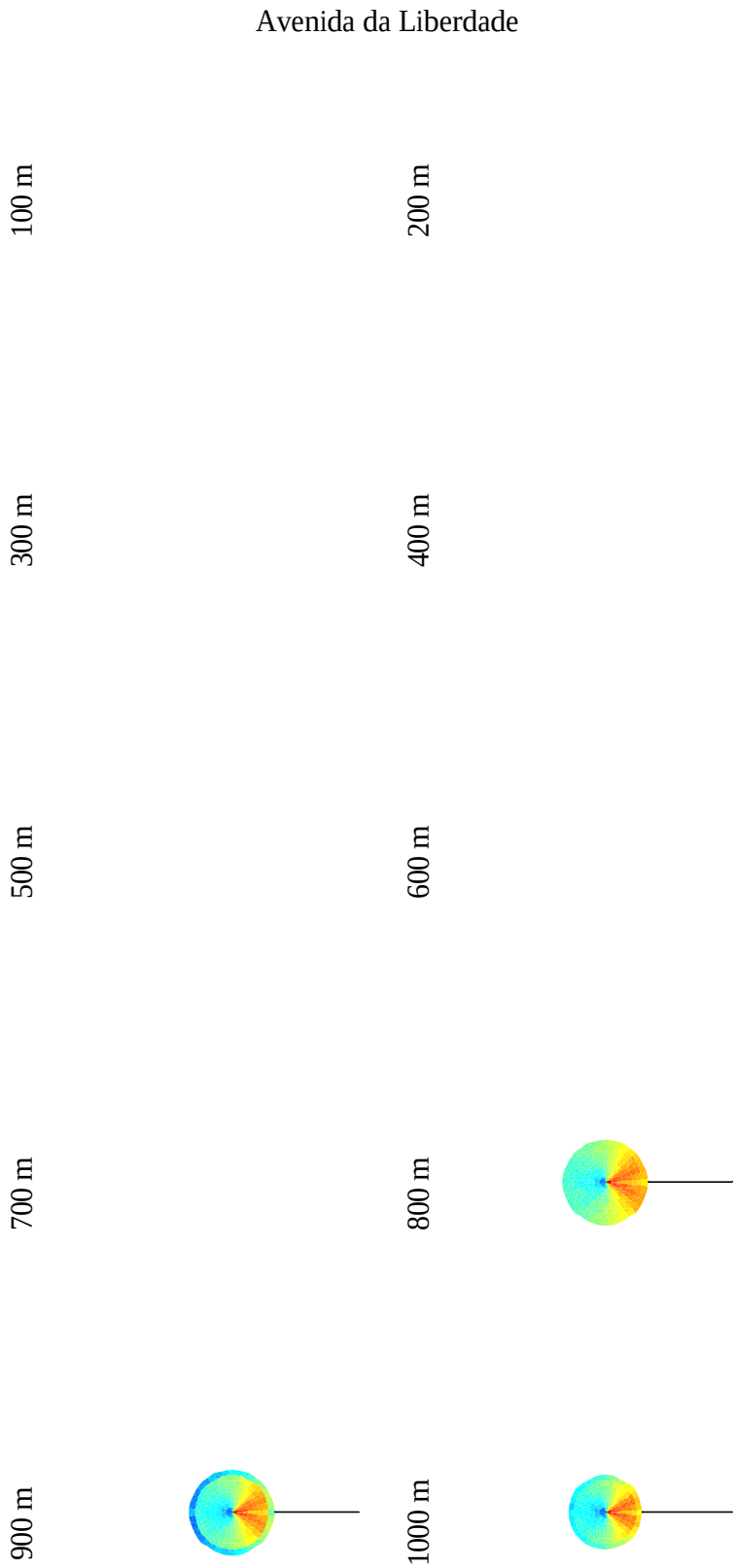

Figure A2.3 – DCIR logarithmic results for simulation set-up 3).

Annex 3

DCIR results for a 20 ns delay resolution

This annex represents the DCIR results obtained for a resolution of 20 ns. Average results a plotted in logarithmic scale with and without resolution contour. Linear scale results are plotted for DCIR average, standard deviation and normalised standard deviation. The same shape of plots is used as for Chapter 4.

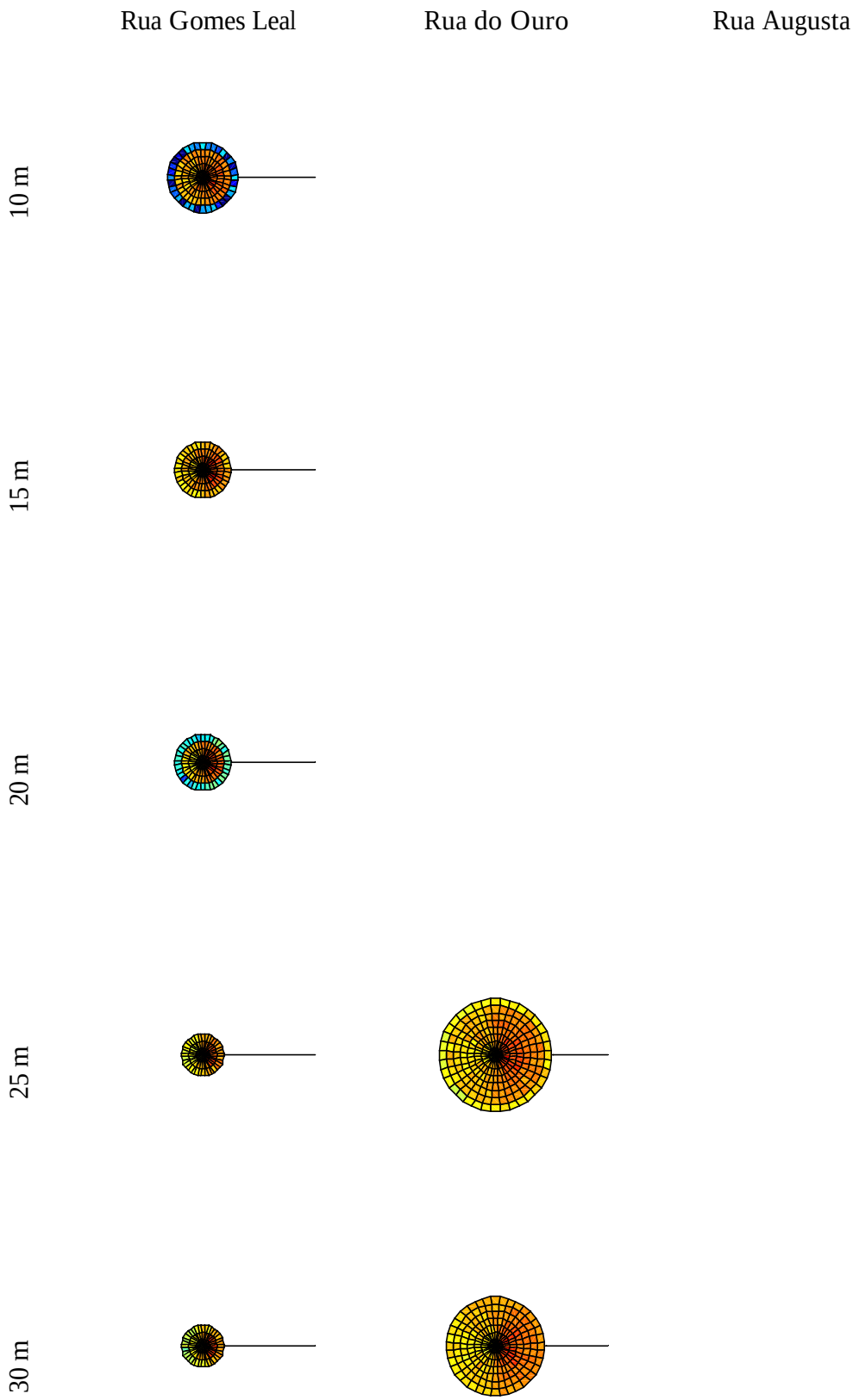

Figure A3.1 – DCIR logarithmic results for simulation set-up 1).

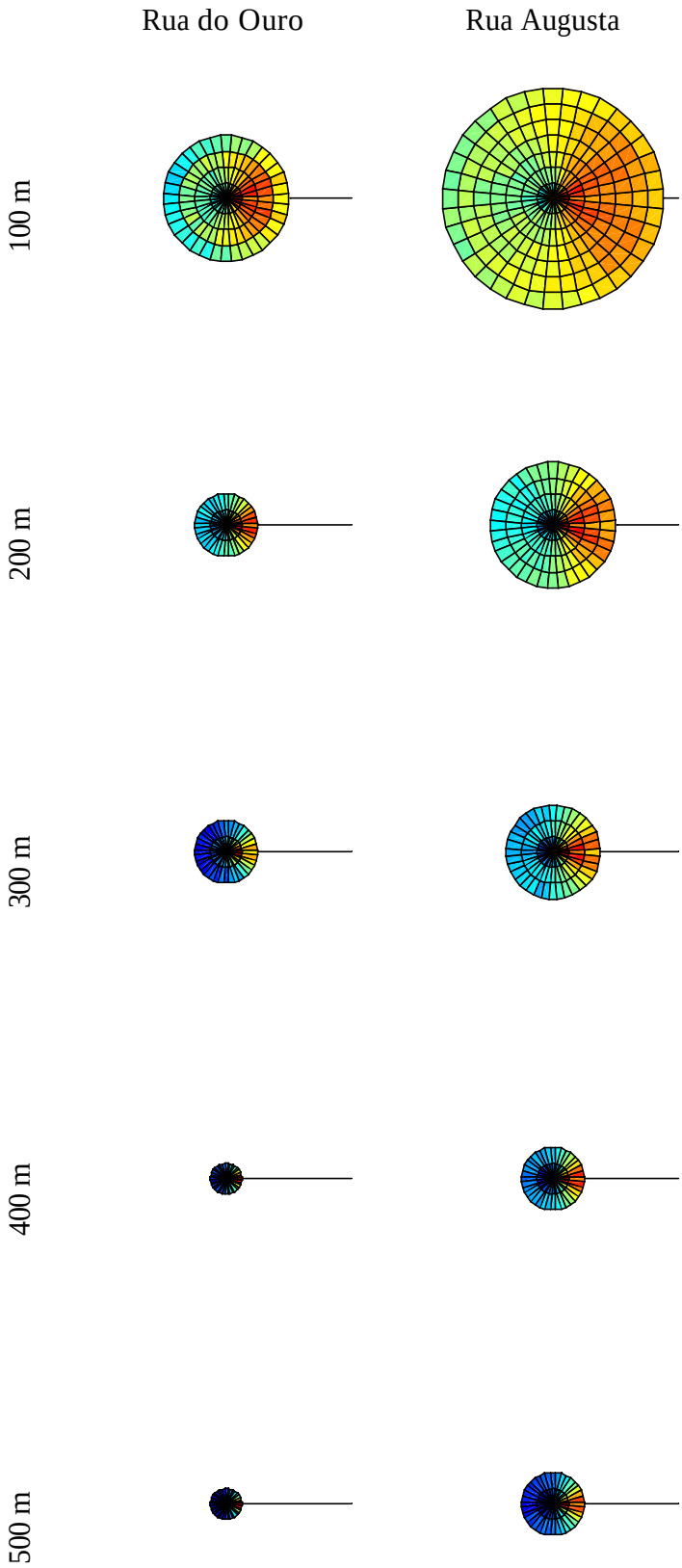

Figure A3.2 – DCIR logarithmic results for simulation set-up 2).

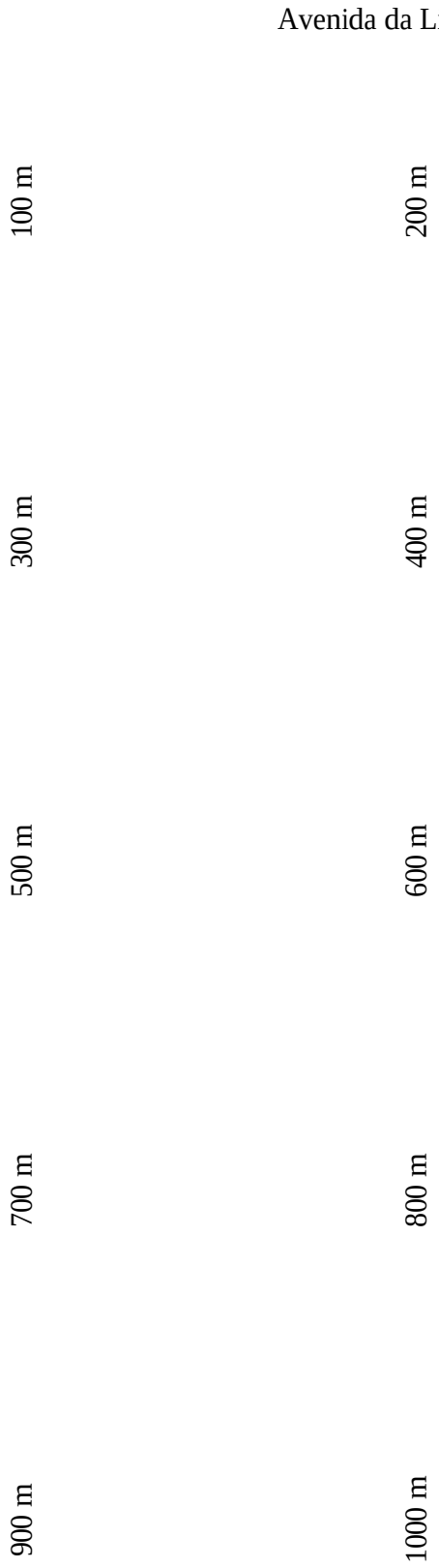

Figure A3.3 – DCIR logarithmic results for simulation set-up 3).

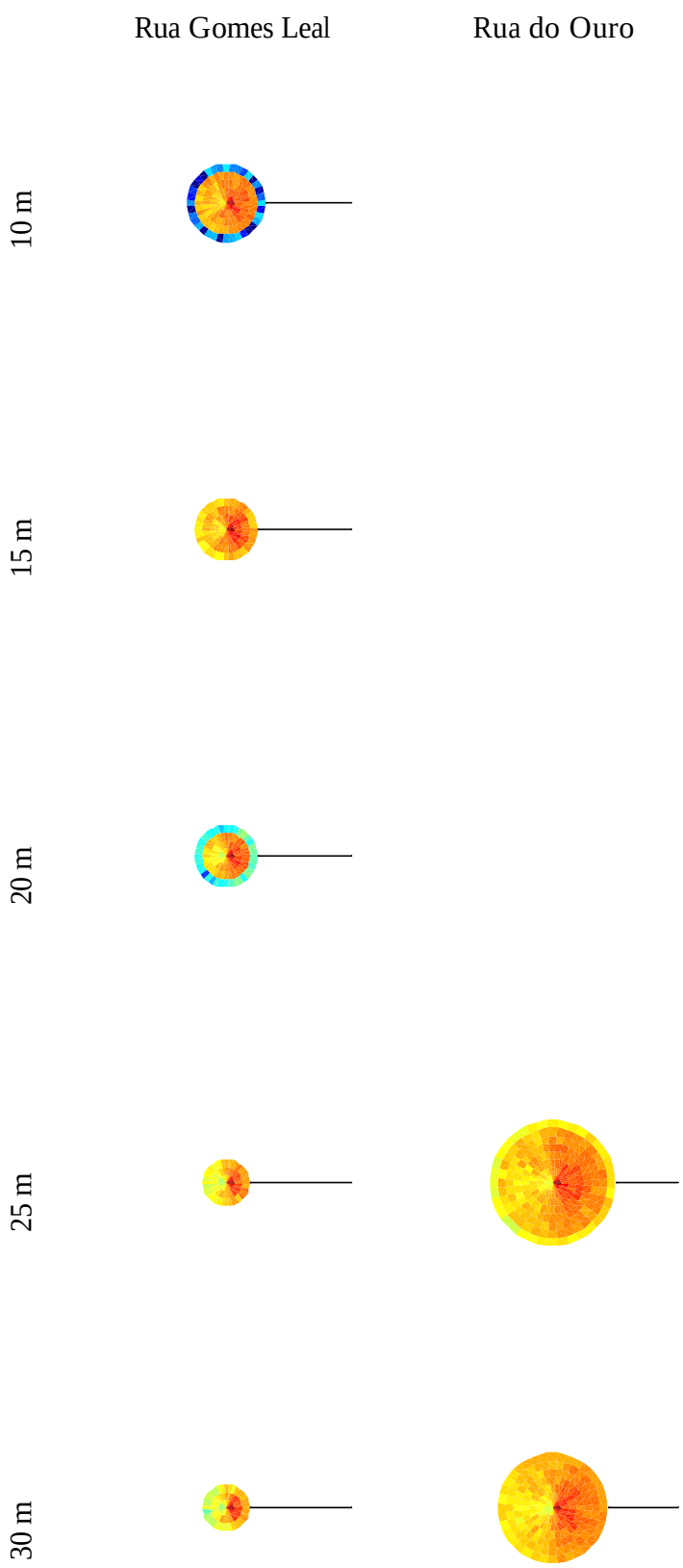

Figure A3.4 – DCIR logarithmic results without resolution contour for simulation set-up 1).

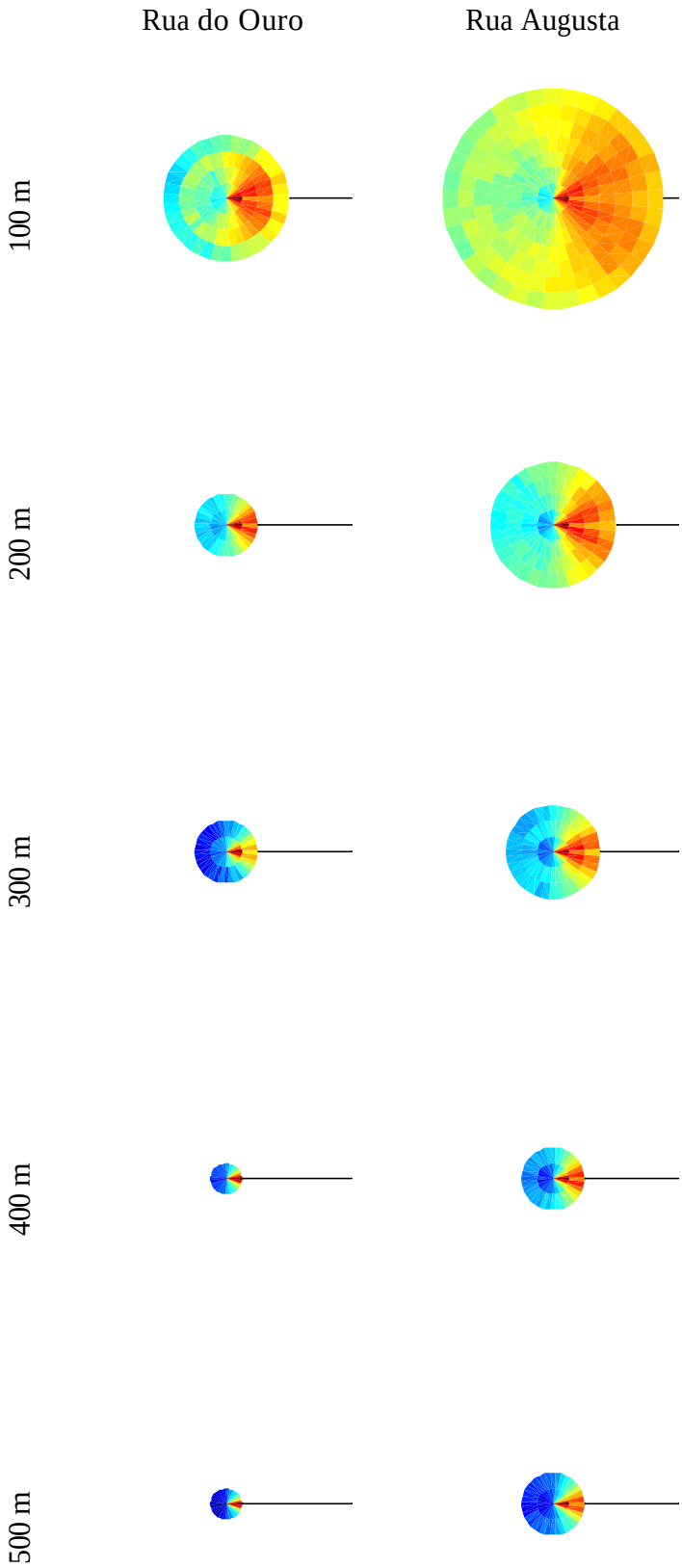

Figure A3.5 – DCIR logarithmic results without resolution contour for simulation set-up 2).

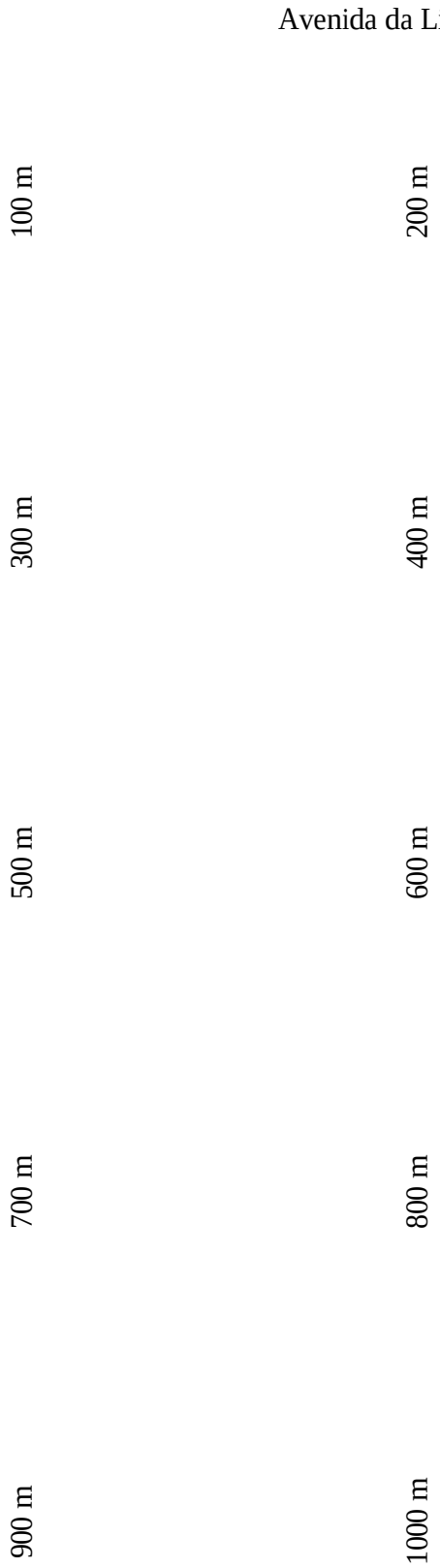

Figure A3.6 – DCIR logarithmic results without resolution contour for simulation set-up 3).

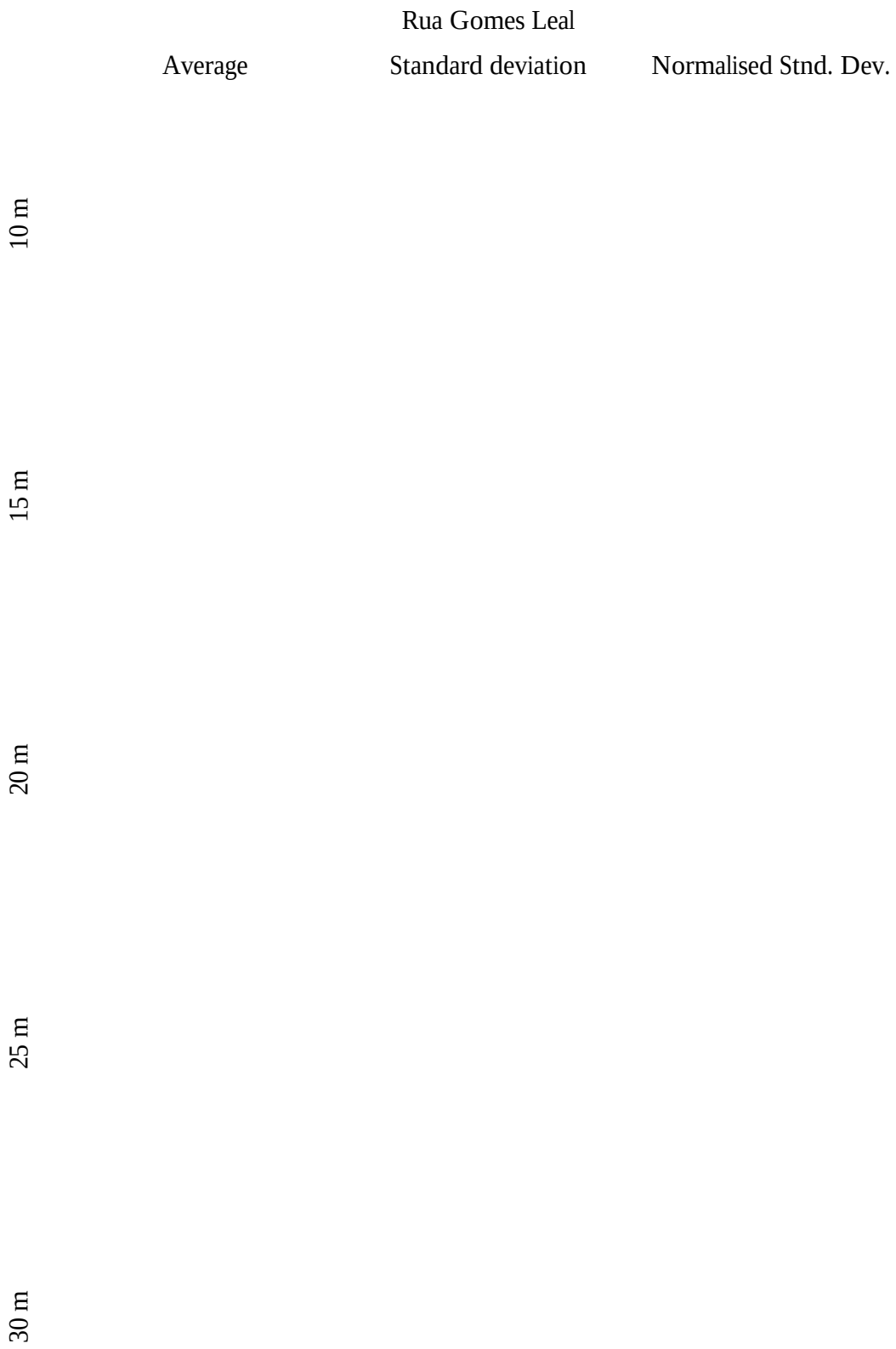

Figure A3.7 – DCIR average and standard deviation results for “Rua Gomes Leal” (simulation set-up 1)).

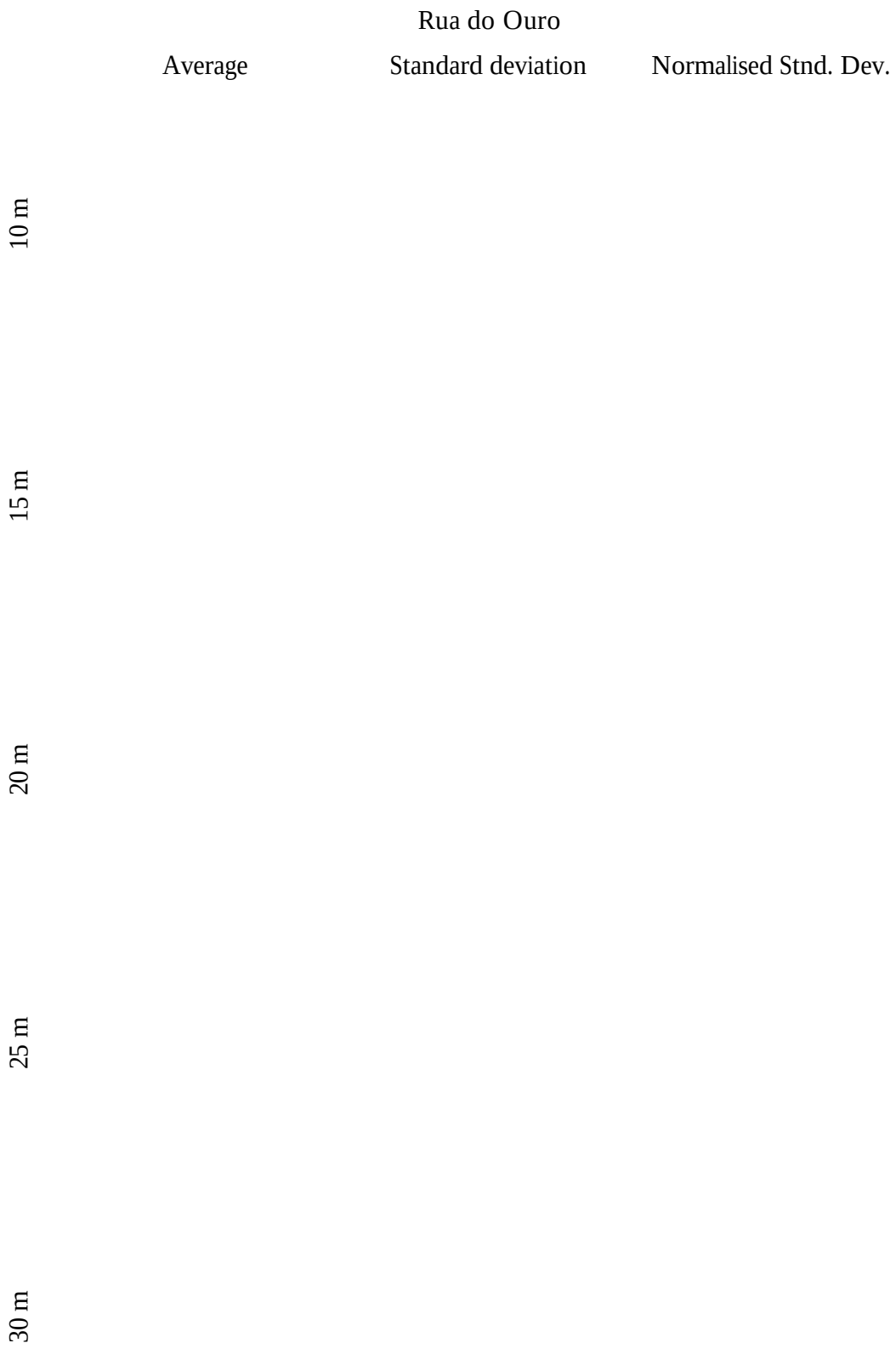

Figure A3.8 – DCIR average and standard deviation results for “Rua do Ouro” at simulation set-up 1).

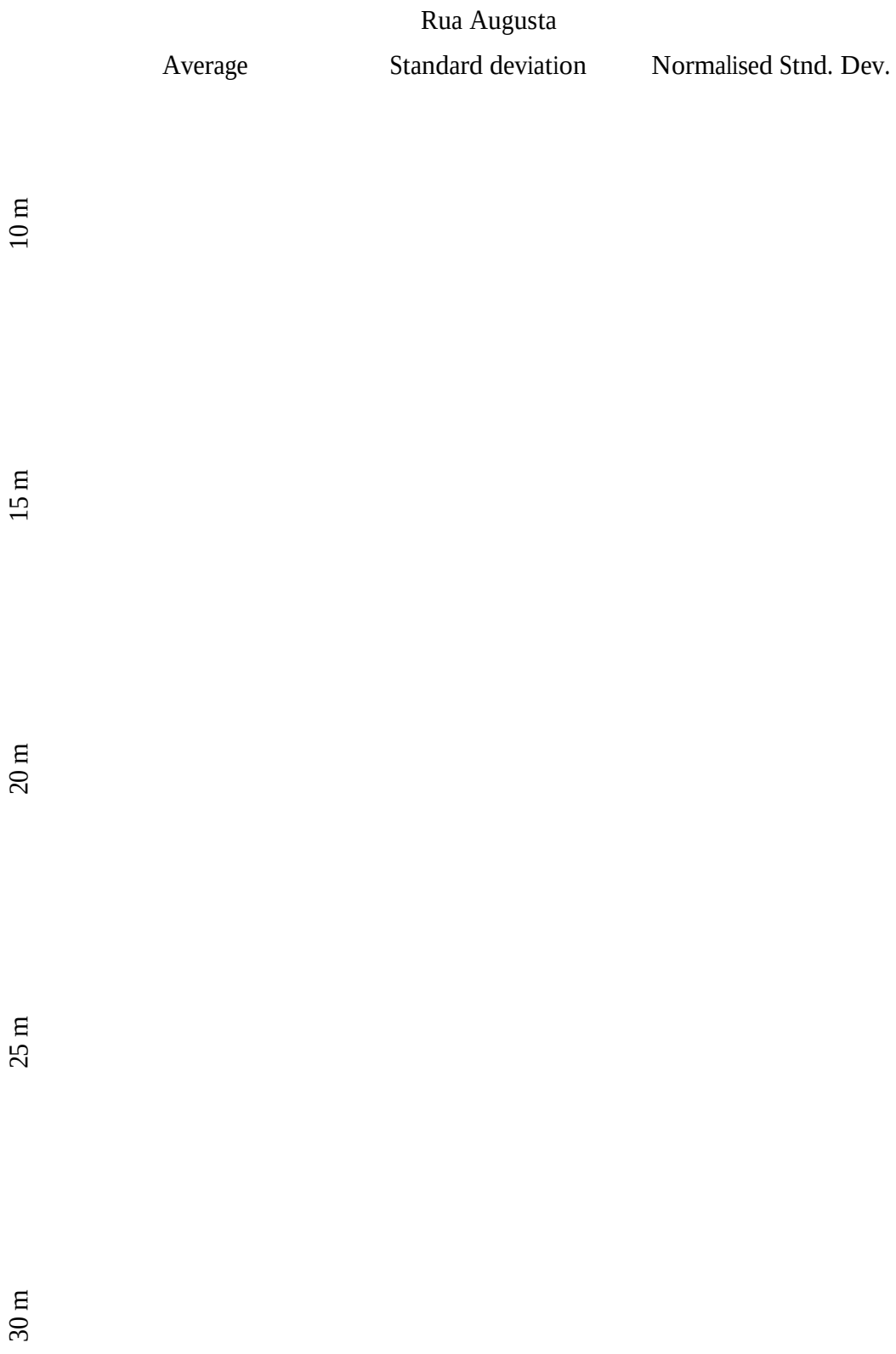

Figure A3.9 – DCIR average and standard deviation results for “Rua Augusta” at simulation set-up 1).

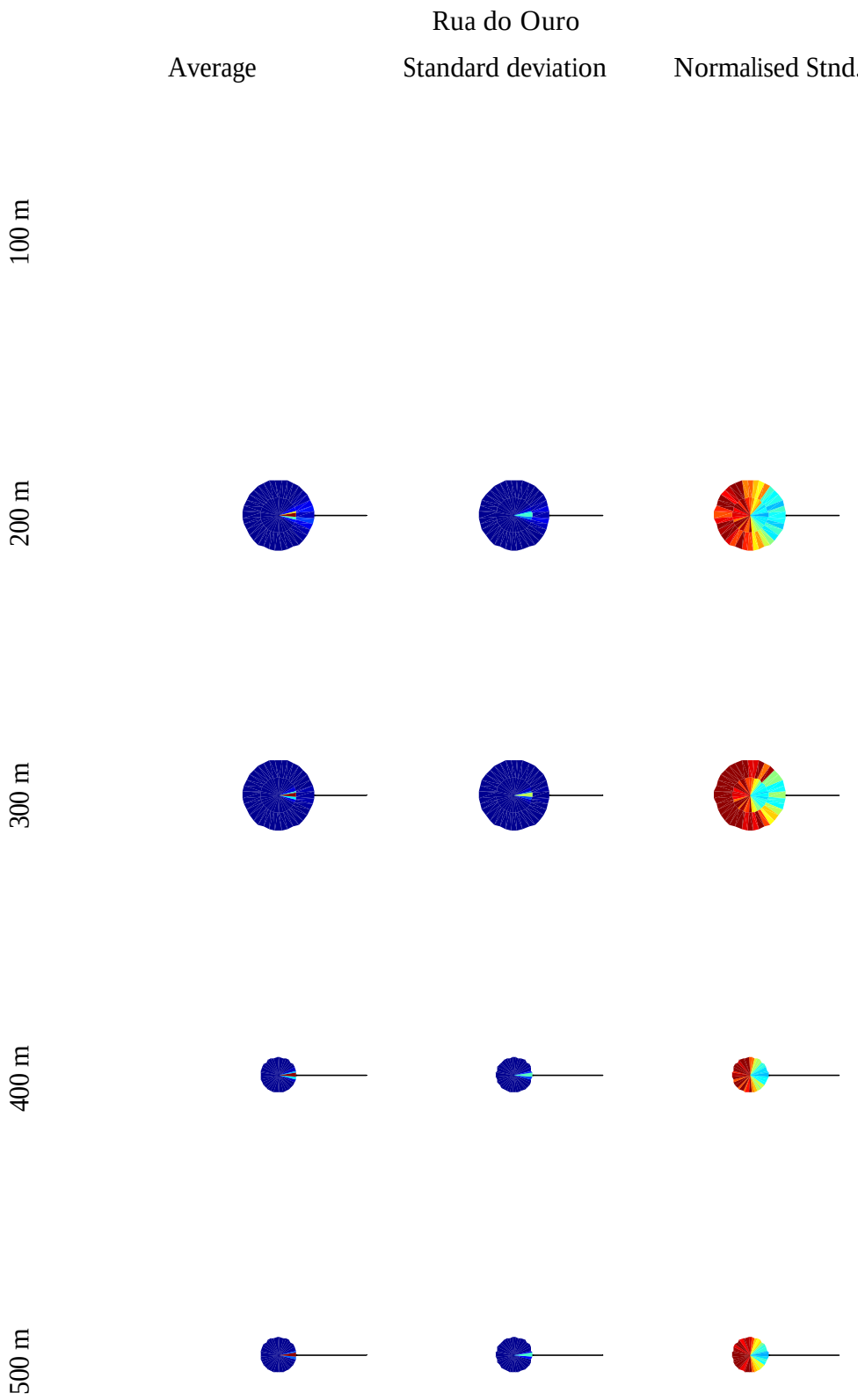

Figure A3.10 – DCIR average and standard deviation results for “Rua do Ouro” at simulation set-up 2).

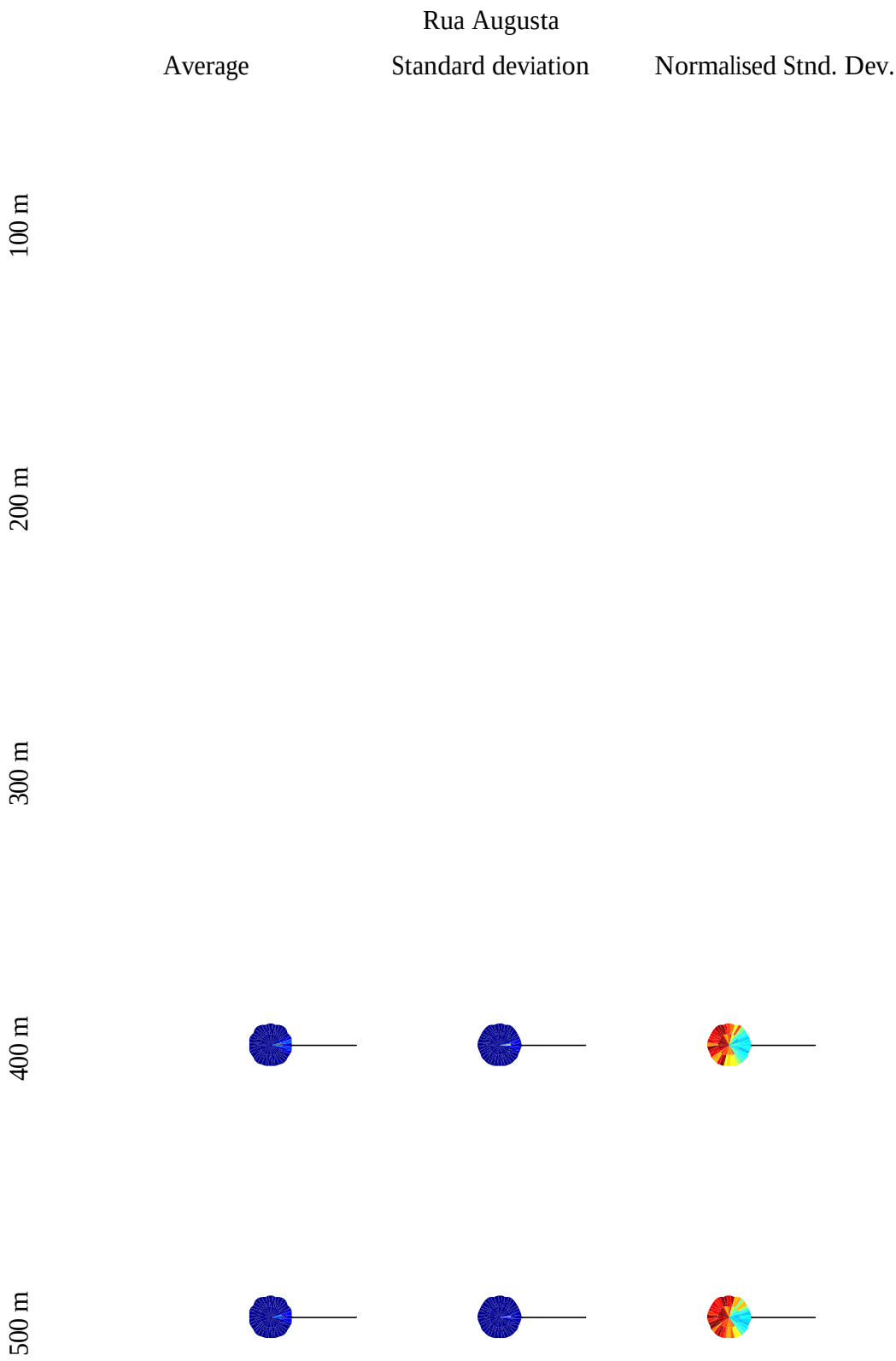

Figure A3.11 – DCIR average and standard deviation results for “Rua Augusta” at simulation set-up 2).

Figure A3.12 – DCIR average and standard deviation results for "Avenida da Liberdade" at the first half of set-up 3).

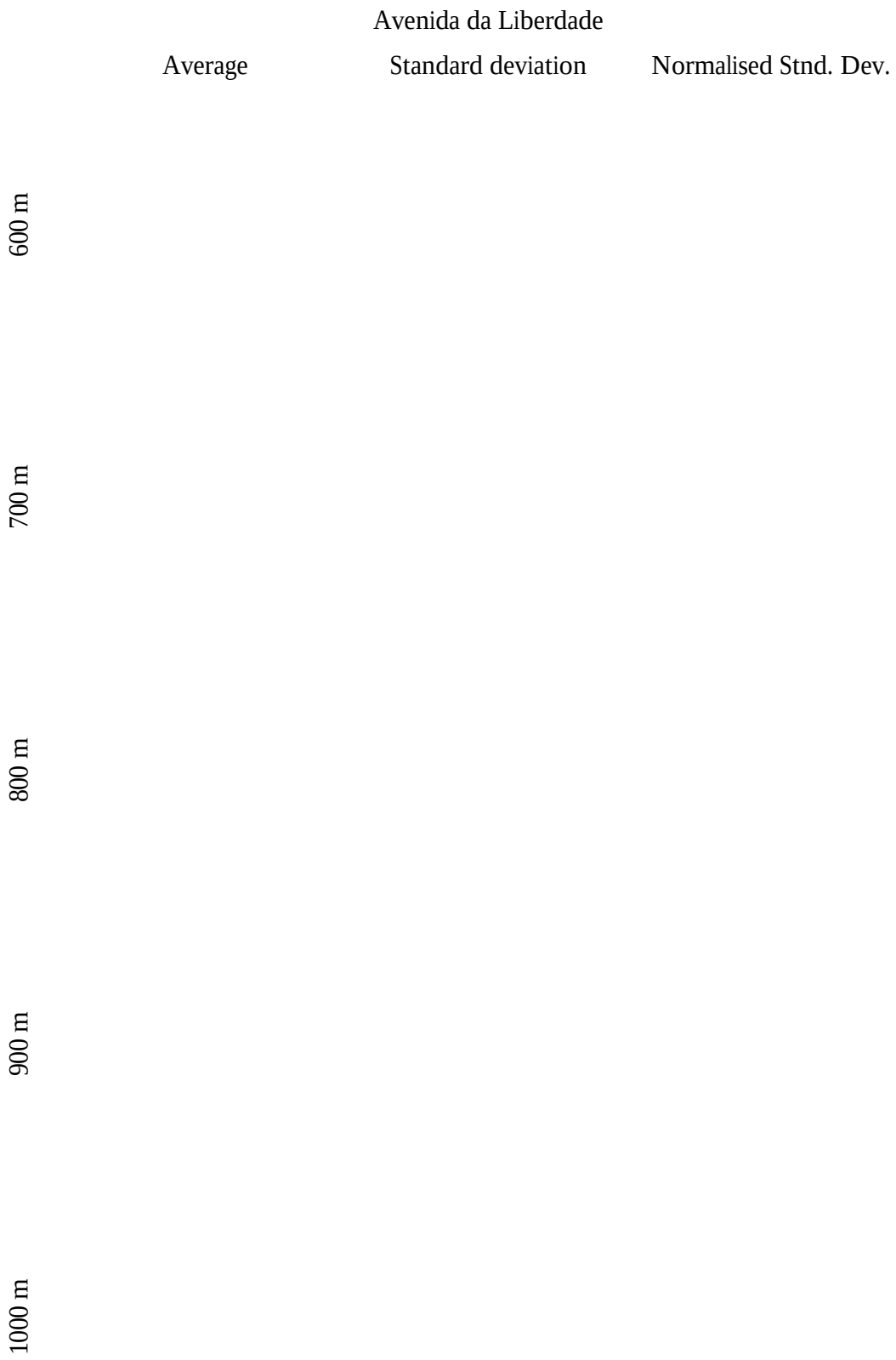

Figure A3.13 – DCIR average and standard deviation results for "Avenida da Liberdade" at the 2nd half of set-up 3).